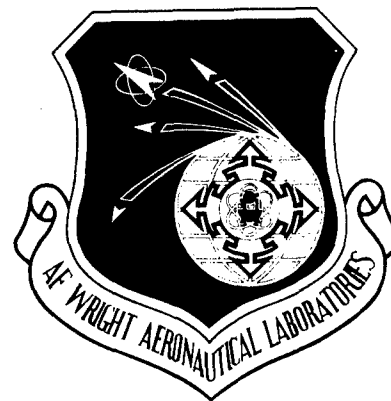


Br Cy

AFWAL-TR-86-4035

ADA 174174

PHYSICAL-CHEMICAL PROPERTIES OF ARTICULATED
RODLIKE POLYMERS



G. C. Berry
R. Furukawa
S. Mohan
C. Wei
C. Kim

Carnegie-Mellon University
4400 Fifth Avenue
Pittsburgh, PA 15213

August 1986

Final Report for Period September 1983 - August 1985

Approved for Public Release, Distribution Unlimited

MATERIALS LABORATORY
AIR FORCE WRIGHT AERONAUTICAL LABORATORIES
AIR FORCE SYSTEMS COMMAND
WRIGHT-PATTERSON AIR FORCE BASE, OHIO 45433-6533

Best Available Copy

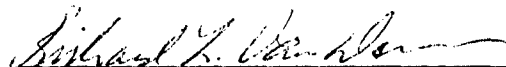
20040219252

When Government drawings, specifications, or other data are used for any purpose other than in connection with a definitely related Government procurement operation, the United States Government thereby incurs no responsibility nor any obligation whatsoever; and the fact that the Government may have formulated, furnished, or in any way supplied the said drawings, specifications, or other data, is not to be regarded by implication or otherwise as in any manner licensing the holder or any other person or corporation, or conveying any rights or permission to manufacture, use, or sell any patented invention that may be in any way be related thereto.

This technical report has been reviewed and is approved for publication.



WALTER W. ADAMS
Work Unit Scientist



RICHARD L. VAN DEUSEN
Chief, Polymer Branch

FOR THE COMMANDER



MERRILL L. MINGES
Director
Nonmetallic Materials Division

"If your address has changed, if you wish to be removed from our mailing list, or if the addressee is no longer employed by your organization please notify AFWAL/MLBP, Wright-Patterson AFB OH 45433 to help us maintain a current mailing list."

Copies of this report should not be returned unless return is required by security considerations, contractual obligations, or notice on a specific document.

Unclassified

SECURITY CLASSIFICATION OF THIS PAGE

REPORT DOCUMENTATION PAGE

1a. REPORT SECURITY CLASSIFICATION Unclassified			1b. RESTRICTIVE MARKINGS N/A		
2a. SECURITY CLASSIFICATION AUTHORITY			3. DISTRIBUTION/AVAILABILITY OF REPORT Approved for public release; distribution unlimited.		
2b. DECLASSIFICATION/DOWNGRADING SCHEDULE					
4. PERFORMING ORGANIZATION REPORT NUMBER(S)			5. MONITORING ORGANIZATION REPORT NUMBER(S) AFWAL-TR-86-4035		
6a. NAME OF PERFORMING ORGANIZATION Carnegie-Mellon University		6b. OFFICE SYMBOL (If applicable)	7a. NAME OF MONITORING ORGANIZATION AFWAL/MLBP		
6c. ADDRESS (City, State and ZIP Code) Pittsburgh, PA 15213			7b. ADDRESS (City, State and ZIP Code) WPAFB, OH 45433-6533		
8a. NAME OF FUNDING/SPONSORING ORGANIZATION Same as 6a		8b. OFFICE SYMBOL (If applicable)	9. PROCUREMENT INSTRUMENT IDENTIFICATION NUMBER F33615-83-C-5044		
8c. ADDRESS (City, State and ZIP Code)			10. SOURCE OF FUNDING NOS.		
			PROGRAM ELEMENT NO.	PROJECT NO.	TASK NO.
			61102F	2303	Q3
11. TITLE (Include Security Classification) (cont. on reverse) Physical-Chemical Properites			12. PERSONAL AUTHOR(S) G.C Berry, S. Mohan, C. Kim, R. Furukawa, C. Wei		
13a. TYPE OF REPORT Final		13b. TIME COVERED FROM Sep 83 TO Aug 85	14. DATE OF REPORT (Yr., Mo., Day) 86/08/29		15. PAGE COUNT 105
16. SUPPLEMENTARY NOTATION					
17. COSATI CODES			18. SUBJECT TERMS (Continue on reverse if necessary and identify by block number)		
FIELD	GROUP	SUB. GR.			
07	04				
11	09				
19. ABSTRACT (Continue on reverse if necessary and identify by block number) Rheological and rheo-optical studies are reported on solutions of rodlike poly(1,4-phenylene 2,6-benzobisthiazole), PBT. Both isotropic and nematic solutions are studied, over a range of polymer concentration c , weight average chain length L_w , and temperature. A single-integral constitutive equation is given that describes the rheological and rheo-optical properties of the isotropic solution. It is based on a memory function based on linear viscoelastic behavior and a strain measure that introduces nonlinear viscoelastic behavior under appropriate strain history. The behavior for the nematic fluid exhibits both similarities and differences with that given by the single-integral relation. In particular, the steady-state behavior at small shear rate is markedly different than that predicted, perhaps related to unstable shear flow of the nematic fluid. (Continued on reverse side)					
20. DISTRIBUTION/AVAILABILITY OF ABSTRACT UNCLASSIFIED/UNLIMITED <input type="checkbox"/> SAME AS RPT. <input checked="" type="checkbox"/> DTIC USERS <input type="checkbox"/>			21. ABSTRACT SECURITY CLASSIFICATION Unclassified		
22a. NAME OF RESPONSIBLE INDIVIDUAL W. W. Adams			22b. TELEPHONE NUMBER (Include Area Code) 513-255-9148		22c. OFFICE SYMBOL AFWAL/MLBP

19. Abstract continued

Rheological data are also given for mixtures of PBT and a nylon in solution. The results reveal marked effects on the rheological properties of the PBT solution, dependent on the nylon concentration.

11. Title continued

of Articulated Rodlike Polymers

FOREWORD

This report on the "Physical-Chemical Properties of Articulated Rodlike Polymers" was prepared in the Department of Chemistry, Carnegie-Mellon University, 4400 Fifth Avenue, Pittsburgh, Pennsylvania 15213, under Contract F33615-83-C-5044 (Project No. 24190142.) It was administered under the direction of the Materials Laboratory, Air Force Wright Aeronautical Laboratories, Wright-Patterson Air Force Base, Ohio, Dr. W. W. Adams.

The report covers work conducted from 1 September 1983 to 30 August 1985. It was submitted in January, 1986. Authors are G. C. Berry, Principal Investigator, R. Furukawa, S. Mohan, C. Wei, and C. Kim.

TABLE OF CONTENTS TITLE

SECTION

1. LINEAR AND NONLINEAR TRANSIENT RHEOLOGICAL BEHAVIOR OF RODLIKE POLYMERS IN SOLUTION	1
2. TRANSIENT AND STEADY-STATE RHEOLOGICAL STUDIES ON NEMATIC SOLUTIONS OF RODLIKE POLYMERS	34
3. RHEOLOGICAL AND RHEO-OPTICAL STUDIES OF A CONSTITUTIVE EQUATION FOR NEMATOGENIC SOLUTIONS OF RODLIKE POLYMERS	64
4. STEADY-STATE AND TRANSIENT RHEOLOGICAL AND RHEO-OPTICAL PROPERTIES OF MIXTURES OF RODLIKE AND FLEXIBLE CHAIN POLYMERS IN ISOTROPIC SOLUTIONS	77
5. REFERENCES	91
6. APPENDICES	93

LIST OF FIGURES

- Figure 1:** 22
The reduced steady-state viscosity η/η_0 versus the reduced shear rate τ/τ_0 for solutions of PBT-53 in methane sulfonic acid. From top to bottom: 25.5 gkg⁻¹ (O, O-, O, Q, -O for 12.5, 23, 30, 40, 60 C, resp.); 28.0 gkg⁻¹ (O-, O for 38, 60, resp.); 29.4 gkg⁻¹ (O, O, O- for 12, 21, 40 C, resp.); 31.7 gkg⁻¹ (O-, Q for 40, 60 C, resp.); and 32.3 gkg⁻¹ (8, 19, 43, 60 C for O, O-, Q, -O, resp.). The solid curves represent Eqn. 21 using the η_i and τ_i in Table 4. The dashed curves represent the data for the solution with $w = 25.5$ gkg⁻¹ to facilitate comparison of the data at various w .
- Figure 2:** 23
The reduced steady-state recoverable compliance R/R_0 versus the reduced shear rate τ/τ_0 for the solutions identified in the caption to Fig. 1. The solid curves represent Eqn. 22 using the η_i and τ_i in Table 4. The dashed curves represent the data for the solution with $c = 25.5$ gkg⁻¹ to facilitate comparison of the data at various w .
- Figure 3:** 24
The reduced steady-state viscosity η/η_0 versus the reduced shear rate τ/τ_0 for solutions of PBT polymers in methane sulfonic acid. From top to bottom: PBT-72, 25.4 gkg⁻¹ (Q, O-, O for 24, 39, 55 C, resp.); PBT-72, 29.4 gkg⁻¹ (O-, O for 39, 58 C, resp.); PBT-72-R, 29.6 gkg⁻¹ (O, Q, O for 23, 39, 58 C); PBT-43, 31.5 gkg⁻¹ (-O, Q, O-, O for 10, 14.5, 18, 23.5 C, resp.). The dashed curves represent the data for PBT-53, $c = 25.5$ gkg⁻¹.
- Figure 4:** 25
The upper three panels give the reduced steady-state recoverable compliance R/R_0 versus the reduced shear rate τ/τ_0 ; the lowest panel gives the reduced dynamic compliance $J'(\omega)/R_0$ versus the reduced frequency τ/τ_0 . The data are for the solution in the corresponding panels identified in the caption to Fig. 3. The dashed curves represent the data for PBT-53, $w = 25.5$ gkg⁻¹.
- Figure 5:** 26
The flow birefringence function versus the reduced shear rate τ/τ_0 for solution of PBT in methane sulfonic acid. From top to bottom: PBT-53, 25.5 gkg⁻¹ (O-, O for 23, 40 C, resp.), 28.0 gkg⁻¹ (O, 60 C), 29.4 gkg⁻¹ (O, O- for 23, 40 C, resp.), 31.7 gkg⁻¹ (O, 40 C); PBT-72, 25.4 gkg⁻¹ (Q, O- for 39, 55 C, resp.); PBT-72R, 29.6 gkg⁻¹ (-O, O, O- for 23, 39 and 60 C, resp.); and PBT-43 (31.5 gkg⁻¹, Q, O- for 15, 23 C, resp.). The solid curve represents Eqn. 12 with Eqn. 28 using the η_i and τ_i in Table 4.
- Figure 6:** 27
Temperature dependence of the viscosity η_0 relative to that η_i of methane sulfonic acid, and the concentration w_0 for the onset of the nematic phase. In the figures, A' and A'' are the values of η_0/η_i and w_0 , respectively, for $T = 313$ K. The symbols denote PBT-53, O; PBT-72, • and PBT-43, ●.
- Figure 7:** 28
The reduced creep compliance $J(t)/R_0$ (open circles) and recoverable compliance $R(t)/R_0$ (filled circles) versus the reduced time t/τ_0 for a solution of PBT-53 in methane sulfonic acid, $w = 25.5$ gkg⁻¹. The symbols O(•), Q, O-, O, -O denote stress σ /Pa equal to 2.8, 15.2, 68.3, 78.7 and 145, resp. The data for O(•) are at 23 C; all others at 13 C.
- Figure 8:** 29
The reduced recoverable compliance function $R(t)/R_0$ versus the reduced time t/τ_0 for a solution of PBT-53 in methane sulfonic acid, $W = 29.4$ gkg⁻¹. The stress σ /Pa is 6.6 (O), 39.3 (O-), and 57.5 (Q) with

$T = 40^\circ, 20^\circ, \text{ and } 40^\circ\text{C}$, respectively. The curve represents Eqn. 14 with the R_i and λ_i given in Table 4.

Figure 9: 30

The reduced flow birefringence relaxation function $\hat{M}(t)/M$ (filled circle) and stress relaxation function $\hat{\eta}_\kappa(t)/\eta_\kappa$ (open circle) for PBT-72, 25.4 gkg⁻¹ (top) and PBT-53, 29.4 gkg⁻¹ (bottom) in methane sulfonic acid. For PBT-72, κ/s^{-1} is 0.0208 (O), 0.0358 (O-), 0.0726 (Q), 0.100 (-O), 0.0126 (•), 0.0502 (•), all at 39 C. For PBT-53, κ/s^{-1} is 0.0227 (O), 0.0455 (O), 0.0851 (Q), 0.186 (-O), 0.0050 (•), 0.0126 (•), 0.0502 (-•), all at 21 C, and 0.0050 (•), 0.0252 (-•), both at 40°C.

Figure 10: 31

The viscosity for solutions of several rodlike polymers over a range of concentration and chain length. Here α^* and $A = KN(1-B)^{-2}$ are empirical parameters obtained by comparison with Eqn. 18 as described in the text. The symbols designate the rodlike polymer/solvent system as given in the caption to Figure 9 in Ref. 1.

Figure 11: 32

The reciprocal of the critical strain γ^* versus weight percent 100w for several PBT-53 solutions in MSA.

Figure 12: 45

Schematic diagram showing the concentration (weight fraction w) and temperatures used in rheological studies on solutions of PBT-53. Regions of isotropic and nematic solutions are indicated on the diagram.

Figure 13: 46

Schematic diagram showing the concentrations (weight fraction w) and temperatures used in rheological studies on solutions of PBT-62. Conditions of w and T for which solutions were observed to be isotropic or nematic are indicated by □ or ▢, respectively. Data for conditions to the left and right sides of the dashed line are given in Figs. 16 and 20, respectively.

Figure 14: 47

The steady-state viscosity of η_κ for solutions of PBT-53 with $T \approx 20^\circ\text{C}$ —the symbols indicate w/gkg⁻¹ of 25.5, O; 29.4, -O; 32.3, O and 42.7 O-.

Figure 15: 48

The steady-state viscosity η_κ and recoverable compliance R_κ for solutions of PBT-62 with $T \approx 60^\circ\text{C}$. The symbols indicate w as in Fig. 13.

Figure 16: 49

η_κ/η_0 and R_κ/R_0 versus $R_0\eta_0\kappa$ for isotropic solutions of PBT-53 (w = 25.5g/kg, with symbols as in Fig. 12). The curves for η_κ/η_0 and R_κ/R_0 represent Eqns. 21 and 40, respectively, with the τ_i and η_i in Table 8.

Figure 17: 50

η_κ/η_0 and R_κ/R_0 versus $R_0\eta_0\kappa$ for isotropic solutions of PBT-62 (symbols as in Fig. 13). The dashed curve represents R_κ/R_0 vs $\tau_c\kappa$ from Fig. 16.

Figure 18: 51

η_κ/η_0 (or η_κ/η_P) and R_κ/R_0 versus $R_0\eta_0\kappa$ (or $R_0\eta_P\kappa$) for isotropic (or nematic) solutions of PBT-53 (w = 32.3 g/kg, with symbols as in Fig. 12). The solid curves for η_κ/η_0 and R_κ/R_0 represent Eqns 21 and 40, respectively with the τ_i and η_i given in Table 8. The dashed curve shows $R_0(t)/R_0$ versus τ_c/t .

Figure 19: 52

η_κ/η_P and R_κ/R_0 versus $R_0\eta_P\kappa$ for nematic solutions of PBT-53 (w = 42.7 g/kg, with symbols as in Fig. 12). The dashed curves represent the curves given in Fig. 18.

Figure 20:	53
η_{κ}/η_P and R_{κ}/R_0 versus $R_0\eta_P\kappa$ for nematic solutions of PBT-62 (symbols κ as in Fig. 13). The curves represent the behavior shown in Fig. 17.	
Figure 21:	54
η_{κ}/η_P and R_{κ}/R_0 versus $R_0\eta_P\kappa$ for solutions of PBT-62 (symbols as in Fig. 13). The curves represent the behavior shown in Fig. 17.	
Figure 22:	55
η_{κ}/η_0 and R_{κ}/R_0 versus $R_0\eta_0\kappa$ for solutions of PBT-62 (symbols as in Fig. 13). The dashed curves represent the behavior shown in Fig. 17.	
Figure 23:	56
Creep $J_{\sigma}(t)$ and recoverable compliance $R_{\sigma}(t)$ versus t/τ (with $\tau = 170s$) for a nematic solution of PBT-53 $^{\sigma}$ ($w = 32.3$ g/kg, $T = 19.5^{\circ}C$). Values of shear stress σ /Pa used are given, along with the parameter γ^* .	
Figure 24:	57
The stress $\sigma(t)$ in a stress-growth experiment versus the strain κt for a solution of PBT-53 ($w = 32.3$ g/kg) at temperatures for which the solution is isotropic ($43^{\circ}C$) and nematic ($19.5^{\circ}C$). Values of κ/s^{-1} are indicated.	
Figure 25:	58
The stress $\sigma(t)$ in a stress-growth experiment versus the strain κt for a nematic solution of PBT-53 ($w = 42.7$ g/kg) at two temperatures.	
Figure 26:	59
The critical strains γ^* and γ^+ plotted (as the inverse) versus the concentration w for solutions of PBT-53.	
Figure 27:	60
Left side: $\eta_0/M_w[\eta](a^*/a_0^*)^3$ versus $Bc_L/M_L a^*$ for isotropic solutions of PBT-53, PBT-62 and other rodlike polymers (see the preceding for identification of the symbols). Here B/a^* is obtained by comparison of Eqn. 18 with experiment (see the preceding), and B/a_0^* is an arbitrary constant. Right side: The same quantities for nematic solution of PBT-62, (a) and PBT-53 (•)	
Figure 28:	61
$R_{\sigma}(t)/R_0$ versus t/τ for two isotropic solutions of PBT-53 ($w/g\ kg^{-1}$ equal to 25.5 and 29.4, long and short dash, respectively) and a nematic solution ($w = 32.3$ g/kg, $T = 19.5^{\circ}C$, solid curve). For the latter, τ is replaced by ηR_{σ} and R_0 is replaced by R_{κ} . With the isotropic solutions, $R_{\sigma}(t) = R_0^{\kappa}(t)$, and with the nematic solution, $\sigma = 14.6$ Pa.	
Figure 29:	62
$\eta_{\kappa}(\tau_{20}/\tau_T)$, R_{κ} and $N_{\kappa}^{(1)}$ versus $(\tau_T/\tau_{20})\kappa$ for an anisotropic solution of poly(γ -benzylglutamate) in τ_{20} for T/K equal to 273 (Δ, Δ) and 293 (O, \bullet). The dashed line and the data on $N_{\kappa}^{(1)}$ are from Ref. 36. The factor τ_T/τ_{20} is unity for $T = 293K$ and chosen to superpose data on R_{κ} versus $(\tau_T/\tau_{20})\kappa$ for $T = 273K$. The range denoted "N $^{(1)}$ anomaly" designates the range for negative $N_{\kappa}^{(1)}$ according to Ref. 38.	
Figure 30:	71
$R_0(t)/R_0$ versus t/τ (with $\tau = \eta_0 R_0$) for an isotropic solution of PBT-53 (0.0294 weight fraction polymer), ---, and $R_{\sigma}(t)/R_{\sigma}$ versus $t/\eta R_{\sigma}$ for a nematic solution of the same polymer (0.0323 weight fraction polymer), _____. For the latter, $R_{\sigma}(t)$, R_{σ} and η_P were determined after steady-state flow with $\eta_P R_{\sigma} \kappa \sim 1$.	
Figure 31:	72
Rheological data 3 for isotropic ($-O, O$) and nematic ($O-, O$) solutions of	

PBT-53 (0.0323 weight fraction polymer. With the latter, η_0 is replaced by η_p , see text. The curves are calculated with Eqns. 3.3 and 3.4 using experimentally determined values of τ_i and η_i .	
Figure 32:	73
$\eta_0/M_w [\eta] (a^*/a_0^*)^3$ versus $BcL/M_w a^*$ for isotropic and nematic solutions of PBT-53 and PBT-62. With the nematic solutions, η_0 is replaced by η_p (a_0^* is a constant).	
Figure 33:	74
The steady-state flow birefringence versus the reduced shear rate $\eta_0 R_0 \kappa$ for an isotropic solution of PBT-53 (0.0255 weight fraction) at several temperatures. The curve is calculated with Eqns. 3.5 and 3.10 using experimentally determined values of τ_i and η_i .	
Figure 34:	75
The reduced flow birefringence relaxation function $\hat{M}(t)/M$ and stress relaxation function $\hat{\eta}(t)/\eta$ for anisotropic solution of PBT-53 (0.0294 weight fraction) for several shear rates, with $\beta_\kappa \approx \tau_\kappa R_\kappa$.	
Figure 35:	81
The zero shear viscosity η as η_0/η , $M[\eta]$ vs. cL for PBT-nylon mixtures (circles with pipe) and PBT in nylon-free solutions --c refers to PBT concentration only, in methane sulfonic acid. For the mixture, the compositions are (see Table 10), 20/80, ; 30/70, ; 40/60, ; 50/50, ; 70/30, ; and 80/20, .	
Figure 36:	82
The viscosity of the nylon-66 polymer used as a function of the nylon concentration (in PBT free solutions).	
Figure 37:	83
The viscosity η versus κ and the dynamic viscosity $\eta^*(\omega)$ versus ω for the 50/50 PBT/nylon mixture.	
Figure 38:	84
Steady-state flow curve for PBT-nylon mixture and PBT solutions; symbols are as in Fig. A.	
Figure 39:	85
Steady-state recoverable compliance curve for PBT-nylon mixture and PBT solutions; symbols are as in Fig. A.	
Figure 40:	86
Steady-state flow birefringence for mixtures (PBT and nylon in solution; symbols are as in Fig. A.	
Figure 41:	87
Stress relaxation for mixture of PBT/nylon and PBT solutions; symbols are as in Fig. A.	
Figure 42:	88
Flow birefringence relaxation for PBT/nylon mixtures in solution; symbol as in Fig. A.	
Figure 43:	89
The shift factor β_κ versus $\tau_c \kappa$	

LIST OF TABLES

Table 1:	Polymer Solutions Used in This Study	18
Table 2:	Rheological Parameters for Solutions of Rodlike Polymers	19
Table 3:	Rheological and Rheo-optical Parameter Solutions of Rodlike Polymer (PBT-53)	20
Table 4:	Retardation and Relaxation Spectra	21
Table 5:	Critical Concentrations for Solutions of Rodlike Polymers	22
Table 6:	Polymers Used in This Study	43
Table 7:	Rheological Parameters for Solutions of Rodlike Polymers	44
Table 8:	Retardation and Relaxation Spectra	45
Table 9:	Leslie Coefficient for Rodlike Polymers	71
Table 10:	Compositions of PBT-Nylon Solutions Studied	81

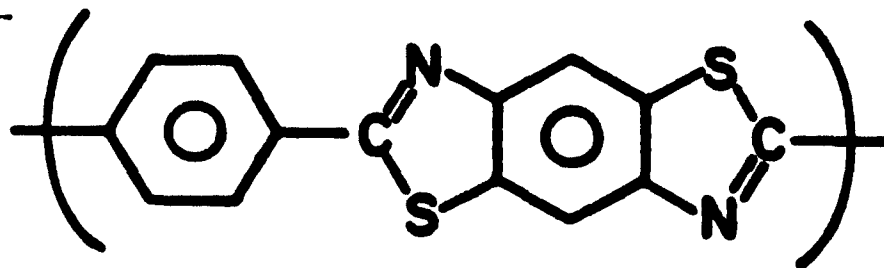
1. LINEAR AND NONLINEAR TRANSIENT RHEOLOGICAL BEHAVIOR OF RODLIKE POLYMERS IN SOLUTION

SUMMARY

Rheological and rheo-optical studies are reported for isotropic solutions of the mesogenic rodlike poly(1,4-phenylene-2,6-benzobisthiazole), PBT. Several PBT samples are used with average contour lengths from 95 to 135 nm. Concentrations were varied over a range just below the concentration c_c for the formation of an ordered (nematic) state. The predictions of a single-integral constitutive equation of the BKZ-type utilizing experimental estimates of the distribution of discrete relaxation times is compared with experimental data on the steady-state viscosity η_κ , the recoverable compliance function R_κ , and the steady-state flow birefringence as functions of the shear rate κ , with satisfactory results. The relaxation of the shear stress and the flow birefringence on cessation of steady-state flow at shear rate κ are also compared with the single-integral constitutive equation, and it is found that in the nonlinear response range the data can be superposed over a wide range in κ . The overall behavior is qualitatively similar to that for flexible chains, which can also be fitted by the single-integral constitutive equations over similar ranges of $\eta_0 R_0 \kappa$, with η_0 and R_0 the limiting values of η_κ and R_κ for small κ . Of course, the dependence of η_0 and R_0 on concentration and molecular weight differs markedly for rodlike and flexible chain polymers.

INTRODUCTION

Elsewhere¹, several steady-state rheological properties were studied in the linear and non-linear response range for rodlike macroions in solution in protic sulfonic acids. The otherwise uncharged polymers are modified to become macroions in solution through protonation by the sulfonic acid. The rheological properties studied included the dependence on shear rate κ of the steady-state viscosity η_κ , recoverable compliance R_κ and flow birefringence function $M_\kappa = \Delta n_\kappa^{(13)} / (\eta_\kappa \kappa)^2$, where $\Delta n_\kappa^{(13)}$ is the flow birefringence in the 1-3 plane. The parameters are defined elsewhere.¹⁻⁵ Here, we will report some transient rheological properties for solutions of the rodlike polymer poly(1,4-phenylene-2,6-benzobisthiazole), PBT:



PBT

Transient properties obtained after initiation of flow include the nonlinear creep compliance $J_\sigma(t)$ and the viscosity growth function $\eta_\kappa(t)$ defined, respectively, as^{5,6}

$$J_\sigma(t) = \gamma(t)/\sigma \quad (1)$$

$$\eta_\kappa(t) = \sigma(t)/\kappa \quad (2)$$

Here $\gamma(t)$ is the strain at time t after imposition of a shear stress σ and $\sigma(t)$ is the shear stress at time t after imposition of a steady rate of shear κ . Of course, for large t , both $\eta_\kappa(t)$ and $t/J_\sigma(t)$ are equal to η_κ .

Transient properties obtained after cessation of steady state flow include the recoverable compliance function $R_\sigma(t)$, the viscosity relaxation function $\hat{\eta}_\kappa(t)$ and the flow birefringence relaxation function $\hat{M}_\kappa(t)$ defined, respectively, as

$$R_\sigma(t) = \gamma_R(t)/\sigma \quad (3)$$

$$\hat{\eta}_\kappa(t) = \sigma(t)/\kappa \quad (4)$$

$$\hat{M}_\kappa(t) = \Delta n_\kappa^{(13)}(t)/(\eta_\kappa \kappa)^2 \quad (5)$$

Here $\gamma_R(t)$ is the recovered strain at time t after cessation of steady flow at shear rate κ (shear stress $\sigma = \eta_\kappa \kappa$), $\sigma(t)$ is the shear stress at time t after cessation of steady flow at shear rate κ , and $\Delta n_\kappa^{(13)}(t)$ is the birefringence (in the 1,3 plane) at time t after cessation of steady flow at shear rate κ . For large t , $R_\sigma(t) = R_\kappa$, whereas both $\hat{\eta}_\kappa(t)$ and $\hat{M}_\kappa(t)$ are zero. For $t = 0$, the latter are η_κ and M_κ , respectively.

For small κ or σ , linear viscoelastic behavior is expected,^{5,6} for which one has the well-known relations

$$\lim_{\sigma=0} J_{\sigma}(t) = J_0(t) = R_0(t) + t/\eta_0 \quad (6)$$

$$\lim_{\sigma=0} R_{\sigma}(t) = R_0(t) \quad (7)$$

$$\lim_{\kappa=0} \eta_{\kappa}(t) = \eta_0(t) = \int_0^t G_0(u)du \quad (8)$$

$$\lim_{\kappa=0} \hat{\eta}_{\kappa}(t) = \hat{\eta}_0(t) = \eta_0 - \eta_0(t) \quad (9)$$

The creep compliance $J_0(t)$ and the linear modulus $G_0(t)$ are related through a convolution integral:

$$\int_0^t G_0(u) J_0(t-u)du = t \quad (10a)$$

$$\int_0^t G_0(u)R_0(t-u)du = t \frac{\hat{\eta}_0(t)}{\eta_0} + \tau_c \frac{N_0^{(1)}(t)}{R_0} \quad (10b)$$

$$\text{where} \quad \tau_c = \eta_0 R_0$$

$$\text{and} \quad N_0^{(1)}(t) = \eta_0^{-2} \int_0^t u G_0(u)du \quad (11)$$

Equations 10 provide a means to compute $J_0(t)$ from $G_0(t)$ or vice versa^{3,6,7}, see below.

As discussed elsewhere¹, according to the "stress-optic" law⁸ M_{κ} is related to the first normal stress function $N_{\kappa}^{(1)}$ (with neglect of $\Delta n^{(23)}$ in comparison with $\Delta n^{(13)}$):

$$M_{\kappa} \sim 2 \mathbb{C}' N_{\kappa}^{(1)} \quad (12)$$

Here, $N_{\kappa}^{(1)} = \nu^{(1)}/2(\kappa \eta_{\kappa})^2$, where $\nu^{(1)}$ is the first normal stress difference for steady flow at shear rate κ , and the coefficient \mathbb{C}' is about equal to the ratio \mathbb{C} of the principal components of the refractive index and stress ellipsoids:^{8,9}

$$\mathbb{C}' = \left(\frac{\cot 2\chi}{N_{\kappa}^{(1)} \eta_{\kappa} \kappa} \right) \mathbb{C} \approx \mathbb{C} \quad (13)$$

with χ the extinction angle locating the cross of isocline (the symbol S_{κ} was used to designate $N_{\kappa}^{(1)}$ in Ref. 1). As indicated in Eqn. 13, the term in parenthesis is expected to

be nearly unity. With Eqn. 12, the limiting value M_0 of M_κ for small κ is given by $M_0 R_0^{-1} \sim 2\mathbb{C}'$. With the stress-optic law, \mathbb{C}' is expected to be independent of polymer concentration or molecular weight for rodlike chains. For small κ , data on the limiting value of the flow birefringence $\Delta n^{(12)}$ in the 1-2 flow plane provide an alternative measure of \mathbb{C}' , with $\Delta n^{(12)}/\eta_0 \kappa \sim 2\mathbb{C}'$.

EXPERIMENTAL

Materials

Polymers PBT 53 and 43 are described in Ref. 1. Polymers PBT 72 and 72R are described in Ref. 10. The latter two represent examples of an otherwise common sample exposed to separate post-polymerization process histories. Sample 72R experienced several precipitation and redissolution cycles, whereas sample 72 was coagulated directly from the polymerization solution.

Methane sulfonic acid was distilled prior to use and stored away from contamination by atmospheric moisture. Polymers were dried *in vacuo* prior to use. Extreme caution was taken to prevent contamination of the solutions by moisture. Even modest amounts of water can lead to intermolecular association in acidic solution of heterocyclic polymers, with substantial effects on rheological properties.¹¹ Methods used here parallel those discussed in Ref. 1.

The wire-suspension cone-and-plate rheometer¹² and the flow birefringence apparatus described in Ref. 1 were used for most of the work reported here. A few data were also obtained with a Rheometrics model RMS 7200 rheometer, equipped with a Birnboim Correlator model DAS-IV, principally to permit estimation of the linear steady-state recoverable compliance. The apparatus was modified to retard the rate of contamination by moisture by use of the protective ring assembly described in Ref. 1 (e.g., see Fig. 1 of Ref. 1).

The temperature for the onset of the ordered nematic phase was determined by observation of the transmitted light with the sample between crossed polaroids in a microscope (approximately 100 x magnification). The sample was held in a special cell fabricated from rectangular glass tubing. (Vitro Dynamics, Inc., Rockaway, NJ). The sample thickness was 0.4 mm; use of cells ca. 0.02 mm thick produced a marked increase of the transition temperature, but no such effect was found for cells of the thickness used. The sample was sealed in the cell to prevent contamination by moisture. After a rapid temperature scan (ca. 0.01K s^{-1}) to provide an approximate estimate for the transition temperature, the temperature was adjusted to give a nematic sample about 5–10 degrees below the transition tem-

perature. After equilibration, the temperature was slowly increased by increments (ca. 1K), allowing the necessary time for equilibration between increments; equilibration times varied from ca. 10 min to several hours, depending on the viscosity. Stability of the anisotropic texture was taken as the criterion of equilibration. The transition temperature was taken as the temperature for the disappearance of the last nematic domains. After conversion to the isotropic state, the process was reversed, with slow cooling to confirm the transition temperature. The process is more difficult, and it is easy to obtain supercooling, by as much as 5K for viscous samples.

RESULTS

The systems studied are identified in Table 1. Values of η_0 , R_0 and $M_0 R_0^{-1}$ are given in Tables 2 and 3. Plots of η_κ/η_0 , R_κ/R_0 and M_κ/R_0 versus $\tau_c \kappa$ are given in Figs. 1 to 5. As seen in the latter figures, reduced plots are obtained at various temperatures in every case but one. The exception is for a solution of PBT-53, $c = 32.3 \text{ gKg}^{-1}$, at a temperature for which the solution has become nematic. This latter behavior is included for illustrative comparison only, and will not be considered further here; such behavior will be amplified in Section 2.

The reduced plots of η_κ/η_0 , R_κ/R_0 and M_κ/R_0 versus $\tau_c \kappa$ are each nearly independent of c for a given polymer for the available example. Moreover, the curves for η_κ/η_0 and R_κ/R_0 versus $\tau_c \kappa$ do not differ markedly among the samples studied. The most marked difference among the reduced curves is for M_κ/R_0 versus $\tau_c \kappa$ for the different samples. Possible reasons for this are discussed below.

Plots of $\ln \eta_0/\eta_s$ and $\ln w_c$ versus T^{-1} are given in Fig. 6. Here, w_c is the concentration for conversion from an isotropic state ($w \leq w_c$) at T to a nematic state ($w > w_c$) at T and η_s is the solvent viscosity. For methane sulfonic acid η_s is 7.67m Pa's at 313K and $\partial \ln \eta_s / \partial T^{-1} = 2800\text{K}$. As seen in Fig. 6, $\partial \ln(\eta_0/\eta_s) / \partial T^{-1} = 1265\text{K}$ for the isotropic samples studied. The data on w_c may also be fitted by an Arrhenius relation with $\partial \ln w_c / \partial T^{-1} = -433\text{K}$, and w_c/gkg^{-1} equal to 32.2, 32.3 and 34.9 at 313K for PBT 72, 53 and 43, respectively. With these results, $\partial \ln(\eta_0/\eta_s w_c^3) / \partial T^{-1} = 34\text{K}$ is nearly negligible, see below. The product $[\eta]w_c\rho$ is equal to 81, 67 and 47 for PBT 72, 53 and 43, respectively ($T = 313\text{K}$).

As with earlier reports¹³, $R_0 T$ is found to decrease with increasing w , and to be independent of T when w is well below w_c . However, as w_c is approached, $R_0 T$ increases with increasing w .

Data on $J_\sigma(t)$ are given in Fig. 7 for PBT 53 ($c = 25.5 \text{ gkg}^{-1}$). As with results reported elsewhere for flexible chain polymers,^{2,3} it appears that $J_\sigma(t) \sim J_0(t)$ for any stress for $t < t^*$ decreases with increasing σ . As with flexible chain polymers, the strain $\gamma^* = \gamma(t^*) = \sigma J_\sigma(t^*)$ is about independent of σ . Values of γ^* are discussed below.

The function $R_\sigma(t)$ is shown in Fig. 8 for PBT-53, $c = 29.4 \text{ gKg}^{-1}$. For small t , $R_\sigma(t)$ is independent of σ , but for large t , $R_\sigma(t)$ is decreased by increased σ . Similar behavior has been reported for flexible chain polymers.^{2,3}

Data on $\eta_\kappa(t)$ obtained here display a broad, shallow maximum with increasing κ at a time t^+ . It is found that t^+ decreases with increasing κ such that the strain $\gamma^+ = \kappa t^+$ is essentially independent of κ . Similar behavior is well known with linear polymers in the range of $\tau_c \kappa$ of interest here⁶. In every case, $\gamma^+ > \gamma^*$. Possibly, $\eta_\kappa(t) \approx \eta_0(t)$ for $\kappa t < \gamma^*$, similar to results reported¹⁴ for flexible chain polymers, but our data at small t are not sufficiently precise to be certain of this.

Data on $\hat{\eta}_\kappa(t)/\eta_\kappa$ and $\hat{M}_\kappa(t)/M_\kappa$ for two solutions at several temperatures are given in Fig. 9. The data are represented in reduced form versus t/β_κ , where the reduction factors β_κ are shown as a function of $\tau_\kappa = \eta_\kappa R_\kappa$ in the inserts. For each function, the reduced curves superpose over the range of κ studied. The rate of relaxation of $\hat{M}_\kappa(t)/M_\kappa$ is considerably less than that of $\hat{\eta}_\kappa(t)/\eta_\kappa$; similar behavior has been reported¹⁵ for flexible chain polymers.

Data on PBT-72R are included to demonstrate the dramatic effects of intermolecular association on the rheological behavior. This polymer, discussed in Ref. 10, is a form of PBT-72 in which (apparently) irreversible intermolecular association of the chains in (nearly) parallel array has been induced through the post-polymerization processing history. As might be expected with such aggregates, the aggregated species have significantly smaller η_0 for a given w and T .

DISCUSSION

Linear Viscoelastic Behavior

In the following we will consider a representation of the linear recoverable compliance $R_0(t)$ in terms of a discrete distribution of $n - 1$ retardation times. Together with η_0 and $\tau_c = \eta_0 R_0$, these will be converted to a discrete distribution of n relaxation times to facilitate computation of functions such as $\eta_0(t)$, $\hat{\eta}_0(t)$ and $\hat{M}_0(t)$. In the next section, the nonlinear creep compliance will be discussed in terms of a single-integral constitutive equation that permits computation of η_κ , $\eta_\kappa(t)$, $\hat{\eta}_\kappa(t)$, R_κ , $N_\kappa^{(1)}$, $N_\kappa^{(1)}(t)$ and $\hat{M}_\kappa(t)$ given the distribution of relaxation times. Finally, comparison of the behavior observed here with that given by mechanistic models will be considered.

In general, the linear creep compliance $J_0(t)$, equal to $R_0(t) + R_0 t/\tau_c$ (see Eqn. 6), can be represented in terms of a discrete set of $2n$ parameters including $\tau_c = \eta_0 R_0$ and $n - 1$ retardation times λ_i together with R_0 and $n - 1$ weight factors R_i , with

$$R_0(t) = R_0 - \sum_{i=1}^{n-1} R_i \exp - t/\lambda_i \quad (14)$$

where $\sum R_i \leq R_0$ ^{5,6}; the contributions comprising $R_0 - \sum R_i$ represent terms with retardation times much shorter than the experimental time scale. By the use of methods based on Eqn. 10, these $2n$ parameters may be converted to an alternative set of $2n$ parameters comprising n relaxation times τ_i and n weight factors η_i such that, for example,^{5,6}

$$\hat{\eta}_0(t) = \sum_{i=1}^n \eta_i \exp - t/\tau_i \quad (15)$$

where $\eta_0 = \sum \eta_i$ and $(\sum \eta_i \tau_i^{-1})^{-1} = R_0 - \sum R_i$. Values of λ_i/τ_c and R_i/R_0 computed for the data in Fig. 8 by use of "Procedure X"¹⁶ are given in Table 4, along with τ_i/τ_c and η_i/η_0 computed from R_0 , τ_c and the distribution of retardation times using a method described elsewhere.^{3,7} The functions $R_0(t)/R_0$ and $\hat{\eta}_0(t)/\eta_0$ computed with these are shown in Figs. 1 and 3. It would be difficult to extract the contribution with the longest relaxation time τ_1 by direct analysis of $\hat{\eta}_0(t)$ by, for example, use of Procedure X owing to experimental limitations at large t . In general, the reduced functions λ_i/τ_c , etc. are independent of temperature.

The linear viscoelastic data discussed above indicate that the distribution of retardation (or relaxation) times is broad. For example, for the average relaxation times $\tau^{(k)}$ defined by¹⁷

$$\tau^{(k)} = \sum' \eta_i \tau_i^{k-1} / \sum' \eta_i \tau_i^{k-2} \quad (16)$$

it is found that $\tau^{(2)}/\tau^{(1)} \sim 10$ for the data in Fig. 8. Here the primes indicate that the summation is limited to the "terminal" relaxation time regime (e.g., the n terms of interest here). In the terms used above $\tau^{(2)} \sim \tau_c$ and $\tau^{(1)} \sim \eta_0 (\sum \eta_i \tau_i^{-1})^{-1} = \eta_0 (R_0 - \sum R_i)$.

With the use of the 'stress-optic' relation discussed in the Introduction, $\hat{M}_0(t)$ is expected to fit the relation (with neglect of $\Delta n_{\kappa}^{(23)}$):

$$\hat{M}_0(t) = \lim_{\kappa \rightarrow 0} \hat{M}_{\kappa}(t) \sim 2 \mathbb{C}' \eta_0^{-2} \sum \eta_i \tau_i \exp - t/\tau_i \quad (17)$$

A plot of this function calculated with the η_i/η_0 and τ_i/τ_c given in Table 4 is included as the curve in Fig. 9; no data on $\hat{M}_0(t)$ are available for the solutions studied here, but an estimation of $\hat{M}_0(t)$ from data on $\hat{M}_{\kappa}(t)$ is considered below.

Following the methods discussed in Ref. 1, a plot of $\eta_0/\eta_s M[\eta] a^{*3}$ versus $cL/M_L a^*$ is given in Fig. 10. Here, $c = w\rho$, with the solution density ρ approximately equal to the solvent density ρ_s for the weight fraction w of polymer interest here, $M_L = M/L$ is the mass per unit contour length and a^* is an empirical parameter chosen to fit the experimental data by the relation

$$\eta_0/\eta_s = K N_A^2 M[\eta] a^{*3} X^3 (1 - BX)^{-2} \quad (18)$$

where $X = cL/M_L a^*$. The plot in Fig. 10 was constructed using the data on $[\eta]$, L_{η} and $M_{\eta} = L_{\eta} M_L$ given in Table 1. Data reported in Ref. 1 are included for comparison. The data are well fitted by Eqn. 18, with the values of $w^*/B = a^* M_L / L_{\eta} \rho B$ given in Table 5 and $KB^{-3} = 1.5 \times 10^{-4}$. These values are conveniently deduced by comparison of bilogarithmic plots of $\eta_0/\eta_s M_{\eta} [\eta]$ versus cL_{η}/M_L with a similar plot of $(BX)^3(1 - BX)^{-2}$ versus BX (Eqn. 18). If these have the same shape, then the vertical and horizontal 'shifts' required to superpose the curves are equal to $\log K N_A^2 (a^*/B)^3$ and $\log a^*/B$, respectively. As seen in Table 5, values of w_c and w^*B^{-1} are equal within experimental error. The correspondence

of w_c and w^*B^{-1} and the temperature dependence of w_c provides a basis for the observed negligible temperature dependence of $\eta_0/\eta_s w_c^3$ remarked above.

With Eqn. 18, the substantial disparity between values of η_0 for PBT 72 and 72R at a given c and T , is subsumed in the parameter w^*B^{-1} . Apparently, the suspected aggregation affects both η_0 and w_c .

Nonlinear Viscoelastic Behavior

In many ways the behavior observed here closely parallels that reported elsewhere^{2,3} for flexible chain polymers. In the latter study, a single-integral constitutive equation of the BKZ type¹⁸ was used to describe behavior for $J_\sigma(t)$, $\eta_\kappa(t)$, η_κ , R_κ , and $N_\kappa^{(1)}$. With $J_\sigma(t)$, it was found that $J_\sigma(t) \sim J_0(t)$ provided the total strain $\sigma J_\sigma(t)$ did not exceed a limiting value γ^* , independent of σ . In accord with many other studies,⁶ the strain $\gamma^+ = \kappa t$ for which $\partial \eta_\kappa(t)/\partial t$ is zero was found to be independent of κ . It was found that γ^+ did not depend strongly on polymer concentration over the range studied, but that $\gamma^* \propto c^{-1}$. As may be seen in Fig. 7, with the creep data on PBT solutions, it is also observed that $J_\sigma(t) \sim J_0(t)$ provided $\sigma J_\sigma(t) \leq \gamma^*$. Moreover, as shown in Fig. 11, $\gamma^* \propto c^{-1}$.

As with flexible chain polymers,³ the rheological behavior described above is accommodated by a BKZ-type single-integral equation which utilizes the linear viscoelastic modulus $G_0(t)$ and a strain function $F(|\gamma|)$ in the forms

$$G_0(t) = \frac{\partial \eta_0(t)}{\partial t} = \sum \eta_i \tau_i^{-1} \exp - t/\tau_i \quad (19)$$

$$F(|\gamma|) = \exp - m (|\gamma| - \gamma')/\gamma'' \quad (20)$$

where m is zero if $|\gamma| \leq \gamma'$ and unity otherwise. In terms of experimental parameters, $\gamma' = \gamma^*$ and $\gamma'' = \gamma^+$. With this relation the steady-state functions are represented by the expressions³

$$\eta_\kappa = \sum \eta_i (1 - q_{\kappa,i}) \quad (21)$$

$$\eta_0 \eta_\kappa R_\kappa = \sum \eta_i \tau_i (1 - q_{\kappa,i} r_{\kappa,i}) \quad (22)$$

$$\eta_\kappa^2 N_\kappa^{(1)} = \sum \eta_i \tau_i (1 - q_{\kappa,i} p_{\kappa,i}) \quad (23)$$

The functions $q_{\kappa,i}$, $r_{\kappa,i}$ and $p_{\kappa,i}$ which depend on $\kappa\tau_i/\gamma''$ and $\alpha = \gamma'/\gamma''$, are given in the Appendix, along with a relation for $\eta_\kappa(t)$, but it may be noted that $q_{\kappa,i}$ is zero for $\kappa\tau_i < 1$, and approaches unity with increasing κ for $\kappa\tau_i > 1$. To a good approximation, $q_{\kappa,i}$, $r_{\kappa,i}$ and $p_{\kappa,i}$ each depend on $\beta\kappa\tau_i$, where $\beta^{-1} = \gamma''f$ with $f^2 = 1 + \alpha - \alpha^2/2$; typically, $f \sim 1$. Comparison of Eqns. 21 - 22 with data on solution of PBT 53 ($c = 29.4 \text{ gKg}^{-1}$) are given in Fig. 8, using the values of τ_i and η_i in Table 4. The comparison is seen to be quite good, with the fits to Eqn. 21 and 22 giving $\beta^{-1} = 1.79$ (for $\alpha = 0.5$), in comparison with $\beta^{-1} = 2.5$ computed with the observed γ'/γ'' and γ'' , using $\gamma' = \gamma^*$ and $\gamma'' = \gamma^+$.

In general, η_κ is closely approximated by $[\eta_0(t)]_{\kappa t=1}$ such that³

$$\eta_\kappa \sim [\eta_0(t)]_{\kappa t=1} = \sum \eta_i (1 - \exp - 1/\kappa\tau_i) \quad (24)$$

and this approximation obtains with the data in Fig. 1 and 3 as well. Equation 24 reflects the approximation $q_{\kappa,i} \sim \exp - 2/5\beta\kappa\tau_i$ and $\beta^{-1} \sim 2.5$. Equations 21 - 24 show that the dependence of η_κ/η_0 and R_κ/R_0 on $\tau_c\kappa$ for the κ of interest here is closely controlled by the distribution of relaxation times obtained for a linear response. The data in Figs. 1-4 shows that η_κ/η_0 and R_κ/R_0 are similar for the several samples studied, but that distinct differences obtain among the samples, indicating differences in the distribution of relaxation times and/or the parameters γ' and γ'' in terms of Eqns. 21 - 22.

If Eqn. 12 is assumed, then data on M_κ/R_0 may be compared with $N_\kappa^{(1)}/R_0$ calculated with the single-integral constitutive relation. As shown in Fig. 5a, the data on M_κ/R_0 versus $\tau_c\kappa$ for solutions of PBT-53 at several concentrations and temperatures form a single curve that can be fitted reasonably well using the estimate $\beta^{-1} = 1.79$ mentioned above, and $M_0/R_0 \sim 3.8 \text{ MP}_a^{-1}$. The latter may be compared with the estimate $M_0/R_0 \sim 3 \text{ MP}_a^{-1}$ given in Table 3 based on data on $\Delta n^{(12)}$ at lower concentrations of PBT-53. Discrepancies at small $\tau_c\kappa$ in Fig. 5a may reflect experimental error in measuring small values of $\Delta n^{(13)}$. The data on M_κ/R_0 versus $\tau_c\kappa$ for PBT 72 and 72R are not too different from each other, but both lie below the data for PBT-53 for a given $\tau_c\kappa$, as do the data for PBT-43. Thus, the data for the latter three solutions indicate a more rapid decrease of M_κ with increasing $\tau_c\kappa$ than is observed with PBT-53. In terms of the proportionality $M_\kappa \propto N_\kappa^{(1)}$ of Eqn. 12, this corresponds to a broadened distribution of relaxation times for the

latter three in comparison with PBT-53. Since the data on R_κ/R_0 and η_κ/N_0 versus $\tau_c \kappa$ do not support the postulate of broadened distribution, one may conclude that additional factors are involved, possibly having to do with the state of interchain association believed to obtain with some of the solutions.

The data in Fig. 9 show that the relaxations $\hat{\eta}_\kappa(t)$ and $\hat{M}_\kappa(t)$ occur more rapidly with increasing κ , behavior also observed with flexible chain polymers. Moreover, the functions $\hat{\eta}_\kappa(t)/\eta_\kappa$ and $\hat{M}_\kappa(t)/M_\kappa$ can both be represented empirically in terms of a reduced time t/β_κ such that

$$\hat{\eta}_\kappa(t/\tau_c)/\eta_\kappa \sim \hat{\eta}_0(t/\beta_\kappa)/\eta_0 \quad (25)$$

$$\hat{M}_\kappa(t/\tau_c)/M_\kappa \sim \hat{M}_0(t/\beta_\kappa)/M_0 \quad (26)$$

According to Eqns. 25 and 26, bilogarithmic plots of $\hat{\eta}_\kappa(t)/\eta_\kappa$ and $\hat{M}_\kappa(t)/M_\kappa$ versus t/τ_c can each be superposed by 'shifts' along the $\log t/\tau_c$ axis that give $\log \beta_\kappa/\tau_c$. For the data in Figs. 10-11, $\beta_\kappa/\tau_c \sim (\tau_\kappa/\tau_c)^\nu$ with $\nu = 0.77$, where $\tau_\kappa = \eta_\kappa R_\kappa$.

In terms of the single-integral equation discussed above,

$$\hat{\eta}_\kappa(t) = \sum \eta_i (1 - q_{\kappa,i}) \exp - t/\tau_i \quad (27)$$

$$\eta_\kappa^2 \hat{N}_\kappa^{(1)}(t) = \sum \eta_i \tau_i (1 - q_{\kappa,i} p_{\kappa,i}) \exp - t/\tau_i \quad (28)$$

Thus, if

$$\hat{M}_\kappa(t) \sim 2 \mathbb{C} \hat{N}_\kappa^{(1)}(t) \quad (29)$$

then both the stress and birefringence relaxation can be predicted with the single-integral equation given data on η_i , τ_i and the nonlinear parameters γ' and γ'' . Although it is not apparent in their form, numerical calculations with Eqns. 27 and 28 show that Eqn. 25 and 26 are approximately obeyed, with $\beta_\kappa \approx \tau_\kappa$ for the τ_i -distributions obtained here. By comparison, with the empirical behavior β_κ is a little larger for a given τ_κ . Nevertheless, the similarity between the experimental result and that observed with Eqns. 27 - 29 is satisfactory, given the limited accuracy of the η_i , τ_i set and the approximate nature of the single-integral constitutive equation obtained with Eqn. 19. It does not seem feasible to

extract analytical approximations such as Eqns. 25 and 26 from Eqns. 27 - 29 given the approximate nature of the numerical comparisons. Nevertheless, with Eqns. 27 - 29, the enhanced relaxation rates with increased κ are attributed to the successive suppression of terms with long τ_i as κ increases, with the result that the remaining terms with shorter τ_i exhibit more rapid relaxation. For example, $q_{\kappa,i}$ is approximately given³ by the relation

$$1 - q_{\kappa,i} \sim (1 + |\beta \kappa \tau_i|^\epsilon)^{-2/\epsilon} \quad (30)$$

where ϵ depends weakly on a (e.g., $\epsilon \sim f^2$). With this approximation, use of Eqn. 27 gives the result

$$\frac{\partial}{\partial \kappa} \frac{\partial \hat{\eta}_\kappa(t)}{\partial t} \sim \beta \sum \eta_i \frac{(\beta \kappa \tau_i)^{\epsilon-1}}{[1 + |\beta \kappa \tau_i|^\epsilon]^{[(2+\epsilon)/\epsilon]}} \exp(-t/\tau_i) \quad (31)$$

which is positive for all t and κ . In effect, with Eqns. 25 and 26, τ_κ is an approximate measure of the effective relaxation time following steady state flow at shear rate κ . With Eqn. 22,

$$\tau_\kappa = \frac{\sum \eta_i \tau_i (1 - q_{\kappa,i} \exp - \tau_i / \tau_\kappa)}{\sum \eta_i} \quad (32)$$

so that τ_κ decreases with increasing κ .

The empirical behavior given by Eqns. 25 and 26 suggests that a set of pseudo-relaxation times and weights computed from pseudo-retardation times and weights obtained from $R_\sigma(t)$ for $\sigma = \eta_\kappa \kappa$ might be used to estimate $\hat{\eta}_\kappa(t)$ and $N_\kappa^{(1)}(t)$.

Molecular Aspects

The threshold volume fraction ϕ_c or concentration c_c for incipient separation of the ordered phase from the isotropic solution is expected to depend on chain length L and diameter d according to a relation of the forms¹⁹⁻²²

$$\phi_c = (6A/L_w) k_D f(L/d) \quad (33a)$$

$$c_c [\eta] \frac{\ln L / d}{L / d} = A(M_z/M_w)^{1/2} k_D f(L/d) \quad (33b)$$

where k_D is a polydispersity factor, equal to unity for a monodispersed polymer, $f(L/d) \sim 1$

for large L/d , A is a constant and $L_\eta \sim (L_z L_w)^{1/4}$. In expressing Eqn. 33b, use is made of the relation²³

$$M_L[\eta] = \pi N_A L_\eta^2 / 24 \ln(L_\eta/d) \quad (34)$$

and c_c is calculated from the threshold volume fraction ϕ_c as $c_c = \bar{v}_2 \phi_c$ where the partial specific volume \bar{v}_2 is equal to $\pi N_A d^2 / 4 M_L$; data in Ref. 10 give $d \sim 0.5$ nm for PBT. For monodispersed polymers, theories of Onsager¹⁹ and Flory²⁰ give A equal to 5/9 and 4/3, respectively. Calculations have been given for chains with a most probable²¹ and a gaussian distribution²² of L , with results, respectively, that can be represented by the expressions (for large L/d), $A(M_z/M_w)^{1/2} k_D \sim 6^{-1/2}$ and $A k_D \sim (4/3)(M_w/M_n)^{1/3}$. The experimental estimates of c_c may be higher than values given by Eqn. 33 owing to the limitations inherent in observing the onset of a birefringent phase. Experimental values of $c_c[\eta](d/L_\eta) \ln(L_\eta/d)$ obtained here (for $T = 313$ K), calculated with $d = 0.5$ nm, range from 0.9 to 1.1. Thus, the experimental values of c_c seem to be in a range predicted by theory given the molecular weight distribution that obtains²⁴ with PBT and related polymers.

The correlation of the data for $\eta_0(c, L)$ with Eqn. 18 appears to be satisfactory. Equation 18 was obtained by Doi^{25,26} using a model based on severe restrictions to rotational molecular motion owing to interchain (hard-core repulsive) interactions. The near correspondence of w^*/B with w_c is in accord with this model. The experimental estimate of $K \sim 1.5 \times 10^{-4}$ is far smaller than the original estimate $K \sim 1$ of Doi, but is in better accord with a numerical estimate of the rotational diffusion of a rod moving in a milieu of randomly distributed rods.²⁷ The considerable variation of $[\eta]$, η_0 and w_c between PBT 72 and 72R is attributed to interchain aggregation of the latter. Nevertheless, the dependence of the reduced parameter $\eta_0/M_\eta[\eta]$ on $cL_\eta/w^* \sim cL_\eta/w_c$ is found to be similar for the two polymers, indicating an approximate compensation for the effects of the aggregation on η_0 and w_c obtaining with PBT 72R.

The experimental values of $R_0 cRT/M_\eta$ are far larger than the value $R_0 cRT/M = 5/3$ given by the Doi and Edwards,²⁶ possibly owing to the effects of molecular weight distribution. The data on R_0 exhibit a previously reported effect¹³ R_0 decreases with increasing w for $w/w_c < 0.7$, then increases with increasing w . This behavior is predicted by a calculation of Marucci²⁸; the latter predicts that $R_0(t) \sim R_0$, which is not the behavior found here.

For small c , it is expected that^{1,29}

$$\lim_{c \rightarrow 0} \underline{C} = \underline{\delta}(\partial n / \partial c)M/RT \quad (35)$$

where $\underline{\delta}$ is the molecular anisotropy. For PBT in methane sulfonic acid $\underline{\delta} \sim 0.6$ and the refractive index increment $\partial n / \partial c \sim 0.55 \text{ mLg}^{-1}$.¹⁰ Consequently, with Eqn. 35 for small c , $M_0 R_0^{-1} \sim 6.9 \text{ MPa}^{-1}$ if M_η is used, in comparison with the experimental value of ca. 3 MPa^{-1} .

A constitutive equation obtained by Doi and Edwards²⁶ for isotropic solutions of rodlike chains based on a mechanistic model similar to that leading to Eqn. 18 leads to a particularly simple result for $G_0(t)$: one relaxation time (e.g., $\eta_1 = \eta_0$ and $\tau_1 = \tau_c$). The considerable disparity between this prediction and the behavior observed here may reflect the effects of molecular weight distribution. Alternatively, relaxation modes not included in the theoretical treatment may also contribute to $G_0(t)$. Possibilities for the latter may include the motions contributing to smaller K in Eqn. 18 than the theoretical expectation, or fluctuation in the local density of interchain interactions related to fluctuation in the local concentration.

The mechanistic treatment of Doi and Edwards leads to single-integral constitutive equation of the type employed here, with the exponential $G_0(t)$ and with $F(|\gamma|)$ that is fitted to within 10% by $(1 + \gamma^2/5)^{-1}$. For the calculations of interest here, Eqn. 20 provides a satisfactory fit to the theoretical estimate,³ provided $\gamma' = 0.6$ and $\gamma'' = 2.13$ (e.g., $\beta^{-1} = 2.38$). Consequently, Eqns. 21 - 23 provide close representation of the expressions that would be obtained with the theoretical single-integral constitutive equation if the latter is generalized to use the empirical η_i, τ_i set and the experimental values of γ' and γ'' . As shown in Figs. 1-5, the functions η_κ/η_0 , R_κ/R_0 and $M_\kappa/M_0 \sim N_\kappa^{(1)}/R_0$ computed with a single relaxation time and $\beta^{-1} = 2.38$ do not correspond to experiment. The theoretical constitutive equation discussed above employs the so-called "independent alignment approximation." For rodlike molecules, the results obtained with and without the use of this approximation are numerically quite similar for the functions of interest here.³⁰ Behavior similar to that embodied in Eqns. 21 - 23 are attributed to molecular weight heterogeneity in a mechanistic calculation.²⁸

As with moderately concentrated solutions of flexible-chain polymers,³ the observed $\gamma' \sim \gamma''$ exceed 0.6, and are proportional to c^{-1} , whereas the observed $\gamma'' \sim \gamma^+$ is not too far from 2.13, and does not depend on c . With flexible chain polymers we suggested that the discrepancy between γ' and 0.6 might be attributed to a looseness in the pseudo-entanglement network caused by the finite chain length of the polymers studied (e.g., $cM/\rho M_c \sim 10$, where M_c is the critical chain length for which $\partial \ln \eta_0 / \partial \ln cM$ changes from 1 to 3.4). A similar effect may be operative here such that γ' would approach 0.6 only if the rodlike chains were very long. In the latter case, however, with rodlike chains, an ordered state would develop, negating the comparisons being made here. Thus, with rodlike chains, the "universal" behavior may be unattainable.

Whereas molecular weight distribution may be a principal source of the distribution of τ_i noted above for the samples studied here, contributions to the distribution could also arise from the postulated looseness of the network constraints to which values of γ' larger than 0.6 are attributed. Thus, D_R , from which the relaxation time of the mechanistic model arises, is closely linked with the translational motion of a rodlike chain along its axis. Fluctuations in the distance over which this translation must occur might contribute to a distribution of τ_i , and such fluctuations could be enhanced if the chains are short, similar to the effect postulated for γ' .

As expected, the relaxations $\hat{\eta}_\kappa(t)$ and $\hat{N}_\kappa^{(1)}(t)$ are both much faster with the theoretical one-relaxation time model than is observed experimentally. With the theoretical model, $N_\kappa^{(1)}(t/\tau_c)/N_\kappa^{(1)}$ is independent of κ , whereas experimentally $N_\kappa^{(1)}(t/\beta_\kappa)/N_\kappa^{(1)}$ is essentially independent of κ , with $\beta_\kappa \sim \tau_\kappa \leq \tau_c$. In effect, τ_κ is a measure of the relaxation time for the deformed sample. With τ_κ given by Eqn. 32 and use of the approximation $1 - q_{\kappa,i} \approx \exp - 2/5 \beta_\kappa \tau_i$, one obtains

$$\tau_\kappa/\tau_c \approx 1 - \hat{N}_0^{(1)}(\tau_\kappa + 2(5\beta_\kappa)^{-1})/R_0 \quad (36)$$

where $\hat{N}_0^{(1)}(t)$ is given by the limit of Eqn. 28 for small κ . As κ is increased, τ_κ decreases owing to successive suppression of contributions from the largest τ_i .

Table 1: Polymer Solutions Used in This Study

Polymer	$[\eta]/\text{mLg}^{-1}$	L_{η}/nm^a	Range w/gkg ⁻¹	Range T/K
PBT 72	1770	135	25.4–29.4	297–331
PBT 72R	1100	100	29.6	296–331
PBT 53	1400	118	1.49–32.3	283–333
PBT 43	900	95	29.4–31.5	288–297

(a) $L_{\eta} = M_{\eta}/M_L$, where $M_L = 220 \text{ dalton nm}^{-1}$ and $M_{\eta} = ([\eta]/K_{\eta})^{1/1.8}$
 with $M_L^{1.8}K_{\eta} = 0.26 \text{ mLg}^{-1.10}$

Table 2: Rheological Parameters for Solutions of Rodlike Polymers

Polymer	w/gkg ⁻¹	T/K	$\eta_0 A^{-1}/\text{kPa}\cdot\text{s}^a$	$R_0 cRT/M_\eta^b$
72	25.4	328	3.94	83
	25.4	312	3.67	86
	25.4	297	3.77	85
	29.4	331	27.5	55
	29.4	312	31.3	61
72R	29.6	331	1.71	(37)
	29.6	312	1.99	(41)
	29.6	296	2.42	44
53	25.5	333	1.89	(60)
	25.5	313	1.83	(60)
	25.5	303	1.73	(62)
	25.5	296	2.10	64
	25.5	286	1.89	69
	28.0	333	6.81	57
	28.0	311	6.30	58
	28.0	293	5.81	(58)
	29.4	313	7.15	70
	29.4	296	7.64	78
	29.4	285	6.80	107
	31.7	333	13.2	85
	31.7	313	20.7	82
	32.3	333	4.83	102
	32.3	316	5.24	97
	32.3 ^c	294	4.54	99
	32.3 ^c	283	5.59	130
43 ^d	29.4	297	0.098	11.8
	29.4	288	0.093	14.0
	31.5	296	0.11	15.3
	31.5	291	0.12	17.2
	31.5	288	0.12	18.1

(a) $A = \exp E(T^{-1} - T_r^{-1})$ with $E = 4065\text{K}$ and $T_r = 297\text{K}$.

(b) R_0 in parenthesis calculated as τ_c/η_0 with τ_c determined from fit of η_κ/η_0 versus κ with curves of η_κ/η_0 versus $\tau_c\kappa$.

(c) Nematic solutions for $T \leq 303\text{K}$.

(d) R_0 determined as $\lim_{\omega \rightarrow 0} J'(\omega)$.

Table 3: Rheological and Rheo-optical Parameter Solutions of Rodlike Polymer (PBT-53)

w/gkg^{-1}	T/K	$\eta_0/\text{Pa}\cdot\text{s}$	$R_0\text{cRT}/\text{M}^a$	$M_0R_0^{-1}/\text{MPa}^{-1}{}^b$
1.49	297	0.145	14.6	3.03
2.10	297	0.340	13.6	2.72
2.80	297	0.580	15.0	3.02
3.50	297	0.780	14.8	--

(a) R_0 determined as $\lim_{\tau_c \omega=0} J'(\omega)$.

(b) $M_0R_0^{-1}$ was calculated as $\Delta n^{(12)}/\eta_\kappa \kappa$

for small κ .

Table 4: Retardation and Relaxation Spectra

λ_i/τ_c	R_i/R_0	τ_i/τ_c	η_i/η_0
PBT-53; $w = 29.4 \text{ gkg}^{-1}$			
2.580	0.580	3.251	0.231
0.210	0.280	0.494	0.480
0.0175	0.130	0.0615	0.197
		0.0010	0.092

PBT-53; $w = 25.5 \text{ gkg}^{-1}$			
5.248	0.430	5.732	0.094
1.022	0.290	1.354	0.258
0.240	0.174	0.381	0.253
0.080 ₅	0.035	0.098 ₈	0.084
		0.025 ₂	0.312

Table 5: Critical Concentrations for Solutions of Rodlike Polymers

Polymer	T/K	w_c/gkg^{-1} ^a	$w^*B^{-1}/\text{gkg}^{-1}$ ^b	Bw_c/w^*
PBT-72	296	29.7	27.5	1.08
	313	32.2	28.9	1.11
	333	34.9	30.4	1.15
PBT-72R	296	--	36.5	
	313	--	38.3	
	333	--	40.3	
PBT-53	296	29.9	31.5	0.95
	313	31.7	32.9	0.96
	333	34.9	34.9	1.00
PBT-43	296	32.2	38.8	0.83
	313	34.9	40.7	0.86
	333	37.9	42.9	0.88

- (a) The concentration for formation of the ordered phases interpolated using the relation $w_c = k \exp - 433/T$, with k equal to 128.4, 128.8 and 139.2 for PBT 72, 53, and 43, respectively.
- (b) Obtained by a fit of Eqn. 18 with data on η_0 , as described in the text.

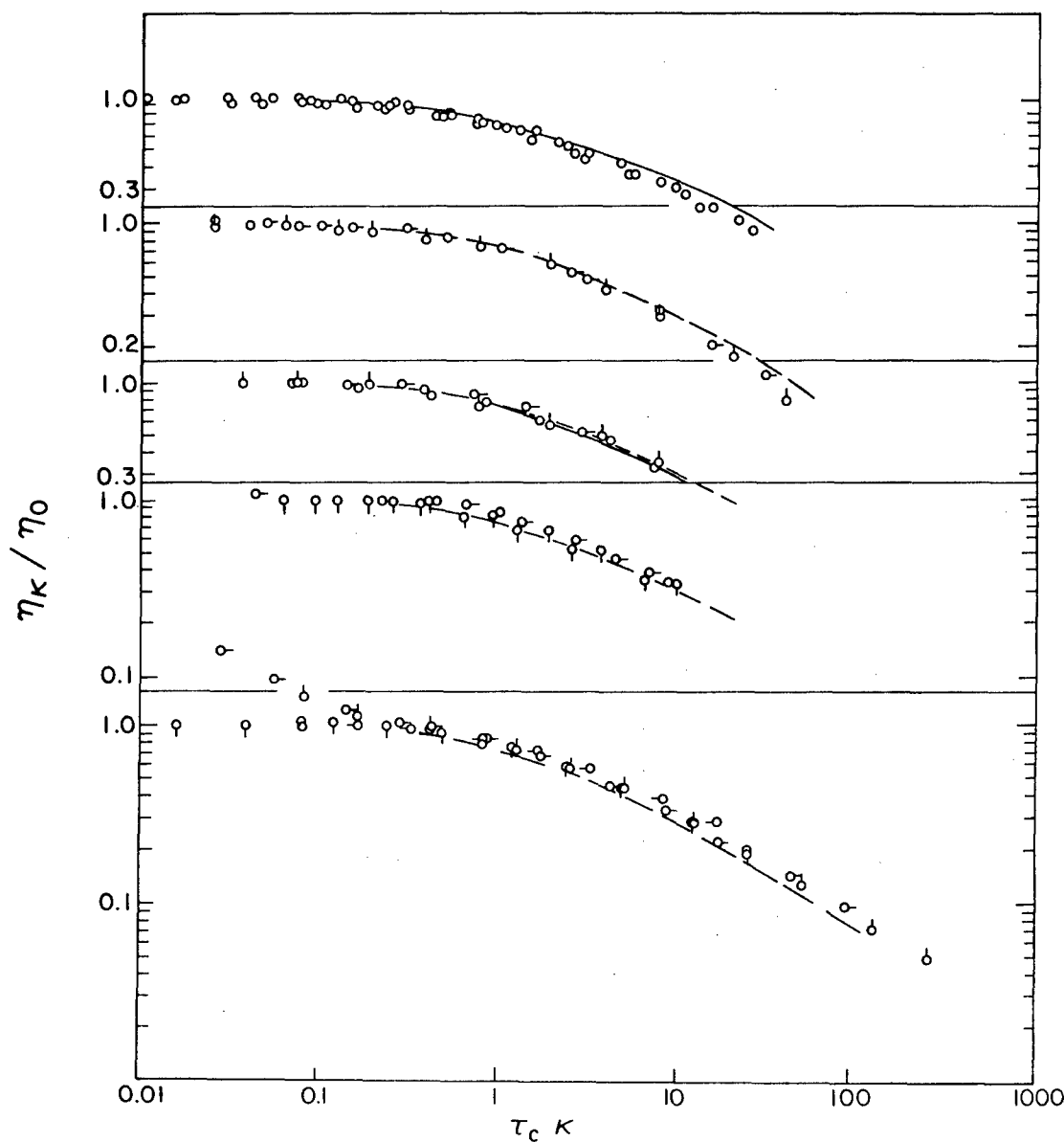


Figure 1:
The reduced steady-state viscosity η_K/η_0 versus the reduced shear rate $\tau_c K$ for solutions of PBT-53 in methanesulfonic acid. From top to bottom: 25.5 g kg⁻¹ (O, □, O, □, O for 12.5, 23, 30, 40, 60 C, resp.); 28.0 g kg⁻¹ (O, □ for 38, 60, resp.); 29.4 g kg⁻¹ (O, □, O for 12, 21, 40 C, resp.); 31.7 g kg⁻¹ (O, □ for 40, 60 C, resp.); and 32.3 g kg⁻¹ (□, 19, 43, 60 C for O, O, O, O, resp.). The solid curves represent Eqn. 21 using the η_i and τ_i in Table 4. The dashed curves represent the data for the solution with $w = 25.5$ g kg⁻¹ to facilitate comparison of the data at various w .

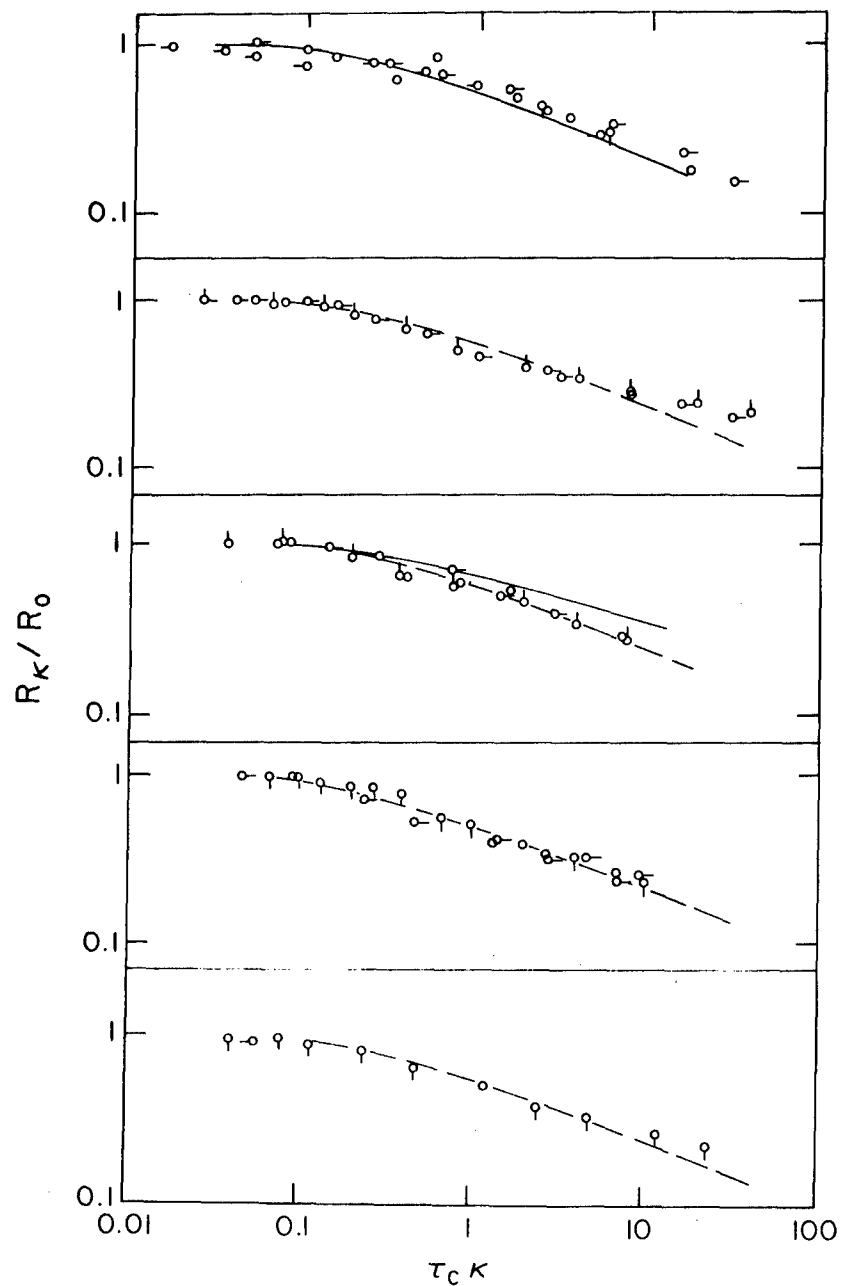


Figure 2:
The reduced steady-state recoverable compliance R_K/R_0 versus the reduced shear rate $\tau_c K$ for the solutions identified in the caption to Fig. 1. The solid curves represent Eqn. 22 using the η_i and τ_i in Table 4. The dashed curves represent the data for the solution with $c = 25.5 \text{ gkg}^{-1}$ to facilitate comparison of the data at various w .

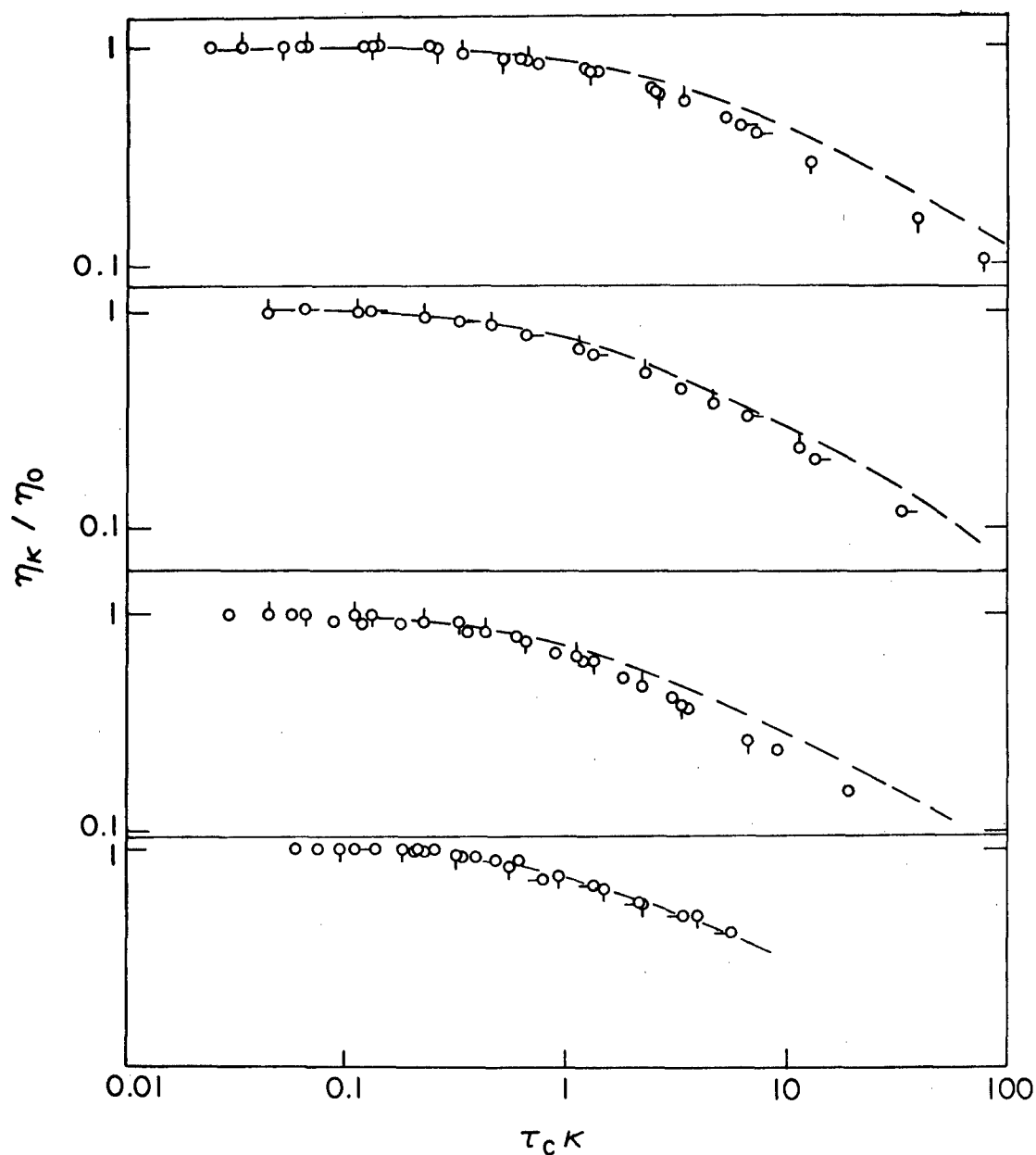


Figure 3:

The reduced steady-state viscosity η_K / η_0 versus the reduced shear rate $\tau_c K$ for solutions of PBT polymers in methanesulfonic acid. From top to bottom: PBT-72, 25.4 gkg⁻¹ (O, O-
O for 24, 39, 55 C, resp.); PBT-72, 29.4 gkg⁻¹ (O, O for 39, 58 C, resp.); PBT-72-R, 29.6 gkg⁻¹ (O, O, O for 23, 39, 58 C); PBT-43, 31.5 gkg⁻¹ (O, O, O for 10, 14.5, 18, 23.5 C, resp.). The dashed curves represent the data for PBT-53, $c = 25.5$ gkg⁻¹.

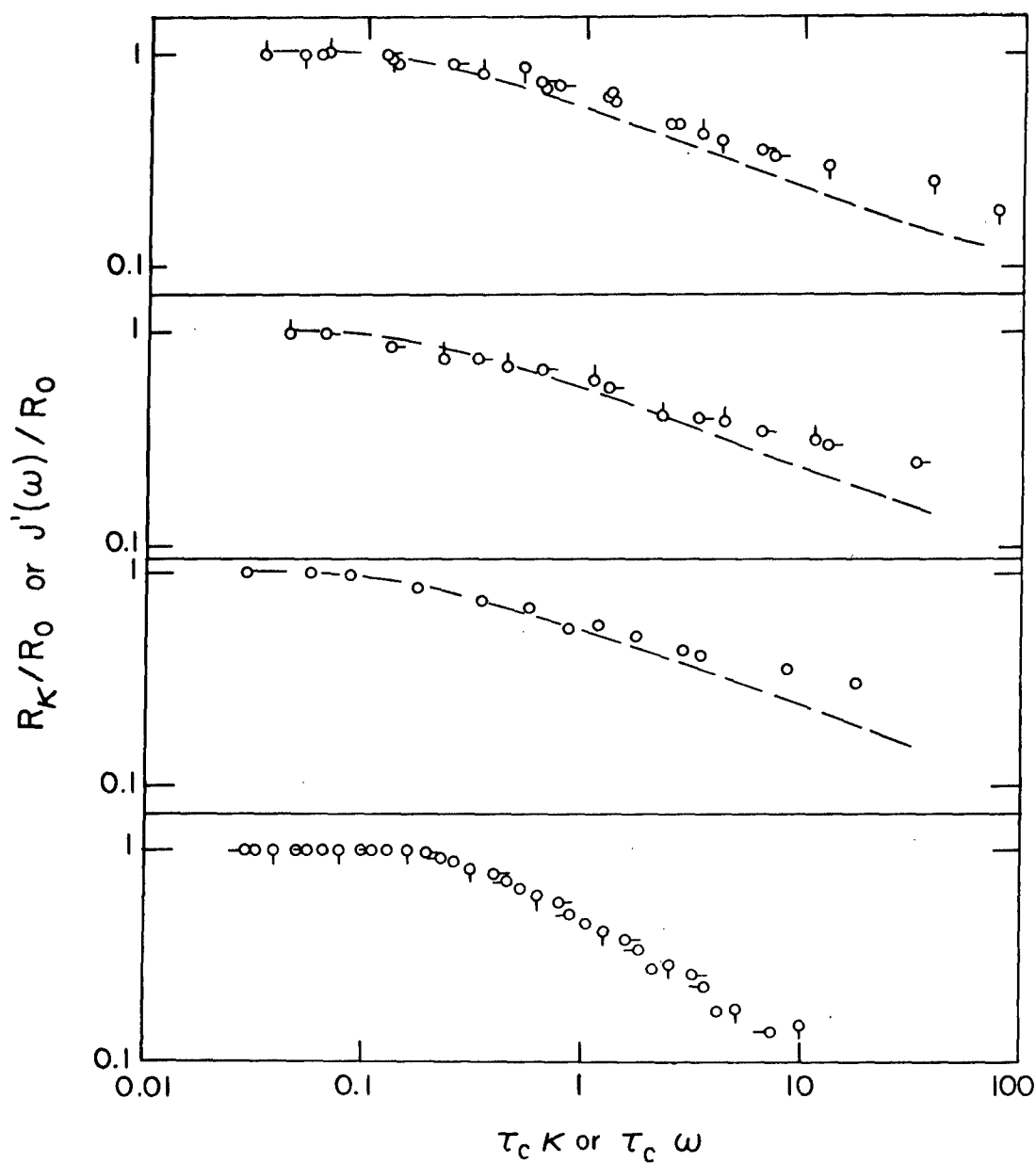


Figure 4:

The upper three panels give the reduced steady-state recoverable compliance R_K/R_0 versus the reduced shear rate $\tau_c K$; the lowest panel gives the reduced dynamic compliance $J'(\omega)/R_0$ versus the reduced frequency $\tau_c \omega$. The data are for the solution in the corresponding panels identified in the caption to Fig. 3. The dashed curves represent the data for PBT-53, $w = 25.5 \text{ g/kg}$.

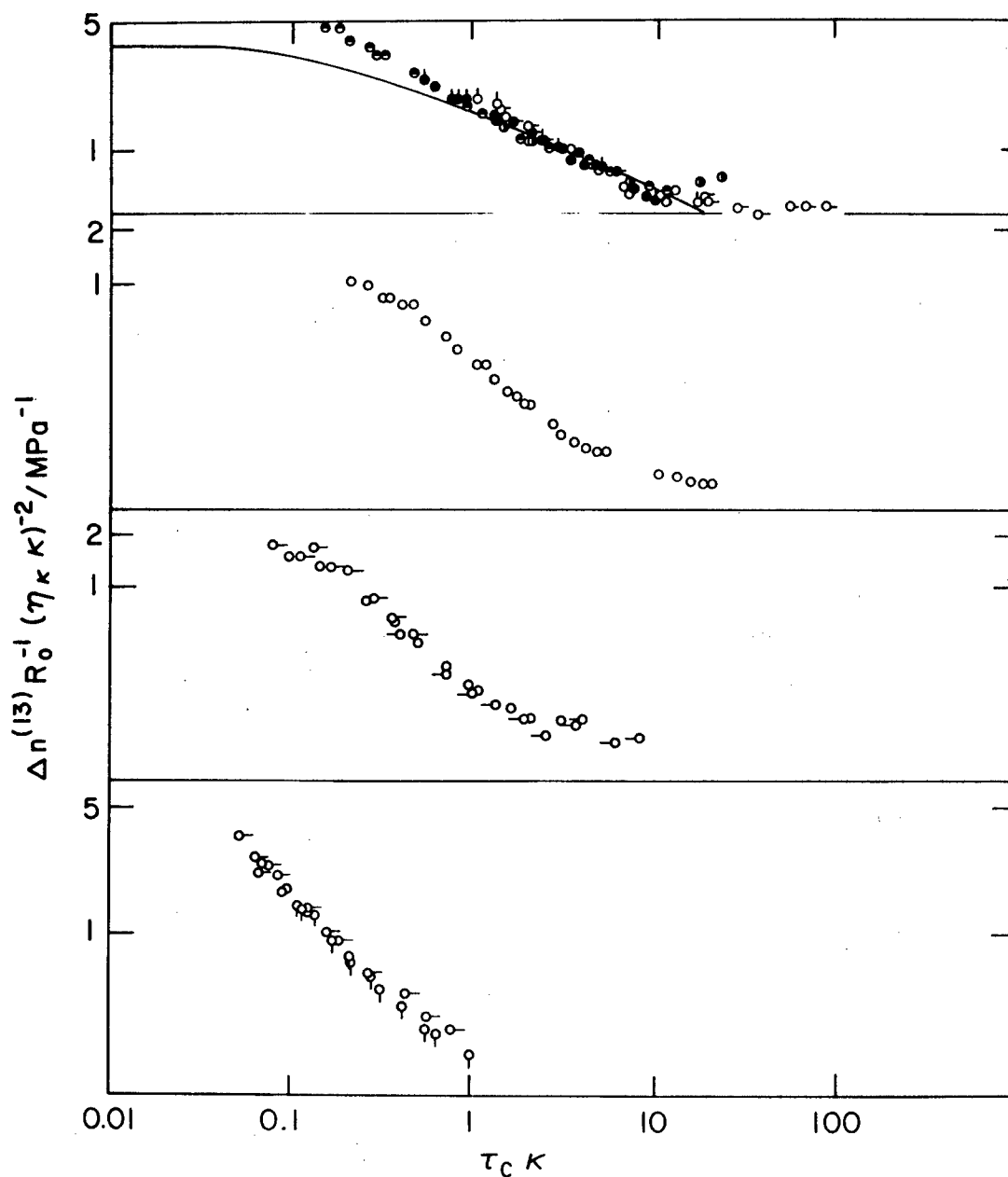


Figure 5:

The flow birefringence function versus the reduced shear rate $\tau_c \kappa$ for solution of PBT in methane sulfonic acid. From top to bottom: PBT-53, 25.5 gkg^{-1} , (\bullet , \blacklozenge for 23, 40 C, resp.), 28.0 gkg^{-1} (\circ , 60 C), 29.4 gkg^{-1} (\circ , \circ for 23, 40 C, resp.), 31.7 gkg^{-1} (\oplus , 40 C); PBT-72, 25.4 gkg^{-1} (\circ , \circ for 39, 55 C, resp.); PBT-72R, 29.6 gkg^{-1} (\circ , \circ , \circ for 23, 39 and 60 C, resp.); and PBT-43 (31.5 gkg^{-1} , \circ , \circ for 15, 23 C, resp.). The solid curve represents Eqn. 12 with Eqn. 28 using the η_i and τ_i in Table 4.

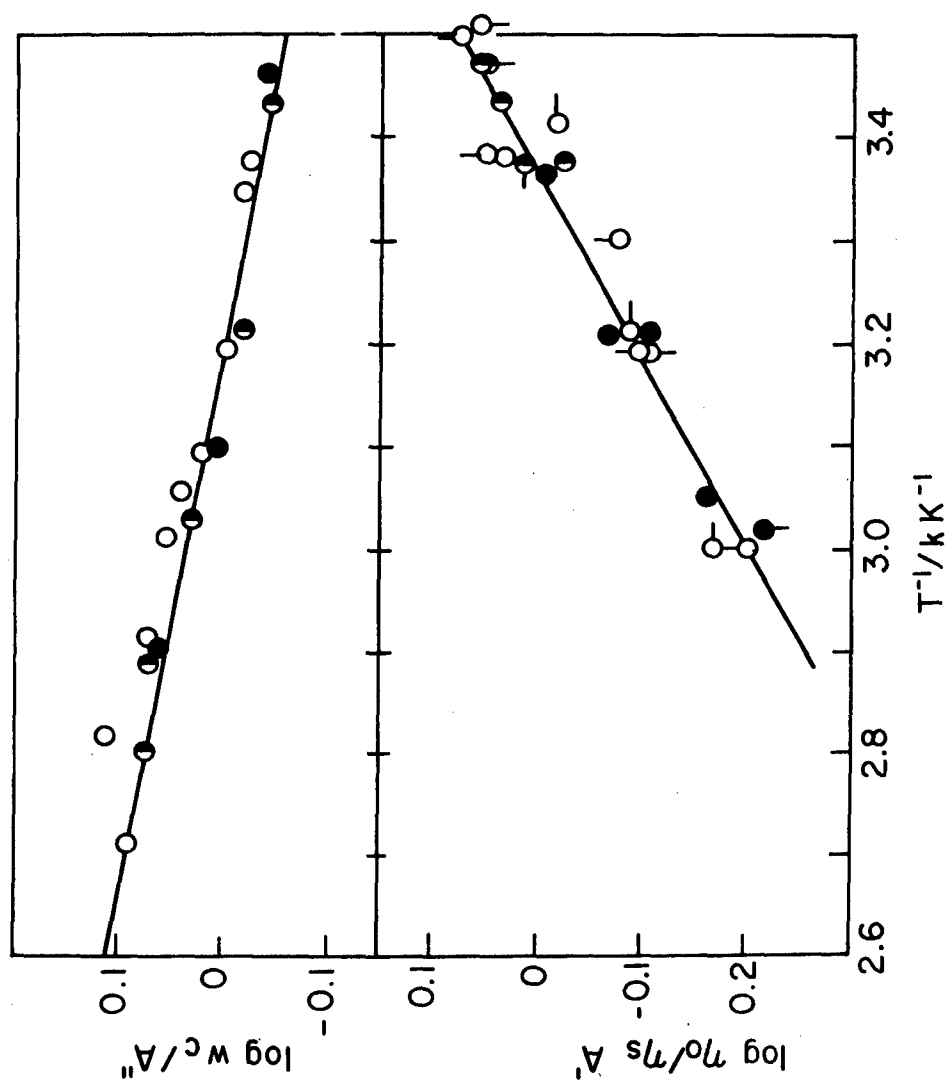


Figure 6: Temperature dependence of the viscosity η_0 relative to that η_s of methane sulfonic acid, and the concentration w_c for the onset of the nematic phase. In the figures, A' and A'' are the values of η_0/η_s and w_c , respectively, for $T = 313K$. The symbols denote PBT-53, \circ ; PBT-72, \bullet and PBT-43, \odot .

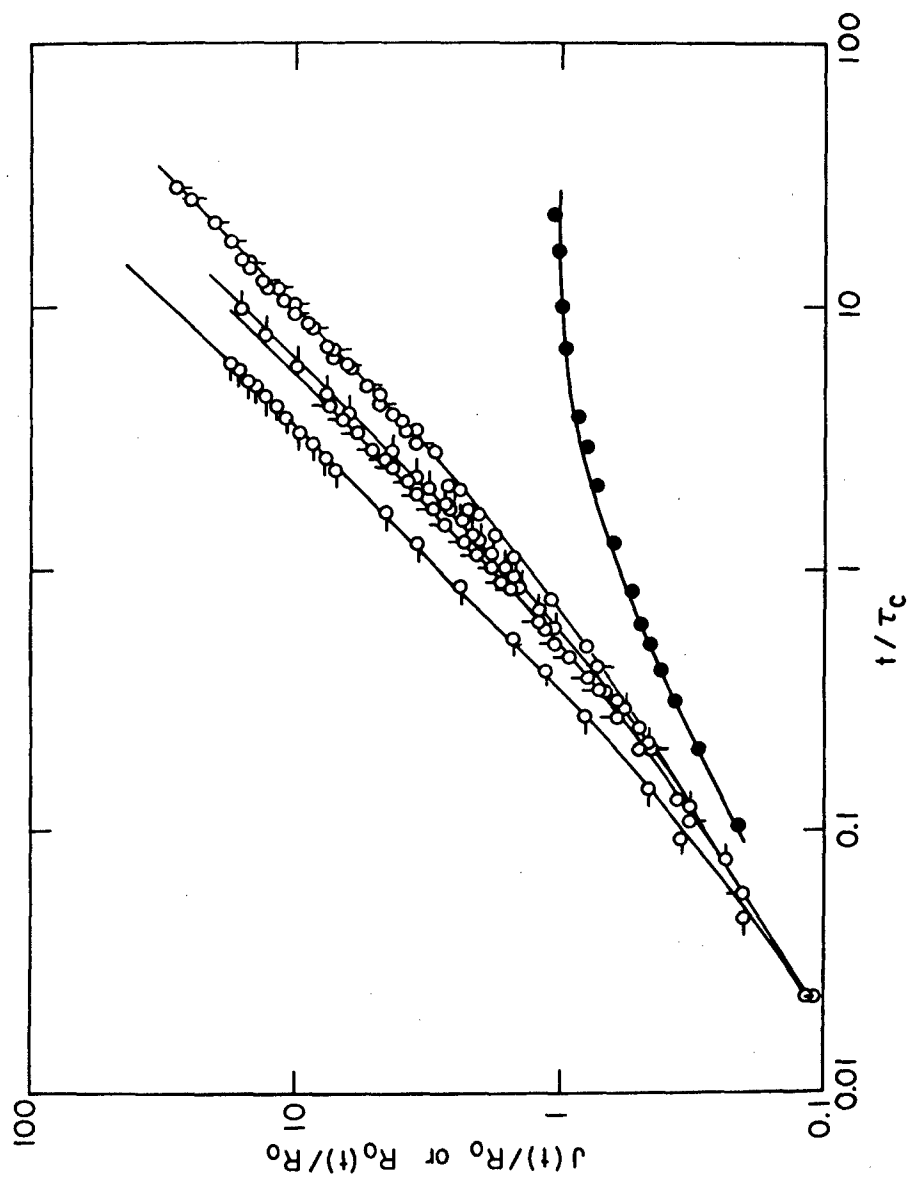


Figure 7:

The reduced creep compliance $J(t)/R_0$ (open circles) and recoverable compliance $R_0(t)/R_0$ (filled circles) versus the reduced time t/τ_c for a solution of PBT-53 in methane sulfonic acid, $w = 25.5 \text{ g/kg}$. The symbols $O(\bullet)$, Q , $O-$, $O-$ denote stress σ/Pa equal to 28, 15.2, 68.3, 78.7 and 145, resp. The data for $O(\bullet)$ are at 23 C; all others at 13 C.

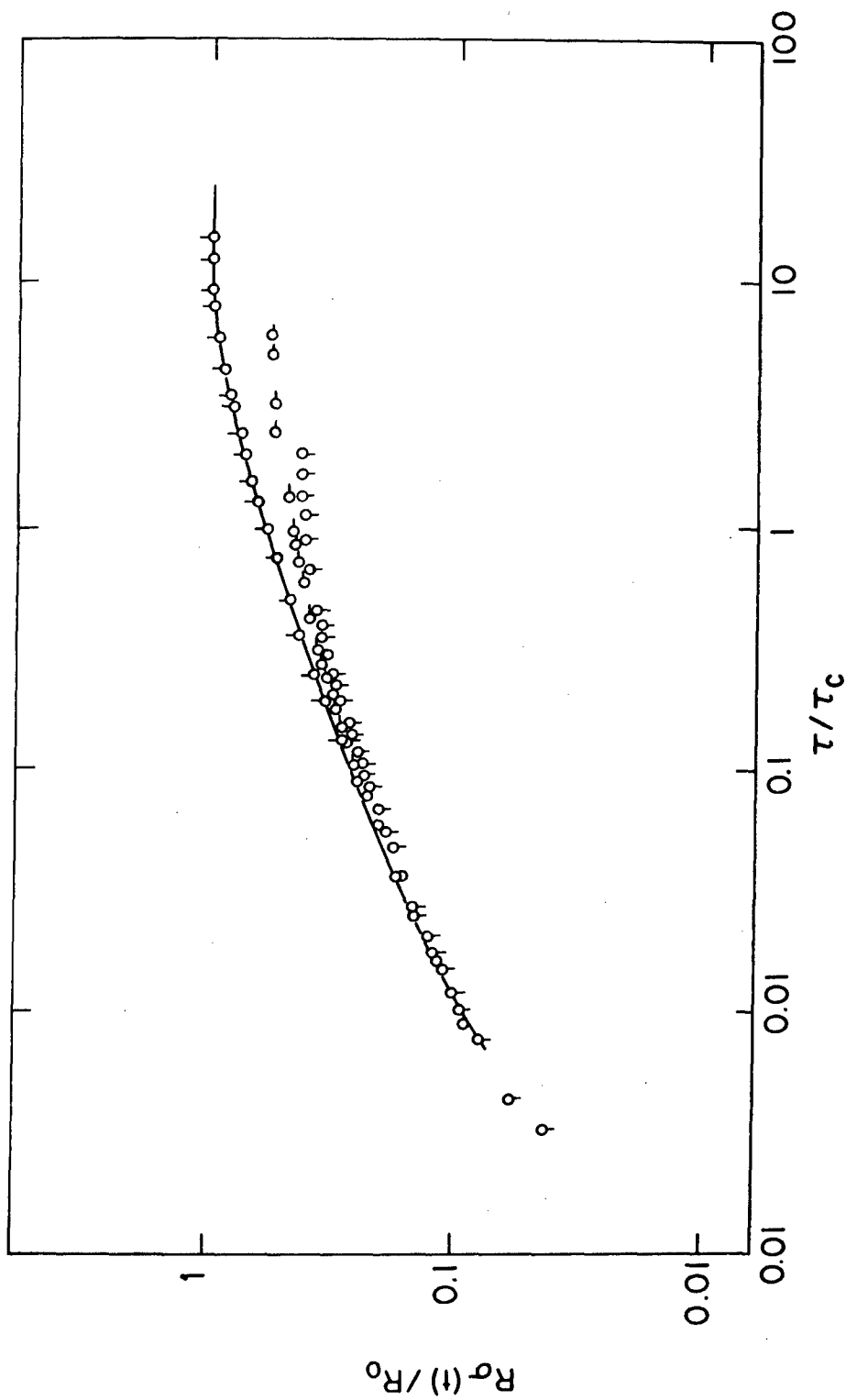


Figure 8: The reduced recoverable compliance function $R(t)/R_0$ versus the reduced time t/τ_c for a solution of PBT-53 in methane sulfonic acid, $W = 29.4 \text{ g/kg}$. The stress σ/Pa is 6.6 (○), 39.3 (□) and 57.5 (□) with $T = 40^\circ$, 20° and 40°C , respectively. The curve represents Eqn 14 with the R_0 and λ given in Table 4.

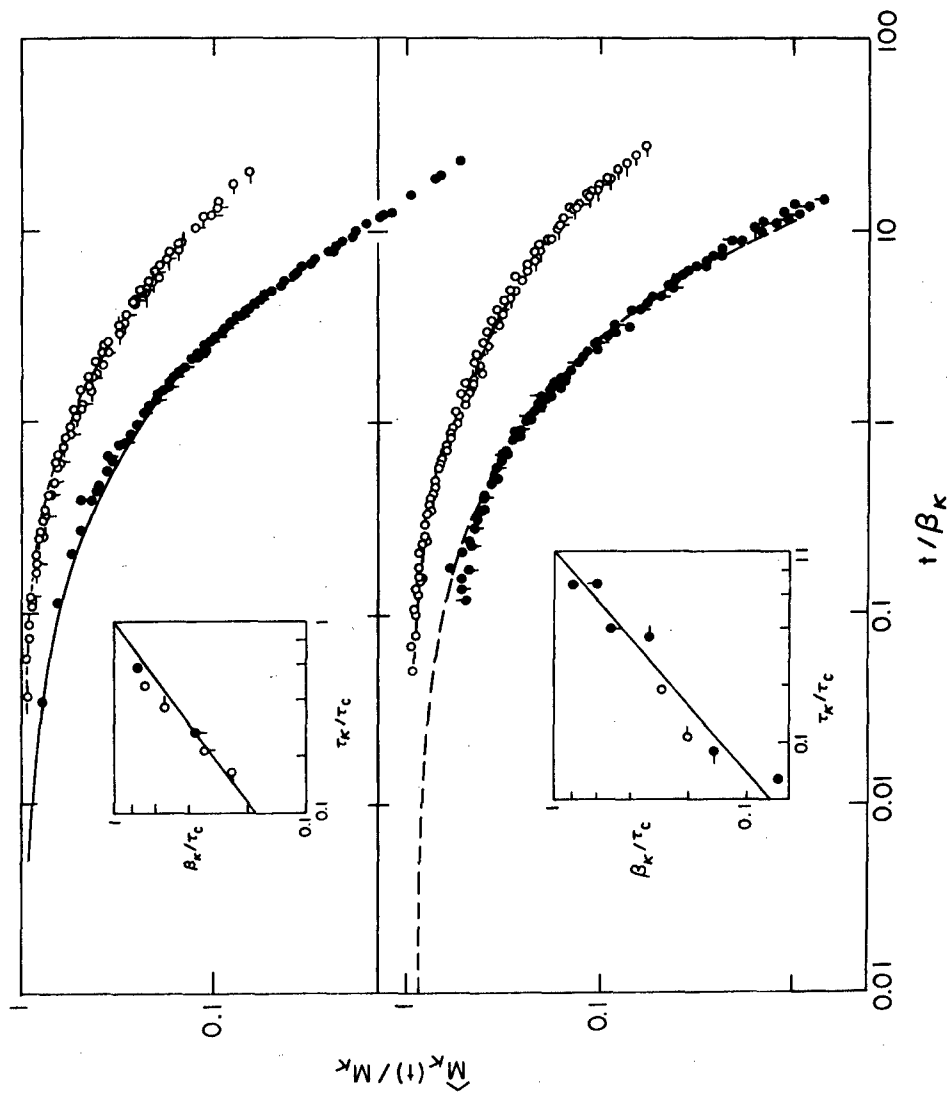


Figure 9:

The reduced flow birefringence relaxation function $\hat{M}_\kappa(t)/M_\kappa$ (filled circle) and stress relaxation function $\hat{\eta}_\kappa(t)/\eta_\kappa$ (open circle) for PBT-72, 25.4 g kg^{-1} (top) and PBT-53, 29.4 g kg^{-1} (bottom) in methane sulfonic acid. For PBT-72, κ/s is 0.0208 (O), 0.0358 (O-), 0.0726 (Q), 0.100 (-O), 0.0126 (●), 0.0502 (●), all at 39°C . For PBT-53, κ/s is 0.0227 (O), 0.0455 (O-), 0.0851 (Q), 0.186 (-O), 0.0050 (●), 0.0126 (●), 0.0502 (●), all at 21°C , and 0.0050 (●), 0.0252 (●), both at 40°C .

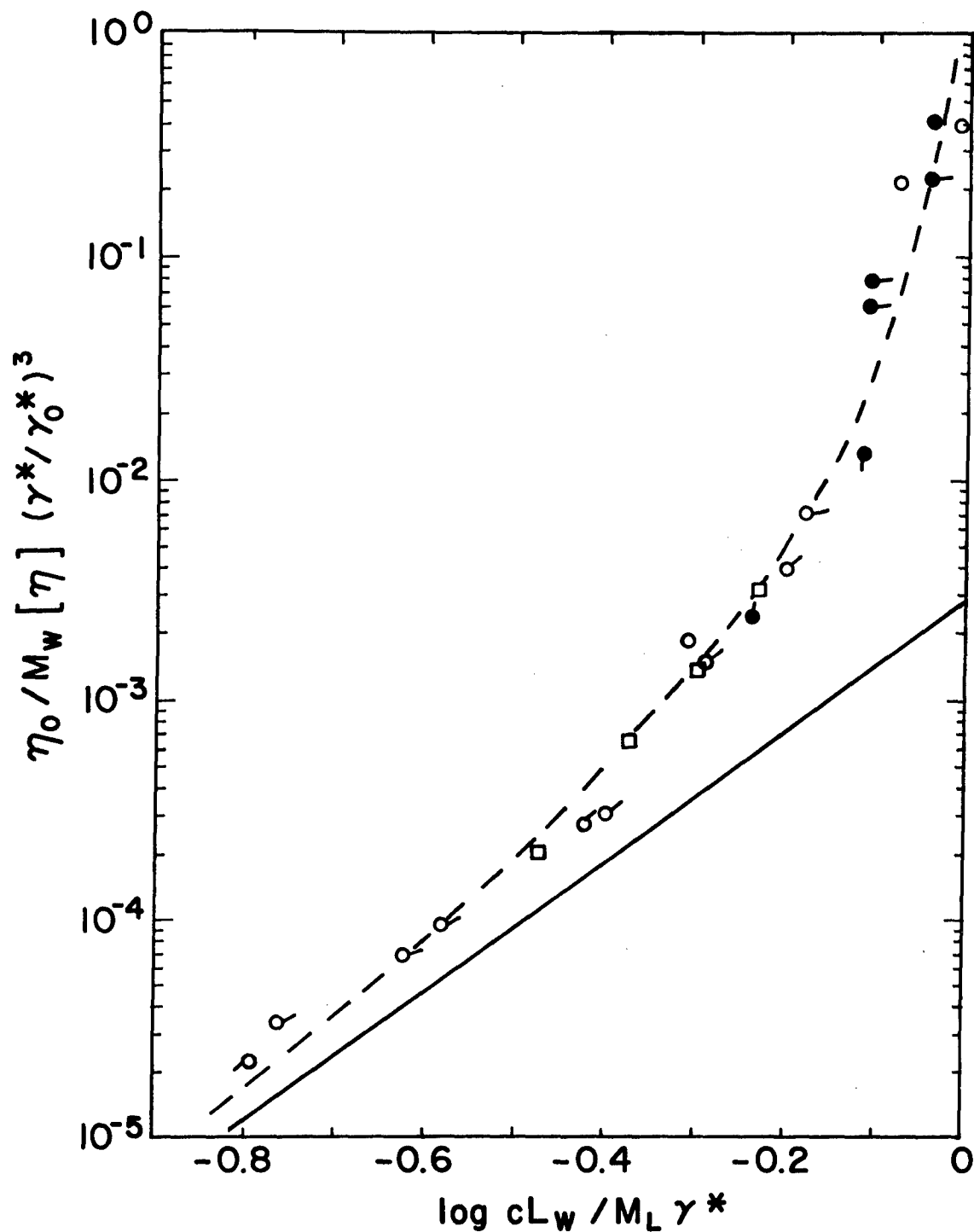


Figure 10:
The viscosity for solutions of several rodlike polymers over a range of concentration and chain length. Here a^* and $A = KN(1-B)^{-2}$ are empirical parameters obtained by comparison with Eqn. 18 as described in the text. The symbols designate the rodlike polymer/solvent system as given in the caption to Figure 9 in reference 1.

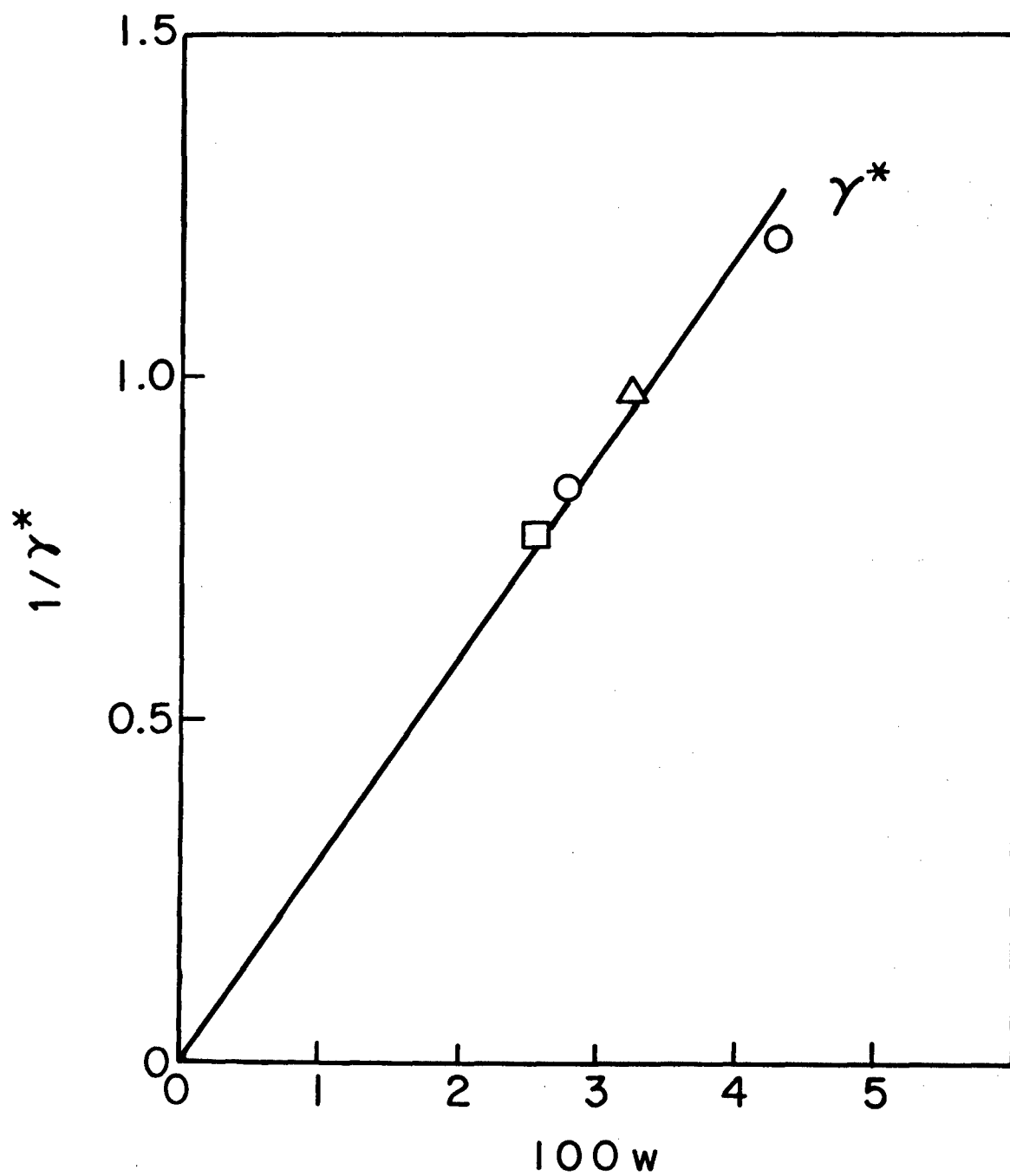


Figure 11:
The reciprocal of the critical strain γ^* versus weight percent $100w$ for several PBT-53 solutions in MSA.

2. TRANSIENT AND STEADY-STATE RHEOLOGICAL STUDIES ON NEMATIC SOLUTIONS OF RODLIKE POLYMERS

SUMMARY

Rheological studies are reported on nematic solutions of the rodlike macroion poly(14-phenylene-2,6-benzobisthiazole), PBT. The data reported include the steady-state viscosity η_κ and recoverable compliance R_κ as functions of the shear rate κ , the creep compliance $J_\sigma(t)$ and the recoverable compliance $R_\sigma(t)$ determined with shear stress σ , and the viscosity growth function $\eta_\kappa(t)$ determined with shear rate κ . The nematic solutions did not exhibit true linear viscoelastic behavior in the range studied ($\sigma \geq 14$ Pa and $\kappa \geq 10^{-4} \text{S}^{-1}$). Neither was any "yield behavior" observed over this range. The steady-state parameters are discussed in terms of a single-integral constitutive equation of the BKZ-type in which the relaxation times are estimated from data on $R_\sigma(t)$ at small σ .

INTRODUCTION

In Ref. 1 and the preceding chapter of this report, the rheological and rheo-optical properties of mesogenic solutions of rodlike macrions are reported for conditions of concentration, rod length and temperature for which the solutions are optically isotropic. Steady-state and transient properties are reported previously, and discussed in terms of a single-integral constitutive equation and molecular theories. Here, some steady-state and transient rheological properties will be presented for nematic solutions of two samples of one of the polymers studied previously, namely, poly(1,4-phenylene-2,6-benzobisthiazole), PBT. The data to be reported include the steady-state viscosity η_κ and recoverable compliance R_κ as functions of the shear rate κ , the creep compliance $J_\sigma(t)$ and recoverable compliance $R_\sigma(t)$ determined with shear stress σ , and the viscosity growth function $\eta_\kappa(t)$ determined with shear rate κ .

The transient function (i.e., $J_\sigma(t)$, $R_\sigma(t)$ and $\eta_\kappa(t)$) are defined in the preceding. There, the limiting values $R_0(t)$ of $R_\sigma(t)$ at small σ , and $\eta_0(t)$ of $\eta_\kappa(t)$ at small κ were expressed in terms of retardation and relaxation times, respectively, as⁶ by equations 14 and

$$\eta_0(t) = \eta_0 - \sum_1^n \eta_i \exp - t/\tau_i \quad (37)$$

where, of course, the set of η_i and τ_i may be determined from the set of R_i and λ_i together with R_0 and $\tau_c = R_0 \eta_0$, and vice versa. Previously, it was found that a single-integral relation for the shear stress $\sigma(t)$ given by³

$$\sigma(t) = \sum \eta_i \tau_i^{-2} \int_0^{\infty} \Delta \gamma(t,u) F[\Delta \gamma(t,u)] \exp(-u/\tau_i) du \quad (38)$$

could be used to predict η_κ and R_κ . Here $\Delta \gamma(t,u) = \gamma(t) - \gamma(t-u)$ and $F(\gamma)$ is given by the expression

$$F(\gamma) = \exp[-m(|\gamma| - \gamma')/\gamma''] \quad (39)$$

where m is zero for $|\gamma| < \gamma'$ and unity otherwise, with γ' and γ'' material parameters. Of course, if $F(\gamma)$ is unity (i.e., $|\gamma| < \gamma'$, then Eqn. (38) reduces to the result for the linear Boltzmann constitutive equation. With Eqns. (38 - 39)³, by Eqns. 21 and

$$\eta_0 \eta_\kappa R_\kappa \approx \sum \eta_i \tau_i (1 - q_{\kappa,i} \exp(-\eta_\kappa R_\kappa / \tau_i)) \quad (40)$$

where

$$q_{\kappa,i} = (1 + a f_i^2 - f_i) \exp(-g_i) \quad (41)$$

with $f_i^{-1} = 1 + a g_i^{-1}$, $g_i = \gamma' / \tau_{i,\kappa}$ and $a = \gamma' / \gamma''$. These relations provided satisfactory fits to data on η_κ and R_κ , given experimental data on η_i and τ_i for the isotropic solutions. Based on studies² of $J_\sigma(t)$, γ' was found to be inversely proportional to c . Mechanistic models with results similar to Eqns. 38 - 39 are discussed in the Chapter 1. These differ from experiment principally in predicting a far narrower distribution of τ_i (or λ_i) than found in our studies.

For the data in Chapter 1, the dependence of η_0 on c and the rodlength L was given by equation 18.¹ Of the latter, B is expected to be nearly unity,²⁵ $a^* M_L / L$ is expected to be nearly equal to the concentration c_c required to form a nematic phase, and the original calculation²⁵ gave $K \sim 1$. With the data reported in Chapter 1, the former two predictions are verified, but $K \approx 1.5 \times 10^{-4}$, in better agreement with revised estimates²⁷.

EXPERIMENTAL

The materials and methods used are described fully in References 1 and 2. The polymers used in this study are listed in Table 6. Sample PBT-53 was studied in solution in methanesulfonic acid (MSA), and PBT-62 was studied in solution in MSA containing 3 weight percent chlorosulfonic acid. The range of the weight fraction w and temperature T spanned in the studies is given in Table 6, and shown schematically in Figs. 12 and 13. With PBT-62, only steady-state data were obtained, e.g., η_κ and R_κ . With PBT-53, in addition to the steady-state data, experiments included $J_\sigma(t)$, $R_\sigma(t)$ and $\eta_\kappa(t)$.

RESULTS

The systematic effects observed on η_κ and R_κ are illustrated in Figs. 14 and 15, respectively, for several concentrations of PBT-62 for $T \approx 60^\circ\text{C}$ and for a solution of PBT-53 for $T \approx 23^\circ\text{C}$. The limiting values η_0 and R_0 obtained for η_κ and R_κ , respectively, at small κ are listed in Table 7.

As seen in Figs. 14 and 15, in some cases η_κ did not go to a limiting value at small κ with the nematic solutions--this feature is discussed further in the next section. In such cases, R_κ did tend to a constant value R_0 at small κ , and usually a range of κ existed for which η_κ was essentially a constant, designated η_P . Values of R_0 and η_P are entered in Table 7 for the nematic fluids.

The data on η_0 are reduced to 24°C using $\partial \ln \eta / \partial T^{-1}$ given in Chapter 1. For the isotropic solution, $\partial \ln \eta / \partial T^{-1}$ is about equal to $\partial \ln \eta_s w_c^3 / \partial T^{-1}$, as expected with Eqn. 18, where w_c is the concentration required to form a stable nematic phase. For the nematic solution, $\partial \ln \eta / \partial T^{-1}$ is smaller, and more nearly equal to $\partial \ln \eta_s / \partial T^{-1}$. Consequently, data on η_P are reduced to 24°C using $\partial \ln \eta_s / \partial T^{-1}$.

Additional data on η_κ and R_κ for PBT-62 and data for PBT-53 are given in Figs. 16 - 22, in plots of the reduced functions η_κ / η_0 (or η_κ / η_P) and R_κ / R_0 versus $\eta_0 R_0 \kappa$ (or $\eta_P R_0 \kappa$). Except for data on nematic solutions with $\eta_P R_0 \kappa < 1$, these plots are independent of T for a given concentration.

Data on $J_\sigma(t)$ versus t are given in Fig. 23 for a nematic solution of PBT-53 ($w = 0.0323$ at 19°C). The behavior is similar to that reported for an isotropic solution of PBT-53 (w

= 0.0255 at 30°C) discussed in Chapter 1. As with the latter, $J_\sigma(t)$ is found to equal the limiting behavior $J_0(t)$ for small σ provided the strain $\gamma(t) = \sigma J_\sigma(t)$ is less than a critical value γ^* , as indicated on Fig. 12. The recoverable compliance function $R_\sigma(t)$ obtained following steady-state deformation is also shown in Fig. 23 for one shear stress ($\sigma = 14.6$ Pa).

Data on $\sigma(t)$ as a function of the strain κt in a stress growth experiment are given in Figs. 24 and 25. In these experiments κ is constant for κt greater than about 0.3, but owing to instrumental limitations, $\gamma(t) \leq \kappa t$ for smaller κt . The data reveal a maximum in $\sigma(t)$ with increasing t such that $\partial\sigma(t)/\partial t$ is zero for κt equal to a value γ^+ that is nearly independent of κ , and smaller than γ^* determined from $J_\sigma(t)$. Values of γ^* and γ^+ determined for isotropic and nematic solutions over a range of c are given in Fig. 26.

DISCUSSION

The decrease of "the viscosity" on the formation of the nematic phase is one of the most characteristic features noted for mesogenic polymer solutions³². The value of η_κ usually referred to in this correlation is η_p defined above. Values of η_p determined here are given in Fig. 27, along with values of η_0 for isotropic solutions reported in Parts 1 and 2; as mentioned above, the latter are well represented by Eqn. 18. In a theoretical treatment related to that used to derive Eqn. 18, Doi has calculated the steady-state viscosity η_{ANISO} for a "uniform" fluid, in a "weak velocity gradient"³³. The fluid is characterized by an order parameter S related to the ratio c/c_c :

$$S = \frac{1}{4} + \frac{3}{4} \left(1 - \frac{8}{9} \frac{c}{c_c} \right)^{1/2} \quad (42)$$

for $c/c_c > 8/9$ and zero for smaller c . With this model, for $c > c_c$,

$$\eta_{\text{ANISO}} = \eta_{\text{ISO}}(c_c) D(S) \quad (43)$$

where $\eta_{\text{ISO}}(c_c)$ is the viscosity of an isotropic solution at concentration c_c , given by Eqn. 18 and $D(S)$ decreases with increasing S :

$$D(S) = (1 - S) \left(\frac{1+S}{1+2S} \right)^2 \frac{1+3S/2}{(1+S/2)^2} \approx (1 - S)/(1 + S/2)^2 \quad (44)$$

With Eqn. 43, $\eta_{\text{ANISO}}/\eta_{\text{ISO}}(c_c)$ is expected to depend on c/c_c through the dependence of S on c/c_c . The data in Fig. 16 conform qualitatively to Eqn. 43 in that η_p decreases from $\eta_{\text{ISO}}(c_c)$ with increasing c/c_c , but η_p appears to level and then increase with larger c/c_c , whereas $D(S)$ decreases monotonically with increasing c/c_c .

The continuous increase of η_κ with decreasing κ in experiments observed with most of the nematic solutions is similar to behavior reported previously in our laboratory³⁴ for nematic solutions of poly(1,4-phenylene-2,6-benzobisoxazole) and poly(1,4-phenylene terephthalate), as well as by a number of others (see the discussion in Ref. 32). The behavior is not always observed over the range of κ studied³², and indeed, is not observed here with the nematic solution of PBT-53 with $w = 42.7 \text{ g kg}^{-1}$. The transient behavior discussed in the following for $J_\sigma(t)$ at small σ and $\eta_\kappa(t)$ at small κ displays unusual behavior in the range for which η_κ increases with increasing κ .

As shown in Figs. 24 and 25, in a stress-growth experiment for the nematic solutions studied, for small κ the stress $\sigma(t)$ increases monotonically with increasing strain κt . In the creep behavior obtained with a nematic solution (Fig. 23), the strain $\gamma(t) = \sigma J_\sigma(t)$ increases monotonically with increasing t , so that at large t , $\gamma(t) \approx \sigma t / \eta_\kappa$ and $\partial \gamma(t) / \partial t$ is a constant. In neither case is there any indication of solid-like behavior at small strain -- i.e., no yield phenomenon is observed. For values of σ such that $\partial \gamma(t) / \partial t$ at steady-state is in the range of κ for which stress-growth experiments give $\eta_\kappa \approx \eta_p$, the creep and stress-growth experiments give the same steady-state viscosity η_p , as would normally be expected. However, different behavior is obtained, for very small κ , for which stress-growth experiments give a larger steady-state viscosity, i.e., $\eta_\kappa > \eta_p$. For example, with PBT-53 at $w = 34.3 \text{ g kg}^{-1}$, $\eta_\kappa \approx 2.4 \eta_p$ for $\kappa = 3.8 \times 10^{-4} \text{ s}^{-1}$ (i.e., $\eta_p R_0 \kappa = 0.053$). For this sample, a creep experiment effected at σ such that $\partial \gamma(t) / \partial t = 3.8 \times 10^{-4} \text{ s}^{-1}$ at steady-state resulted in a smaller steady-state viscosity, $\eta_\kappa = 1.2 \eta_p$. Values of R_0 determined after steady-state flow in these experiments were equivalent. In a creep experiment, $\partial \gamma(t) / \partial t$ is larger at small t than at steady-state (i.e., large t). Thus, in the example cited the reduced η_κ obtained in creep is in the range expected for a stress-growth experiment with κ equal to $\partial \gamma(t) / \partial t$ obtained at small t in the creep experiment. The quiescent, relaxed nematic fluids studied here are characterized by a texture such that locally, the axes of the rodlike chains are parallel, but with no correlation among these axes over

the entire sample. The behavior of η_κ at small κ or σ may be caused by effects on this texture. In particular, domains with the molecular axes of the rodlike chains oriented perpendicular to the flow plane may be depopulated with increasing κ (or $\partial\gamma(t)/\partial t$), resulting in reduced η_κ . A similar suggestion has been made on the basis of flow birefringence data¹¹. If this view is correct, then comparison of η_p with η_{ANISO} may be inappropriate, since the latter is computed for a uniform fluid whereas η_p could be for fluid with the molecular axes oriented preferentially in the flow plane, so that one could have $\eta_p < \eta_{\text{ANISO}}$ as the Miesowicz viscosities are unequal.^{12,13} The failure to observe an increase in η_κ with decreasing κ for some nematic fluids (e.g., PBT-53 with $w = 42.7 \text{ g kg}^{-1}$) may indicate suppressed domain structure (perhaps owing to incomplete relaxation of prior deformation) or insufficiently small κ to observe the effect.

With increasing κ , the $\sigma(t)$ obtained in stress-growth experiments display a maximum for strain κt about equal to a constant γ^+ (independent of κ) for a given c — γ^+ appears to decrease slowly with increasing c . This behavior is not unusual, and is observed with isotropic solutions of the polymers studied here, with γ^+ being slightly larger for the latter. Similarly, with increasing σ , the $\gamma(t)$ obtained in creep experiments are given by $\sigma J_0(t)$ provided $\gamma(t)$ is smaller than a constant γ^* (independent of σ) for a given c , with $\gamma(t) > \sigma J_0(t)$ for larger $\gamma(t)$. This is similar to behavior obtained with isotropic solutions of the rodlike chains, with γ^* being somewhat smaller for the nematic solution than for the isotropic fluids. The combined behavior for stress-growth and creep suggests that as with Eqn. 38, the rheological constitutive equation for nematic fluids may involve a critical strain criterion. The behavior at small κ (or σ) suggests that Eqn. 38 may not itself suffice.

With the nematic fluids studied here, no proper linear viscoelastic behavior was observed, so that the τ_i (or λ_i) distribution could not be rigorously determined. Nevertheless, since for the nematic solutions, η_κ and R_κ are (nearly) independent of κ over a reasonable range of κ for $R_0\eta_p\kappa$, in the range 0.1 to 1, it is reasonable to compute (apparent) values of R_i and λ_i from data in $R_\sigma(t)$ for corresponding levels of σ . Values of R_i and λ_i determined for the data on $R_\sigma(t)$ in Fig. 23 are given in Table 8 -- the data are normalized by the values of R_κ and η_κ obtained with the σ used to determine $R_\sigma(t)$ (i.e., $\sigma = 14.6 \text{ Pa}$). Of course, the data in Table 8 reproduce $R_\sigma(t)$ in Fig. 23. Their use to estimate η_κ and R_κ will be discussed below. The set of λ_i for the nematic solution is similar in breadth to

those obtained with an isotropic solution of PBT-53 ($w = 29.4 \text{ g kg}^{-1}$), given in Table 8 for comparison, so that as shown in Fig. 28, $R_0(t)/R_0$ for the latter is similar to $R_\sigma(t)/R_\kappa$ for the nematic solution. By comparison, $R_0(t)/R_0$ and the λ_i set for a solution of PBT-53 ($w = 25.5 \text{ g kg}^{-1}$) are noticeably different.

As shown in Part 2, for isotropic solutions, η_κ/η_0 and R_κ/R_0 may be represented in terms of Eqns. 21 and 40 given the parameters η_i and τ_i (or R_i and λ_i). With these fluids (as with flexible chain polymers³) over a wide range $\tau_c\kappa$ (with $\tau_c = \eta_0 R_0$), the approximations

$$\eta_\kappa \simeq [\eta_0(t)]_{\kappa t=1} \quad (45)$$

$$R_\kappa \simeq [R_0(t)]_{\kappa t=1} \quad (46)$$

provide direct correspondence between linear and nonlinear properties. In particular, with a narrow distribution of τ_i , R_κ is essentially independent of $\tau_c\kappa$ over a wide range of $\tau_c\kappa$. With the isotropic solutions studied here, the distribution of τ_i is reasonably broad, so that R_κ decreases markedly with increasing $\tau_c\kappa$, as discussed in the preceding, in good agreement with Eqn. 46. Similar behavior is shown in Fig. 18 for a nematic solution, where $R_\sigma(t)$ for a low σ corresponding to the range for which $\eta_\kappa \approx \eta_p$ and $R_\kappa = R_0$. As mentioned above, for the isotropic solutions the functions η_κ/η_0 and R_κ/R_0 versus $\tau_c\kappa$ are independent of T for a given material. In the interests of completeness, reduced curves for isotropic solutions of PBT-53 and 62 given in Parts 1 and 2 are included in Figs. 16 and 17. For PBT-53, η_κ/η_0 and R_κ/R_0 are fitted well by Eqns 21 and 40, respectively, using η_i and τ_i determined by linear viscoelastic studies. As may be seen in Fig. 17, the decrease of R_κ/R_0 with increasing $\tau_c\kappa$ is more pronounced with the isotropic solutions of PBT-62 than those of PBT-53, indicating a broader τ_i (or λ_i) distribution with the PBT-62 solutions.

The set of τ_i and η_i given in Table 8 for the nematic solution with $w = 32.3 \text{ g kg}^{-1}$ were computed from the λ_i and R_i given in Table 3. The τ_i and η_i were calculated using the expressions for linear viscoelasticity, despite the nonlinearity discussed in the preceding. The functions η_κ/η_p and R_κ/R_0 versus $R_0\eta_p\kappa$ computed using these τ_i and η_i in Eqns. 21 and 40 are shown in Fig. 18 -- these curves were computed with $\gamma' = 1.0$ and $\gamma'' = 2.4$, in accord with the experimental data. The computed η_κ/η_0 are in good accord with the

experimental η_κ/η_P ; the computed R_κ/R_0 tend to lie 20–40% above the measured values for large $R_0\eta_P\kappa$. Apparently, the quasi-linear treatment of the data used to estimate τ_i and η_i , etc., is useful in the range studied here, provided $R_0\eta_P\kappa$ is at least as large as the value needed to obtain the "plateau" in η_κ (e.g., $R_0\eta_P\kappa > 0.1$ for PBT-53 with $w = 32.3 \text{ g kg}^{-1}$).

Note that the treatment given above would not lead to negative first normal stress $\nu_\kappa^{(1)}$, as has been reported for an ordered solution of poly (γ -benzylglutamate), (PBG). Thus, with the single-integral equation used to obtain Eqns. 21 and 40, the reduced parameter $N_\kappa^{(1)} = \nu_\kappa^{(1)}/2(\kappa\eta_\kappa)^2$ is given by equation 23. With Eqn. 23, $N_\kappa^{(1)}$ is always positive. Data were obtained in our laboratory on a solution of PBLG in cresol for which negative values of $N_\kappa^{(1)}$ were obtained³⁸—the solution was provided by R. S. Porter. The results for η_κ , given in Fig. 29 were in good agreement with data reported by Porter and Kiss over the range of κ for which the data overlapped. Data obtained here at lower κ did not become independent of κ . Values of R_κ were found to decrease smoothly with increasing κ , through the range of κ for which $N_\kappa^{(1)}$ is reported to be negative. On the basis of the behavior observed for η_κ and R_κ , one can speculate that the τ_i (or λ_i) distribution would be very broad for the PBG solution. With Eqns. 21 and 23, $N_\kappa^{(1)}$ may become very small with η_κ/η_0 not too much less than unity with some τ_i -distribution, but $N_\kappa^{(1)}$ will always be positive.

With a PBT-62 solution studied for which c was slightly less than c_c so that the quiescent fluids were (macroscopically) isotropic, the data on η_κ versus κ did not display any range of κ for which η_κ was independent of κ . Rather, as shown in Figs. 15 and 21, η_κ decreased slowly with increasing κ at small κ . For these solutions, the decrease in R_κ with increasing κ was much smaller than observed with isotropic solutions (see Fig. 10). This behavior, which is found only over a narrow range of conditions with c close to, but less than c_c , may be caused by a tendency for the isotropic solutions to develop orientational order characteristic of the nematic state under the influence of a shear stress, so that η_κ decreases slowly with increasing κ .

As shown in Fig. 22, the data on η_κ/η_0 versus $\tau_c\kappa$ for solution with c near c_c for the temperature of the measurement do not superpose with each other and differ from data

on the isotropic solutions at lower c . For example, with PBT-62, the data on η_{κ}/η_0 versus $\tau_c \kappa$ for the solution with $w/g \text{ kg}^{-1}$ equal to 30.0 and 34.3 do not superpose over the temperature range studied. In terms of Eqn. 21 or 40, it appears that the distribution of τ_i sharpens with decreasing T for this solution. The behavior of R_{κ}/R_0 , which becomes nearly independent of $\tau_c \kappa$ at low T , is also consistent with an effectively narrowed distribution of τ_i .

Table 6: Polymers Used in This Study

Polymer	$[\eta]/\text{mLg}^{-1}$	L_{η}/nm^a	Range w/gkg^{-1}	Range T/K
PBT-62	2,650	170	15.0-82	272-353
PBT-53	1,400	120	25.5-42.7	283-333

a. $L_{\eta} = M_{\eta}/M_L$, where $M_L = 220 \text{ dalton nm}^{-1}$ and $M_{\eta} = ([\eta]/K_{\eta})^{1.8}$
 with $M_L^{1.8}K_{\eta} = 0.26 \text{ mLg}^{-1}$.

Table 7: Rheological Parameters for Solutions of Rodlike Polymers

Polymer	w/g kg ⁻¹	T/K	$\eta_0 A^{-1}/\text{kPa}\cdot\text{s}^a$	$R_0 cRT/M_\eta^b$
53	25.5(I) ^c	333	1.89	(60)
	25.5(I)	313	1.83	(60)
	25.5(I)	303	1.73	(62)
	25.5(I)	296	2.10	64
	25.5(I)	286	1.89	69
	29.4(I)	313	7.15	70
	29.4(I)	296	7.64	78
	29.4(I)	285	6.80	107
	32.3(I)	333	4.83	102
	32.3(N)	316	4.05	97
	32.3(N)	294	4.34	112
	32.3(N)	283	6.90	130
	42.7(N)	316	12.3	190
	42.7(N)	296	11.0	180
	42.7(N)	284	9.6	172
	15.0(I)	333	0.28	18
	15.0(I)	318	0.31	17
	15.0(I)	293	-0.27	21
	25.2(I)	333	22.8	42
	25.2(I)	297	41.0	31
	25.2(I)	277	52.0	18
62	30.0(I)	353	45.6	63
	30.0(I)	333	41.7	53
	30.0(I)	313	60.4	44
	30.0(I)	293	74.7	35
	30.0(I)	283	86.4	30
	30.0(I)	272	71.1	23
	34.3(I)	333	13.2	31
	34.3(I)	313	13.1	21
	34.3(N)	293	3.1	33
	34.3(N)	283	3.0	25
	47.3(N)	333	0.61	940
	47.3(N)	313	0.53	970
	61.1(N)	333	0.94	2030
	82.0(N)	333	0.83	3630
	82.0(N)	297	0.47	3640

Table 8: Retardation and Relaxation Spectra

λ_i/τ_c	R_i/R_0	τ_i/τ_c	η_i/η_0
PBT-53; $w = 32.3 \text{ g kg}^{-1}$ (NEMATIC) ^a			
8.30	0.262	8.59	0.037
2.65	0.104	2.79	0.065
1.04	0.312	1.40	0.266
0.193	0.170	0.353	0.323
		0.086	0.149
0.042	0.111	0.0075	0.160

PBT-53; $w = 29.4 \text{ g kg}^{-1}$ (ISOTROPIC) ^b			
2.580	0.580	3.251	0.231
0.210	0.280	0.494	0.480
0.0175	0.130	0.0615	0.092
		0.0010	0.092

PBT-53; $w = 25.5 \text{ g kg}^{-1}$ (ISOTROPIC)			
5.248	0.430	5.732	0.094
1.022	0.290	1.354	0.258
0.240	0.174	0.381	0.253
0.080 ₅	0.035	0.098 ₈	0.084
		0.025 ₂	0.312

(a) R_0 , η_0 and τ_c replaced by values obtained from creep with shear stress

$$\sigma = 14.6 \text{ Pa, see text; } \tau_c = \eta_0 R_0.$$

(b) See Part 2.

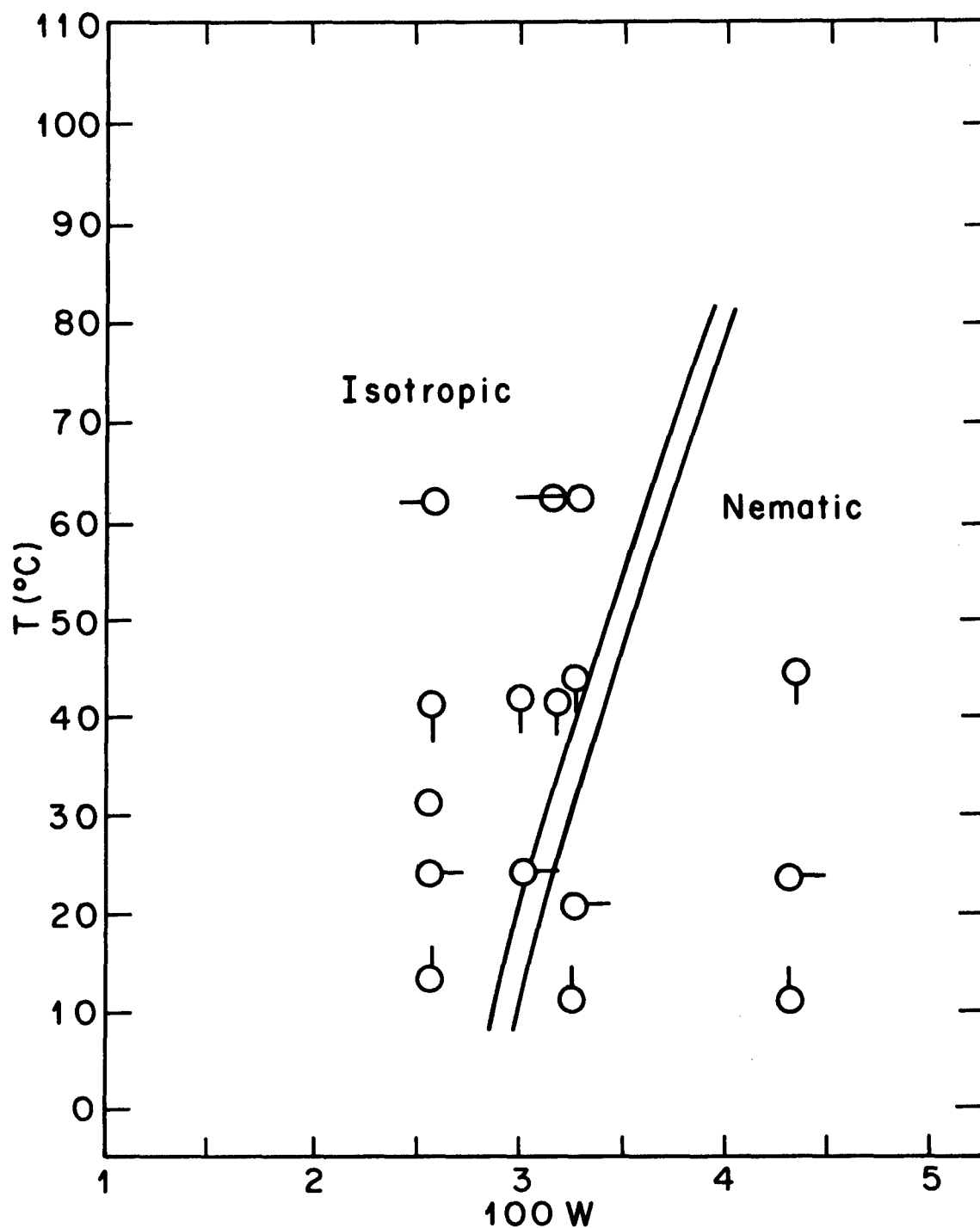


Figure 12:
Schematic diagram showing the concentration (weight fraction w) and temperatures used in rheological studies on solutions of PBT-53. Regions of isotropic and nematic solutions are indicated on the diagram.

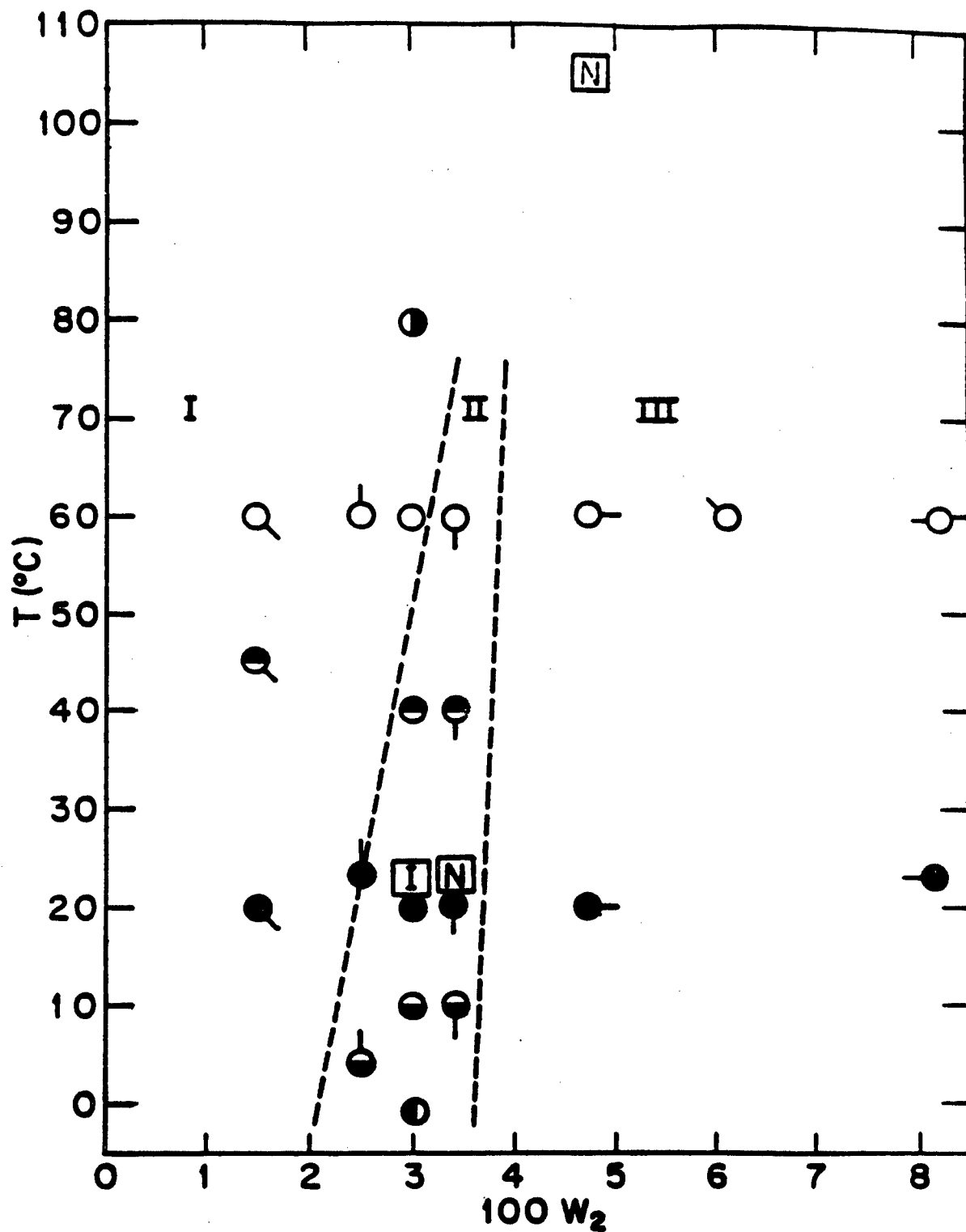


Figure 13:
Schematic diagram showing the concentrations (weight function w) and temperatures used in rheological studies on solutions of PBT-62. Conditions of w and T for which solutions were observed to be isotropic or nematic are indicated by \square or \blacksquare , respectively. Data for conditions to the left and right sides of the dashed line are given in Figs. 16 and 20, respectively.

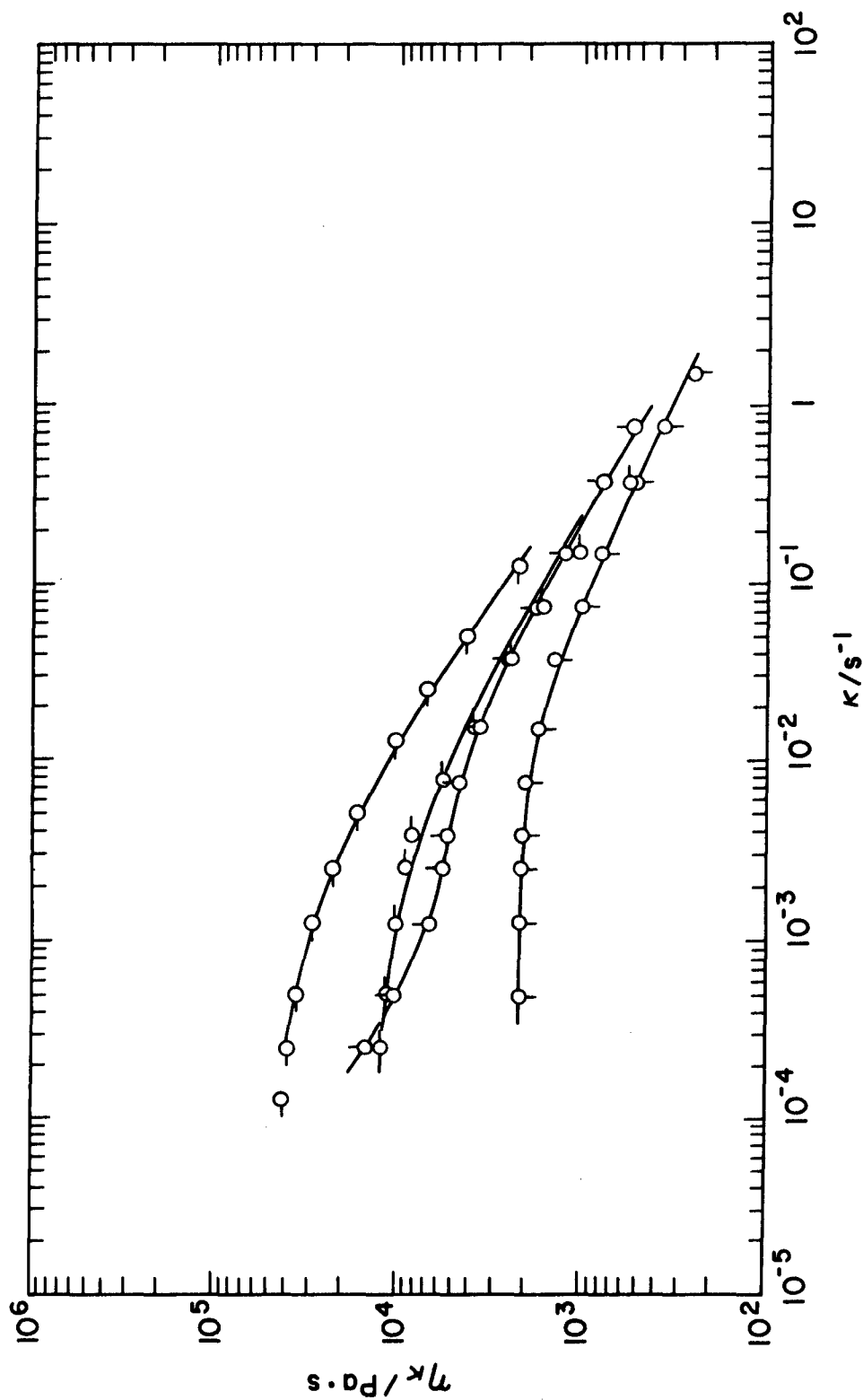


Figure 14:
The steady-state viscosity of η for solutions of PBT-53 with $T \approx 20^\circ\text{C}$ --the symbols indicate w/gkg of 25.5, O; 29.4, -O; 32.3, O and 42.7 O-.

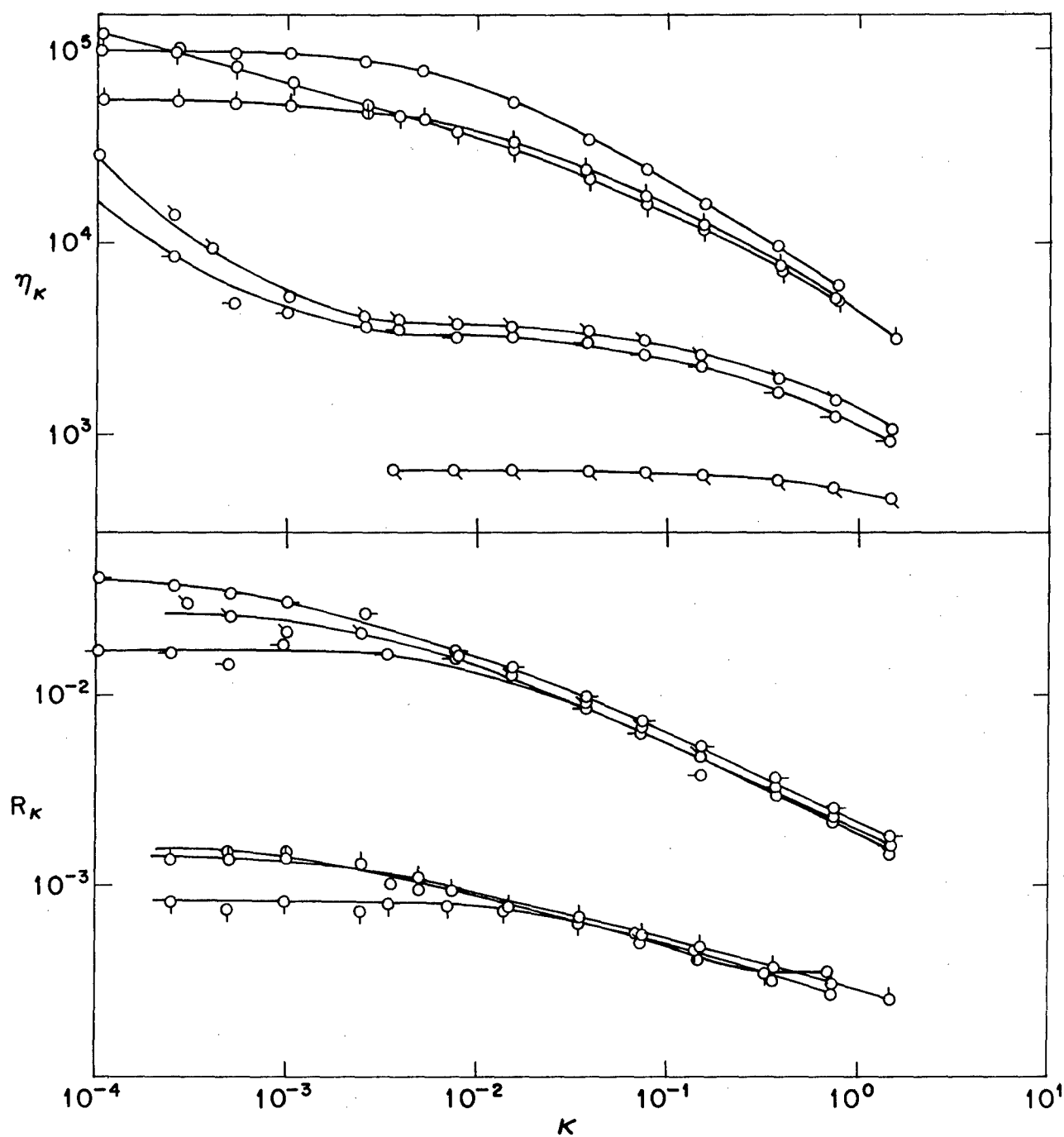


Figure 15:
The steady-state viscosity η_κ and recoverable compliance R_κ for solutions of PBT-62 with $T \approx 60^\circ\text{C}$. The symbols κ indicate w as in Fig. 13.

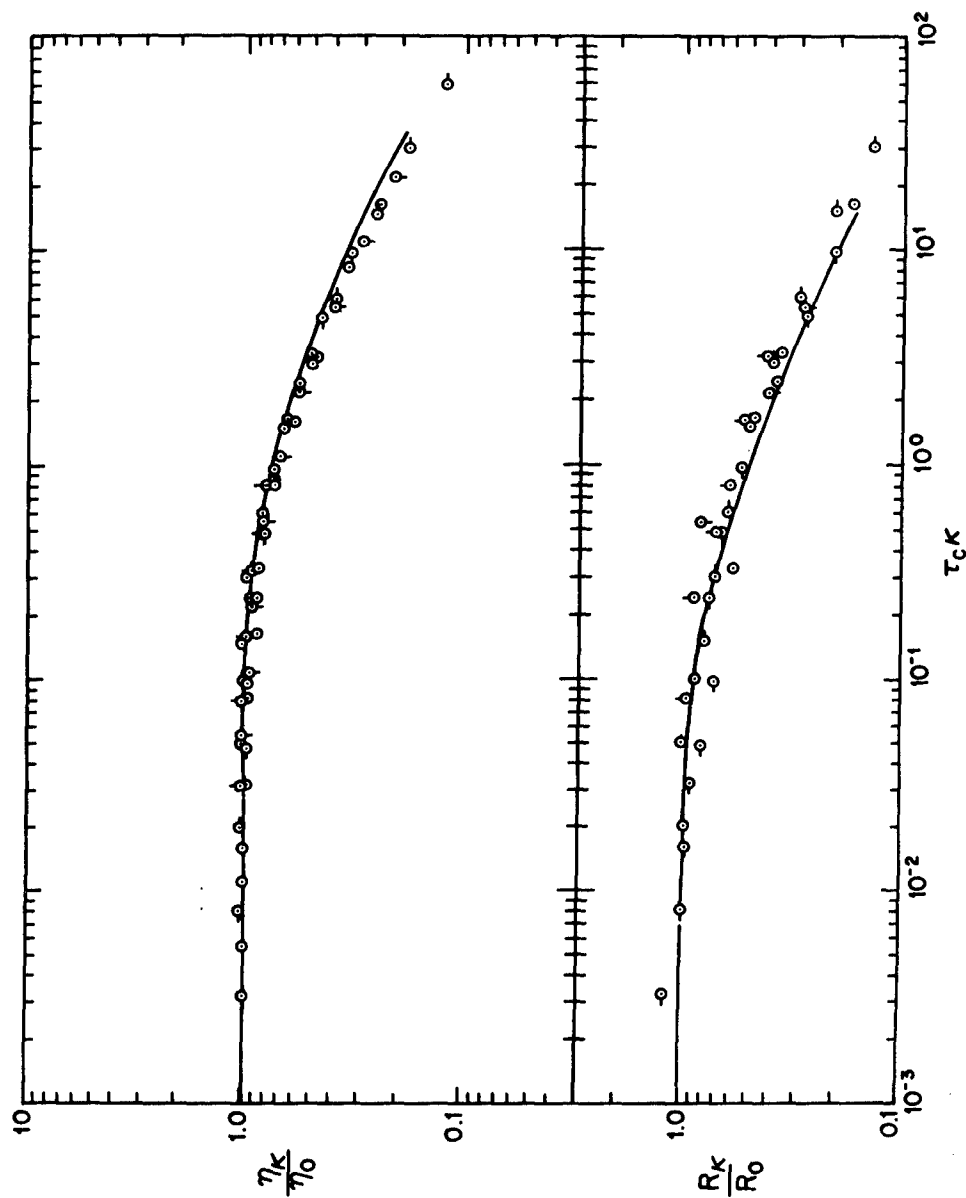


Figure 16: η_k/η_0 and R_k/R_0 versus $R_0\eta_0\kappa$ for isotropic solutions of PBT-53 ($w = 25.5\text{g/kg}$, with symbols as in Fig. 12). The curves for η_k/η_0 and R_k/R_0 represent Eqns. 21 and 40, respectively, with the τ_i and η_i in Table 8.

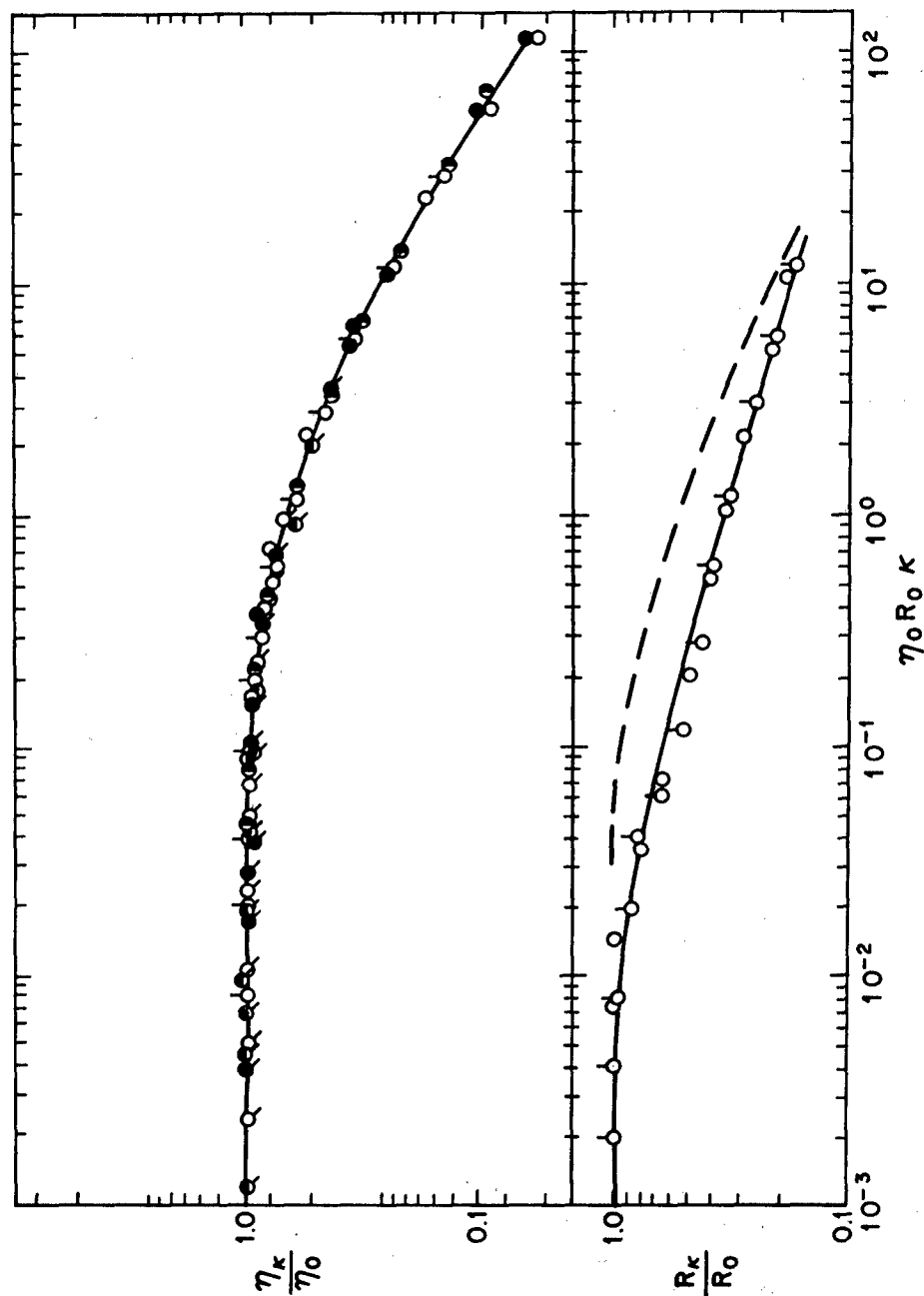


Figure 17:
 η_κ/η_0 and R_κ/R_0 versus $R_0 \eta_0 \kappa$ for isotropic solutions of PBT-62 (symbols as in Fig. 13).
 The dashed curve represents R_κ/R_0 vs τ_κ from Fig. 16.

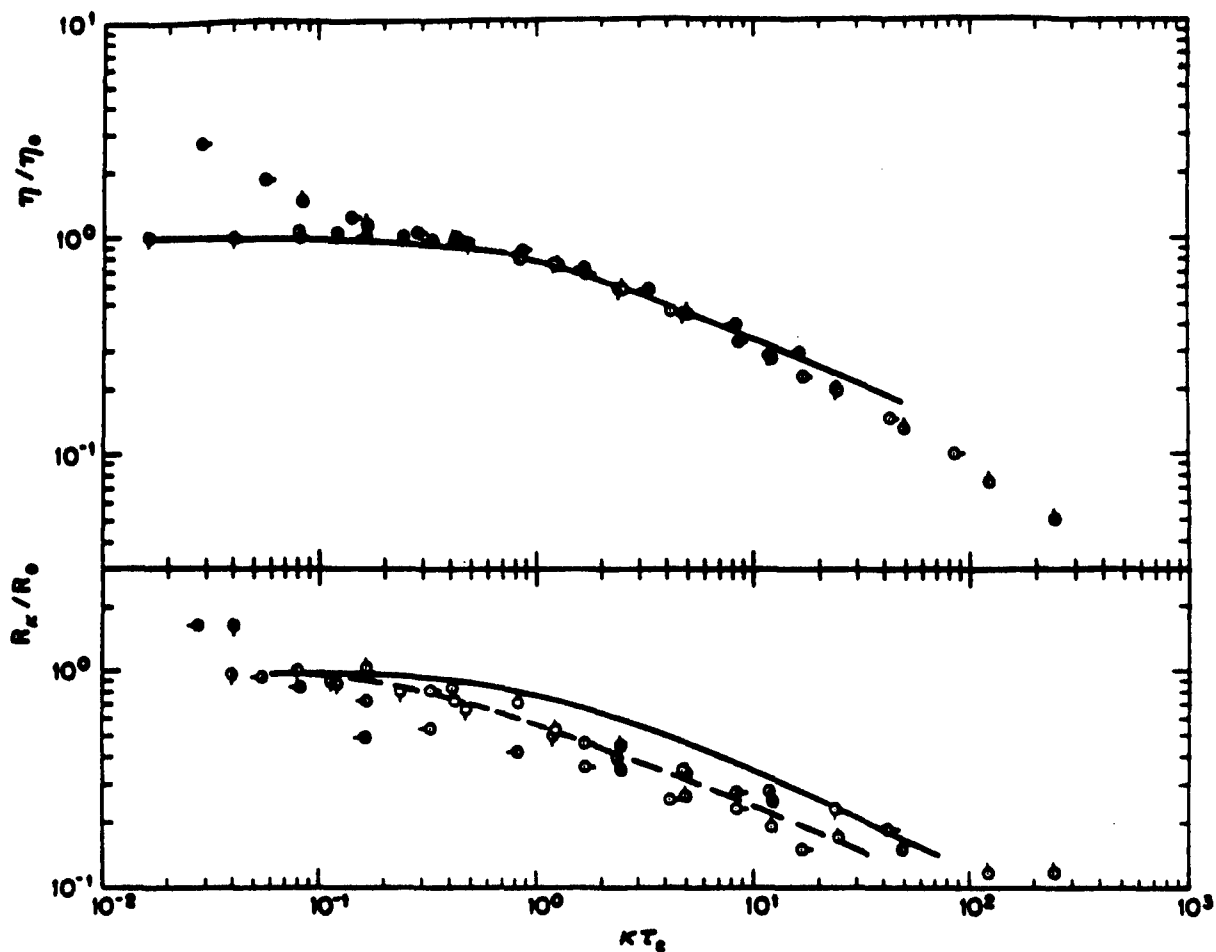


Figure 18:
 η/η_0 (or η^*/η_p) and R_x/R_0 versus $R_0\eta_0\kappa$ (or $R_0\eta_p\kappa$) for isotropic (or nematic) solutions of PBT-53 ($w = 32.3$ g/kg, with symbols as in Fig. 12). The solid curves for η^*/η_0 and R_x/R_0 represent Eqs 21 and 40, respectively with the τ_i and η_i given in Table 8. The dashed curve shows $R_0(t)/R_0$ versus τ_c/t .

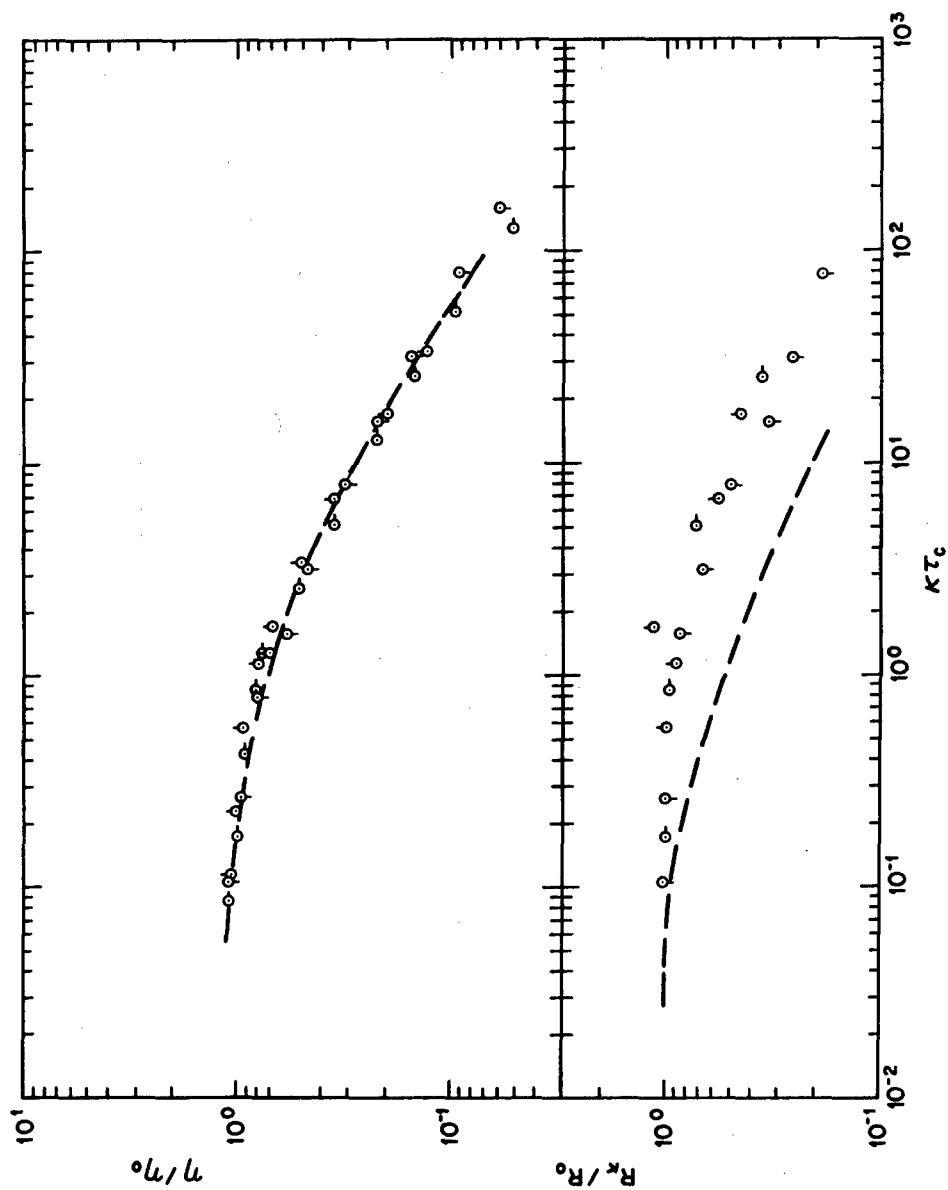


Figure 19: η/η_0 and R_κ/R_0 versus $R_0\eta_P\kappa$ for nematic solutions of PBT-53 ($w = 42.7$ g/kg, with symbols as in Fig. 12). The dashed curves represent the curves given in Fig. 18.

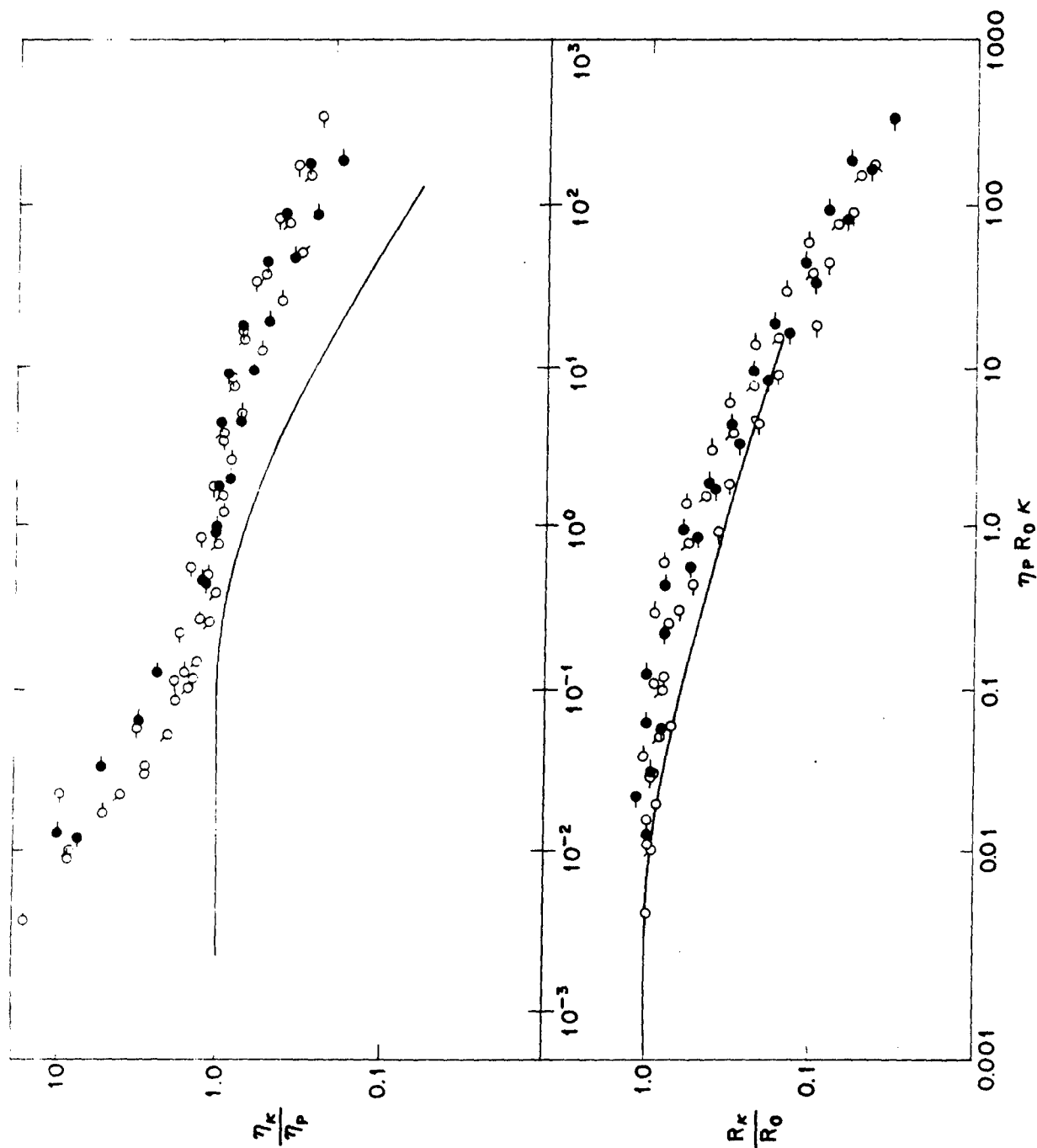


Figure 20:
 η_K/η_P and R_K/R_0 versus $\eta_P R_0 K$ for nematic solutions of PBT-62 (symbols as in Fig. 13).
 The curves represent the behavior shown in Fig. 17.

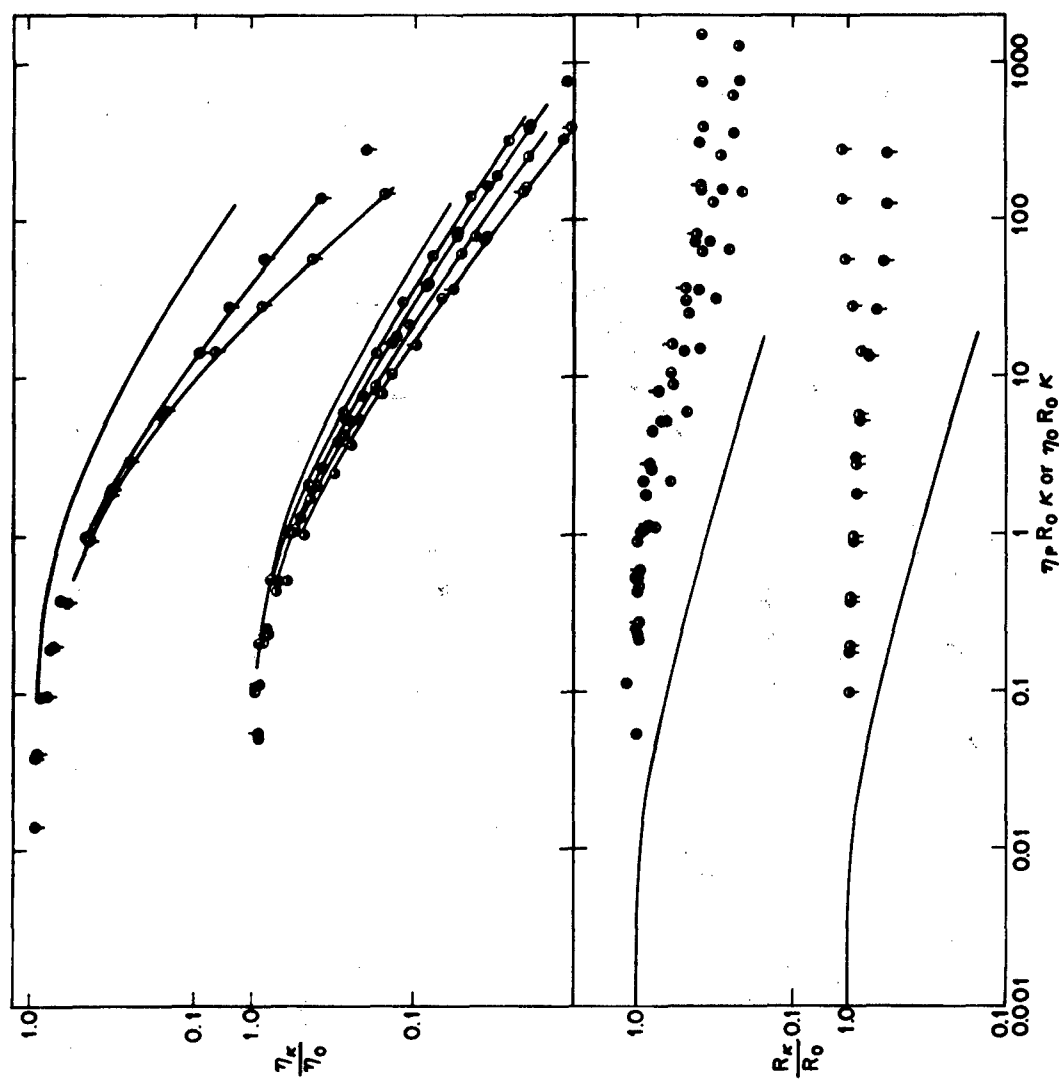


Figure 21: η_K/η_P and R_K/R_0 versus $R_0 \eta_P K$ for solutions of PBT-62 (symbols as in Fig. 13). The curves represent the behavior shown in Fig. 17.

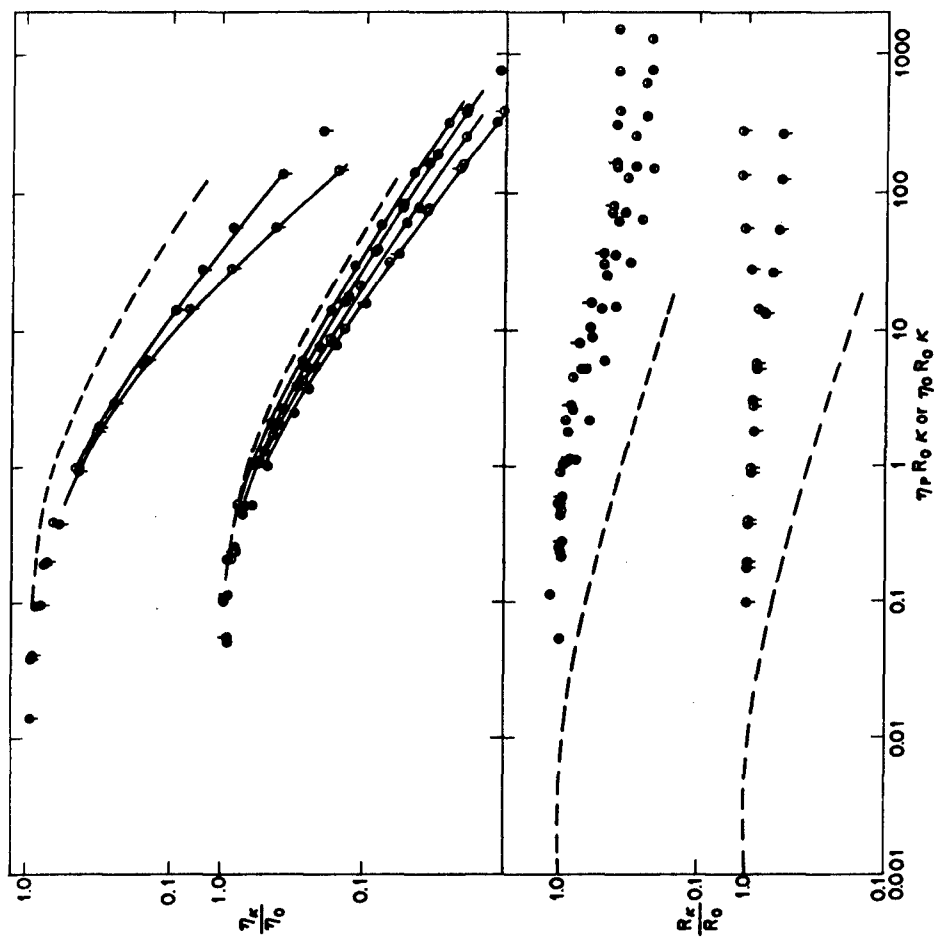


Figure 22: η_r/η_0 and R_r/R_0 versus $R_0 \dot{\gamma}_r \kappa$ for solutions of PBT-62 (symbols as in Fig. 13). The dashed curves represent the behavior shown in Fig. 17.

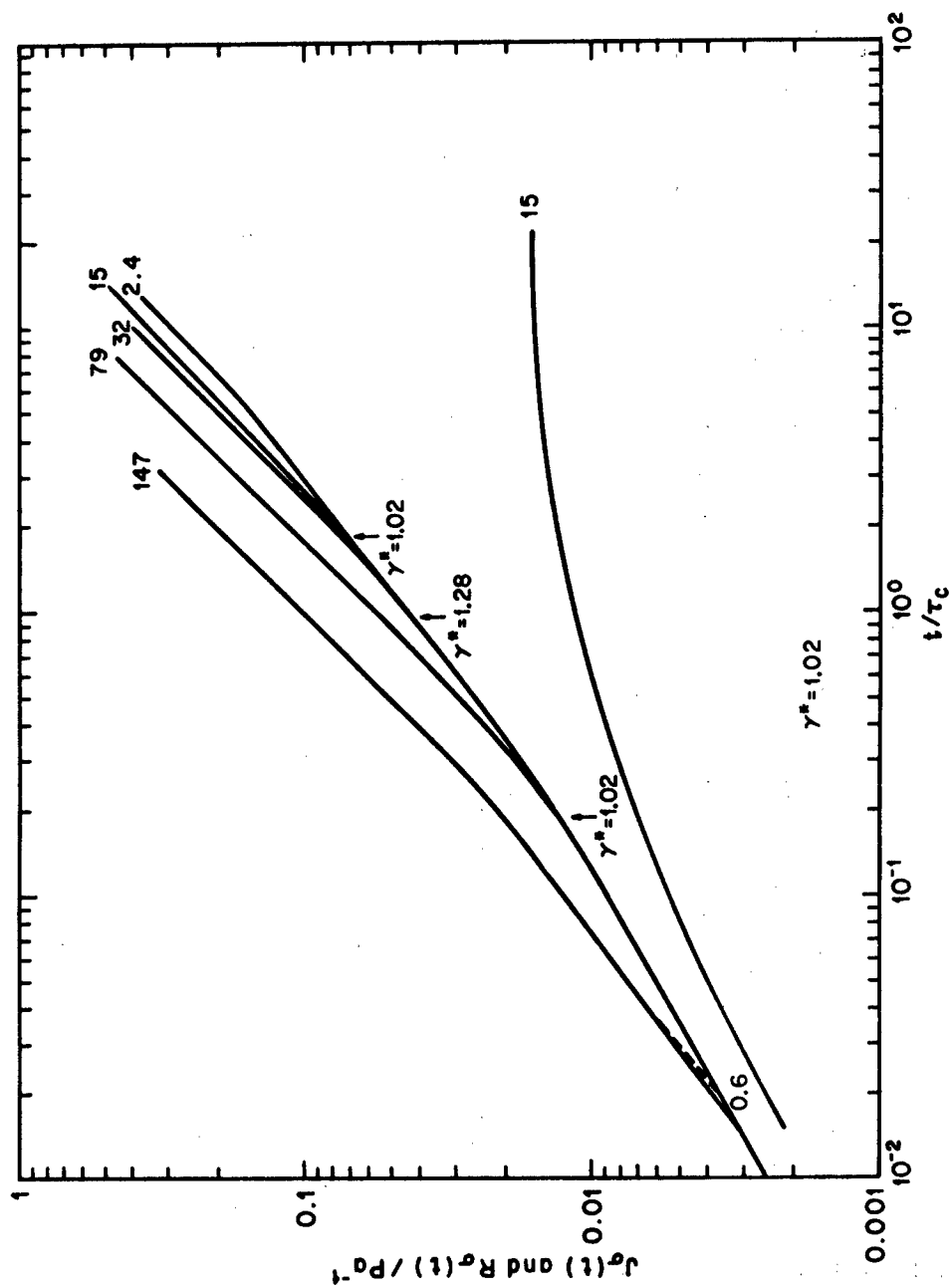


Figure 23:
Creep $J_{\sigma}(t)$ and recoverable compliance $R_{\sigma}(t)$ versus t/τ_c (with $\tau_c = 170\text{s}$) for a nematic solution of PBT-53 ($w = 32.3 \text{ g/kg}$, $T = 19.5^\circ\text{C}$). Values of shear stress σ/Pa used are given, along with the parameter γ .

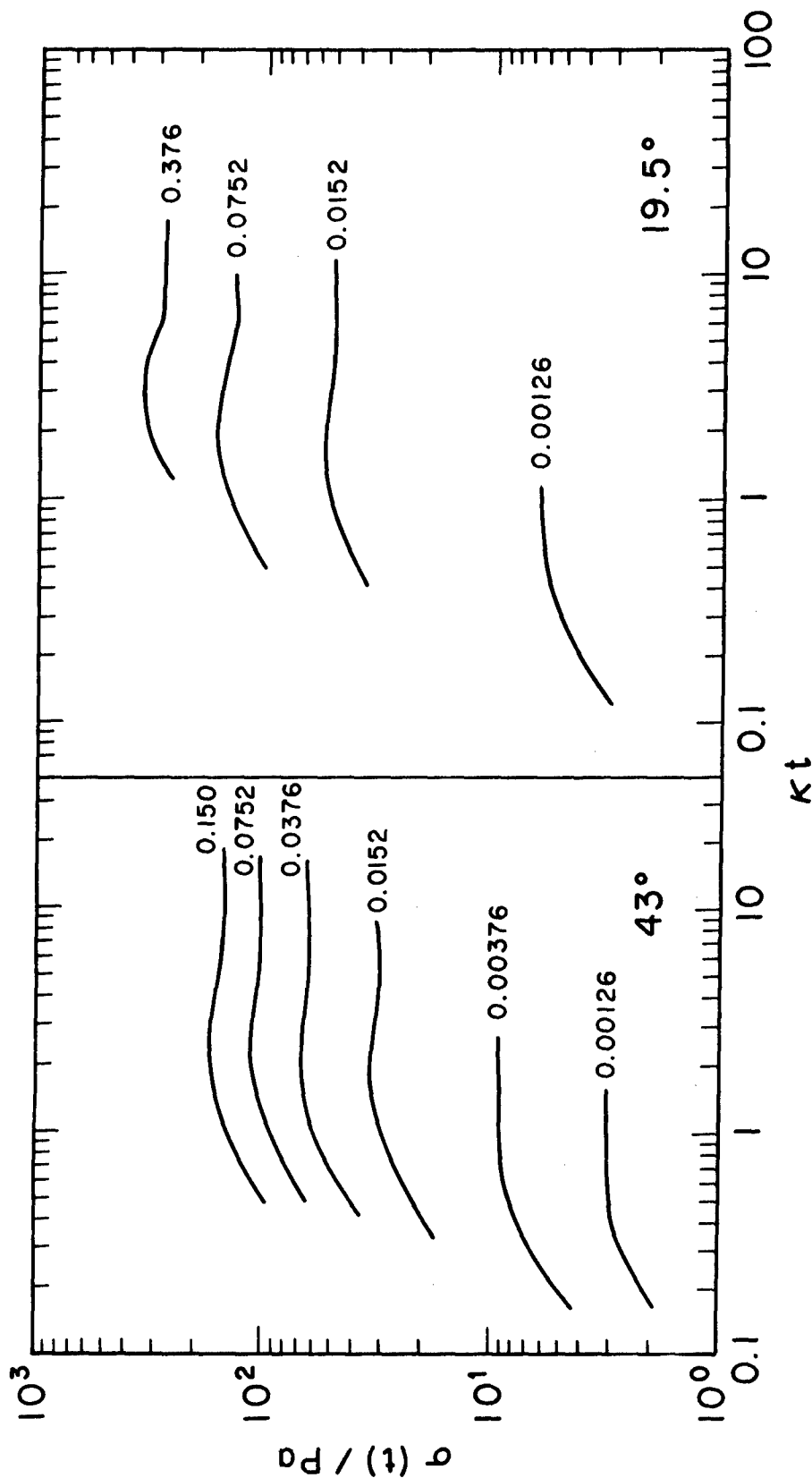


Figure 24:
The stress $\sigma(t)$ in a stress-growth experiment versus the strain κt for a solution of PBT-53 ($w = 32.3$ g/kg) at temperatures for which the solution is isotropic (43°C) and nematic (19.5°C). Values of κ/s are indicated.

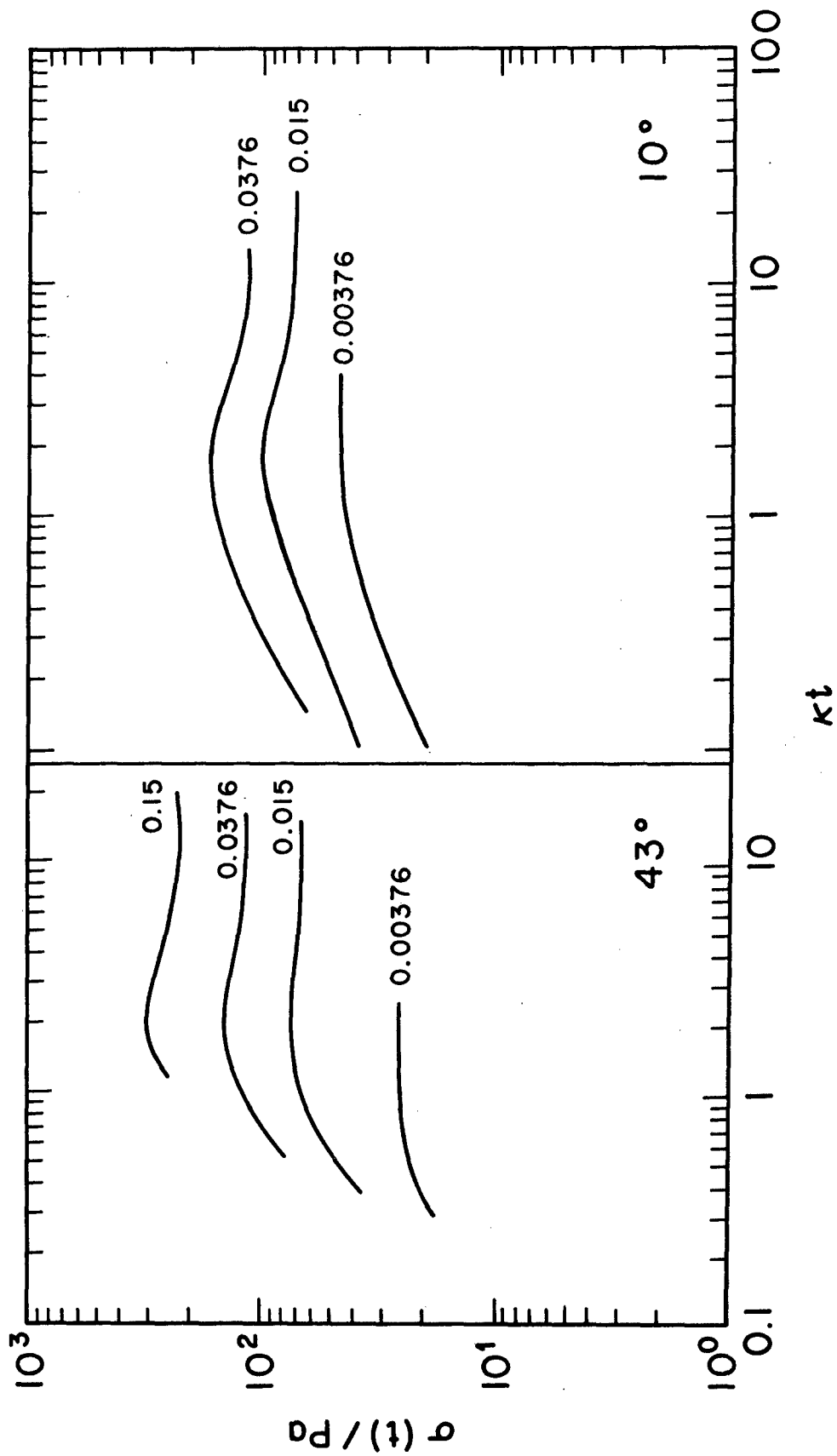


Figure 25:
The stress $\sigma(t)$ in a stress-growth experiment versus the strain κt for a nematic solution of PBT-53 ($w = 42.7$ g/kg) at two temperatures.

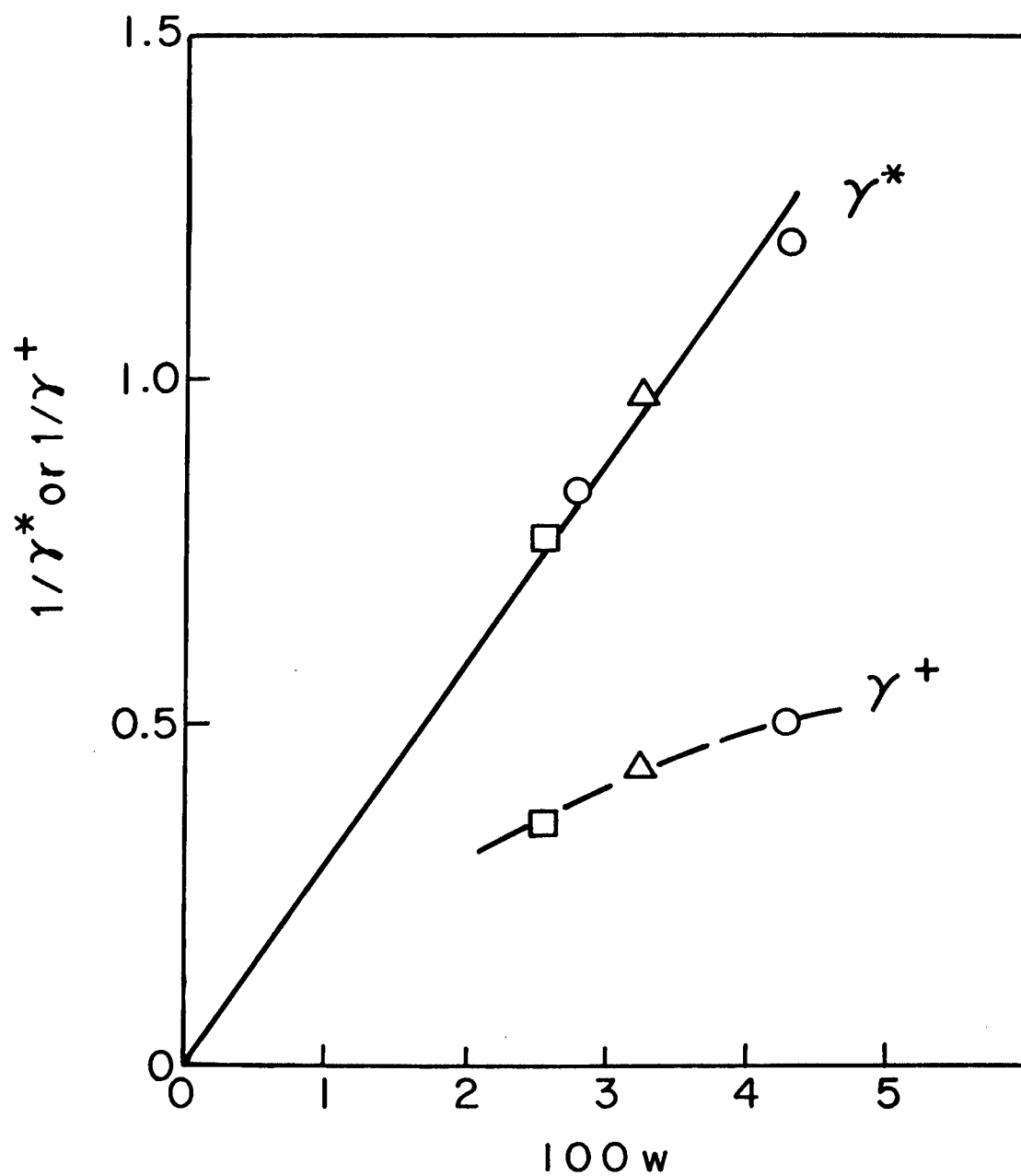


Figure 26:
The critical strains γ^* and γ^+ plotted (as the inverse) versus the concentration w for solutions of PBT-53.

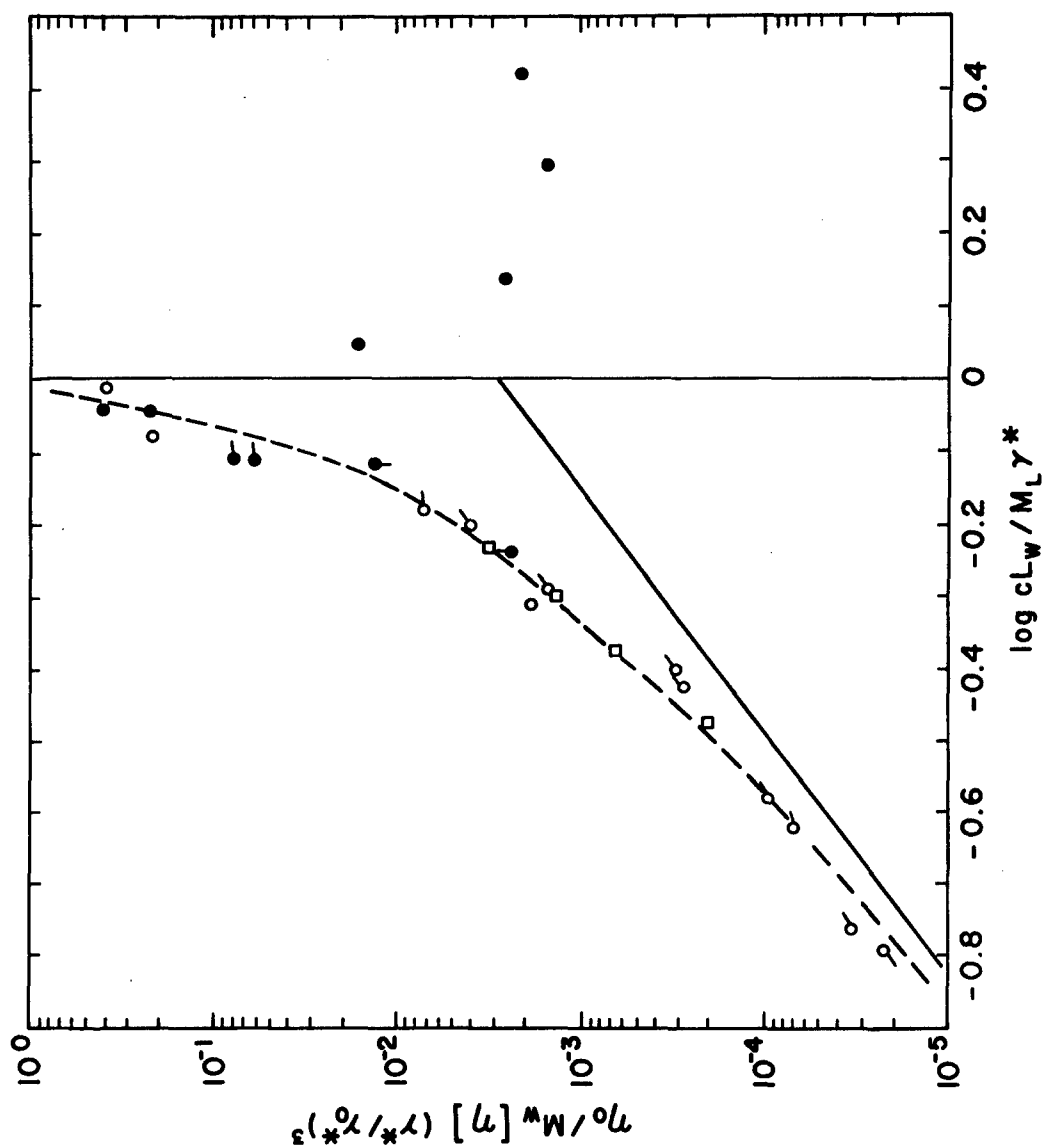


Figure 27:

Left side: $\eta_0/M_w[\eta](\gamma^*/\gamma_0)^3$ versus $BcL_w/M_L\gamma^*$ for isotropic solutions of PBT-53, PBT-62 and other rodlike polymers (see the preceding for identification of the symbols). Here B/a^* is obtained by comparison of Eqn. 18 with experiment (see the preceding), and B/a^* is an arbitrary constant.

Right side: The same quantities for nematic solution of PBT-62, (a) and PBT-53 (•)

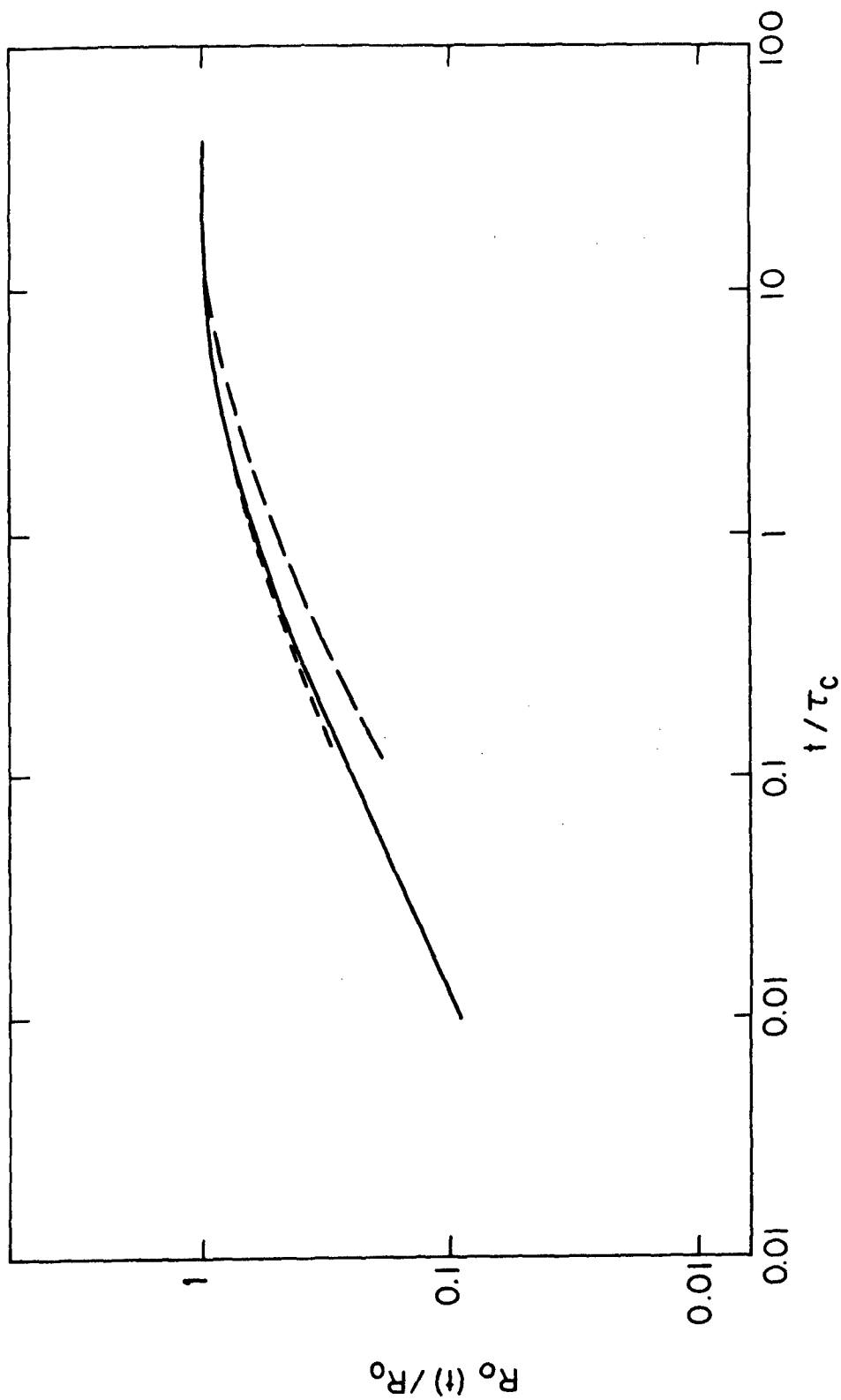


Figure 28:
 $R(t)/R_0$ versus t/τ for two isotropic solutions of PBT-53 (w/g kg⁻¹ equal to 25.5 and 29.4, long and short dash, respectively) and a nematic solution (w = 32.3 g/kg, T = 19.5°C, solid curve). For the latter, τ is replaced by γR_x and R_0 is replaced by R_x . With the isotropic solutions, $R_0(t) = R_0(t_f)$ and with the nematic solution, $\sigma = 14.6$ Pa.

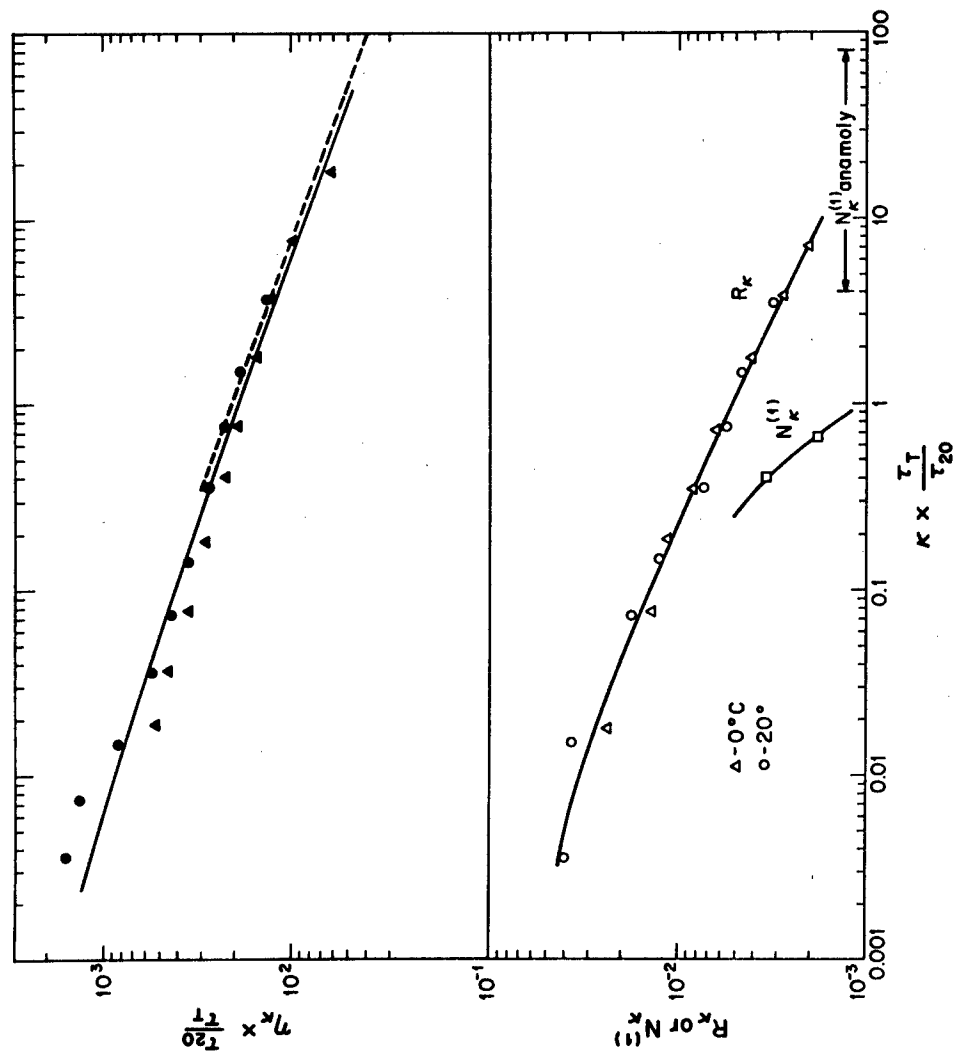


Figure 29: $\eta_{\kappa}(\tau_{20}/\tau_{\kappa})$, R_{κ} and $N_{\kappa}^{(1)}$ versus $(\tau_1/\tau_{20})_{\kappa}$ for an anisotropic solution of poly(γ -benzylglutamate) in cresol for T/K equal to 273 (Δ , Δ) and 293 (\circ , \circ). The dashed line and the data on $N_{\kappa}^{(1)}$ are from reference 36. The factor τ_1/τ_{20} is unity for $T = 293$ K and chosen to superpose data on R_{κ} versus $(\tau_1/\tau_{20})_{\kappa}$ for $T = 273$ K. The range denoted "N $_{\kappa}^{(1)}$ anomaly" designates the range for negative $N_{\kappa}^{(1)}$ according to reference 38.

3. RHEOLOGICAL AND RHEO-OPTICAL STUDIES OF A CONSTITUTIVE EQUATION FOR NEMATOGENIC SOLUTIONS OF RODLIKE POLYMERS

SUMMARY

Rheological and rheo-optical studies on solutions of the rodlike poly(1,4-phenylene-2,6-benzobisthiazole), are described for both isotropic and nematic-solutions. The data include both steady-state and transient behavior. For isotropic solutions, it is found that a single-integral constitutive equation (a form of the BKZ equation) represents the data available. For nematic solutions, unexplained behavior is observed for small κ , perhaps related to unstable flow in simple shear predicted for such solutions by some mechanistic theories for the parameters in the Leslie-Erickson constitutive equation. For larger κ , the flow behavior may be represented by a modified form of the single-integral equation.

INTRODUCTION

The following describes rheological and rheo-optical studies¹ on nematogenic solutions of the rodlike poly(1,4-phenylene-2,6-benzobisthiazole), PBT, carried out over a range of concentration c and chain length L encompassing the isotropic and nematic phases. The studies include measurements of the creep compliance $J_\sigma(t)$ determined from the strain $\gamma(t)$ obtained with a constant shear stress σ (e.g., Eqn. 1), the recoverable $R_\sigma(S, \theta)$ determined after creep of duration S , with θ the elapsed time for creep recovery,

$$R_\sigma(S, \theta) = \frac{\gamma(S) - \gamma(\theta)}{\sigma} \quad (47)$$

the stress-growth function $\eta_\kappa(t)$ determined from the stress $\sigma(t)$ obtained with a constant shear rate κ (e.g., Eqn. 2), the viscosity relaxation function determined from the stress $\sigma\theta$ following cessation of steady state flow at constant κ

$$\hat{\eta}_\kappa(\theta) = \sigma(\theta)/\sigma \quad (48)$$

and the corresponding birefringence $\Delta n^{(13)}$ expressed below as the function, given by equation 5, and

$$M_\kappa(t) = \Delta n^{(13)}(t)/(\kappa \eta_\kappa)^2 \quad (49)$$

where η_κ is the steady-state viscosity obtained as the asymptotic value of $\eta_\kappa(t)$ for large t and $\Delta n^{(13)}$ is measured in the 1-3 flow plane, with flow in the 2-direction for a shear-gradient in the 1-direction. In using these relations, it is convenient to define

$$\lim_{S \rightarrow \infty} R_\sigma(S, \theta) = R_\sigma(\theta) \quad (50)$$

$$\lim_{\theta \rightarrow \infty} R_\sigma(\theta) = R_\kappa^{(S)} \quad (51)$$

Since the materials studied here are fluids,

$$\lim_{t \rightarrow \infty} J_\sigma(t) = J_\kappa^{(S)} + t/\eta_\sigma \quad (52)$$

In general, $J_\kappa^{(S)} \neq R_\kappa^{(S)}$ and $\eta_\kappa > \eta_0$, but for a linear viscoelastic fluid, $J_\kappa^{(S)} = R_\kappa^{(S)} = R_0^{(S)}$ and $\eta_\sigma = \eta_\kappa = \eta_0$, and

$$J_0(t) = R_0(t) + t/\eta_0 \quad (53)$$

$$\int_0^t J_0(t-u) G_0(u) du = t \quad (54)$$

$$\eta_0(t) = \eta_0 - \hat{\eta}_0(t) = \int_0^t G_0(u) du \quad (55)$$

$$R_0^{(S)} = \lim_{t \rightarrow \infty} R_0(t) = \frac{\int_0^\infty u G_0(u) du}{\left[\int_0^\infty G_0(u) du \right]^2} \quad (56)$$

With nonlinear behavior, these relations are not obeyed. In the following, the data will be compared with predictions made with a BKZ-type single-integral constitutive equation⁵ given by⁶

$$\sigma^{(m)}(t) = \int_0^\infty [\Delta \gamma(t, u)]^m F[\Delta \gamma(t, u)] \frac{\partial G_0(u)}{\partial u} du \quad (57)$$

with $\sigma^{(1)}(t)$ and $\sigma^{(2)}(t)$ equal to the shear stress $\sigma(t)$ and first-normal stress difference $\nu^{(1)}(t)$, respectively. Here $\Delta \gamma(t, u) = \gamma(t) - \gamma(t-u)$, F is a decreasing function of $\Delta \gamma(t, u)$ for nonlinear behavior--for $F=1$, linear behavior is recovered with Eqn. (57).

With nematic solutions, the rheological properties are inherently anisotropic. According to the constitutive equation of Leslie³⁹ and Erickson⁴⁰, the steady-state shear viscosity η_0

(determined for flow in a wide gap in a region for which the stress tensor is a linear function of the velocity gradient tensor) may be expressed in the form

$$\eta_0 = \eta_b + \frac{1}{2}(1-\lambda^{-1})[(\eta_c - \eta_b) + \frac{1}{2}a_1(1+\lambda^{-1})] \quad (58a)$$

$$2\eta_b = a_3 + a_4 + a_6 \quad (58b)$$

$$2(\eta_c - \eta_b) = a_5 - a_2 - a_3 - a_6 \quad (58c)$$

$$\lambda^{-1} = (a_2 - a_3)/(a_2 + a_3) \quad (58d)$$

where λ and the a_i are related to the order parameter S for the quiescent nematic fluid, see below. Stable simple shear obtains only if $\lambda > 1$, with the rodlike chains at angle $(\arccos \lambda^{-1})/2$ with the flow direction.

EXPERIMENTAL

The experimental methods used and molecular characteristics of the polymers studied are reported in the preceding.¹ Briefly, solutions were prepared in methane sulfonic acid (MSA). Polymers 53,62 and 72 have contour lengths L_w of 120,170 and 135 nm, respectively. Rheological data were obtained with a cone and plate rheometer constructed to permit measurement of $\gamma(t)$ with a specified stress history, or $\sigma(t)$ with a specified strain history. The flow birefringence data were obtained with the fluid between glass (pyrex) parallel plates, using measurement of the intensities $I_+(\phi)$ and $I_{11}(\phi)$ transmitted between crossed and parallel polars, respectively, where ϕ is the angle between the flow direction and the polarization direction of the incident beam. This arrangement permits measurement of $\Delta n^{(13)}$ for the birefringence in the 1-3 flow plane.¹

DISCUSSION

Isotropic Solutions

Results for $J_\sigma(t)$ and $R_\sigma(t)$ for isotropic solutions reveal linear behavior $J_0(t)$ for small enough σ , but also show that $J_\sigma(t) = J_0(t)$ for $t < t^*$, and $J_\sigma(t) > J_0(t)$ for $t > t^*$, where t^* decreases with increasing σ . The strain $\gamma(t^*) = \sigma J_\sigma(t^*)$ is found² to be nearly independent of σ , and universally proportional to c . This behavior is consistent with Eqn. (57), with $F(\gamma) = 1$ for $\gamma(t) < \gamma^*$. Similar behavior has been reported with flexible chain polymers,⁶ and analyzed with Eqn. (57) with

$$F(\gamma) = \exp m \frac{|\gamma| - \gamma'}{\gamma'} \quad (59)$$

$$G_0(t) = \sum G_i \exp -t/\tau_i \quad (60)$$

where m is zero if $|\gamma| < \gamma'$ and unity otherwise. For example, with these expressions, the steady-state parameters calculated with Eqn. (57) are given by³ equations 21 - 23. The needed parameters G_i and τ_i have been computed from the corresponding parameter R_i and λ_i , defined by use of equations 14 and relations based on Eqn. (54).³ Typical results for $R_0(t)$ are given in Figure 30. As shown in Figure 31 both η_κ/η_0 and R_κ/R_0 are fitted well by Eqns. 3.3 and 3.4 for the isotropic solutions. The τ_i distribution is found to be broader than that calculated by Doi and Edwards,²⁶ for which there is essentially one relaxation time.

The limiting viscosity η_0 is shown in Figure (3a) in a form for comparison with the theoretical relation^{25, 26} given by equation 18. The data are fitted by Eqn. (18) with $a^* = c_c L/M_L$ and B slightly smaller than unity, where c_c is the concentration for the appearance of nematic phase. These are in the range expected theoretically. The empirical value $K = 1.5 \times 10^{-4}$ is smaller than the original prediction,^{25, 26} but in accord with subsequent treatments.²⁷ With $a^* = c_c L/M_L$, the dependence of $\eta_0/\eta_s c_c^3$ is expected to be independent of temperature. This behavior is observed for the system studied.

In the range of cL with η_0 increasing markedly with increasing c , $R_0^{(S)}$ is found to be nearly independent of c , or to increase with increasing c . Similar behavior has been predicted theoretically by Marrucci.²⁸

With the stress-optic law in the form⁸ equation 12 for either $M_\kappa(t)$ or $\hat{M}_\kappa(\theta)$, Eqn. (57)

can be used with flow birefringence data. Since $N_{\kappa}^{(1)}$ is expected to be $R_0^{(S)}$ for small κ , it is seen that $2C = M_0/R_0^{(S)}$. Results in Figure 33 for M_{κ} are seen to be in satisfactory agreement with Eqn. (23). The results for $M_0/R_0^{(S)}$ are about thirty percent larger than values obtained at lower concentration. The data on M_{κ} show that the rodlike molecules are well aligned in the flow direction, but that for $\eta_0 R_{\kappa}^{(S)} > 1$, the orientation is not as great as would be expected had linear viscoelastic behavior obtained. The relaxation function $\hat{\eta}_{\kappa}(\theta)/\eta_{\kappa}$ and $\hat{M}_{\kappa}(\theta)/M_{\kappa}$ shown in Figure 34 are in qualitative accord with Eqn. (57), for which the behavior is similar to that obtained with flexible chain polymers in that the birefringence relaxes more rapidly than the stress.⁴¹

Nematic Solutions

Typical results shown in Figure 31 reveal an effect at small κ different from that observed with isotropic solutions (at only slightly smaller c), and not included in Eqn. (57). Thus, η_{κ} decreases with increasing κ , reaching a plateau $\eta_{\kappa} = \eta_p$ for $\eta_p R_{\kappa}^{(S)} = 1$. At the same time $R_{\kappa}^{(S)}$ is independent of κ for $\eta_p R_{\kappa}^{(S)} < 1$. It is tempting to attribute the behavior at small κ to effects of the anisotropy leading to Eqns. (58). In the latter, η_p and η_c represent the ratio σ/κ for steady state shear flow with the rodlike molecules held parallel to the flow direction and the direction of the shear gradient, respectively. Since $\eta_c > \eta_p$, effects which decrease λ toward unity cause a decrease in η_0 . In theoretical treatments^{36, 37} based on the diffusion equation of Doi and Edwards²⁶, λ and the Leslie-coefficient α_i are all functions of the order parameter S for the quiescent material.

$$S = \frac{1}{2} (3 \langle \cos^2 \theta \rangle - 1) \quad (62)$$

where θ is the angle between the rodlike molecules with the average calculated using the equilibrium distribution of θ , and S depends on c/c_c , increasing toward unit with increasing c/c_c . If steady-state flow at finite κ can be represented by Eqn. (58) with a modified order parameter S replacing the order parameter for the quiescent fluid, then η_0 might be expected to decrease as κ increases. With the α_i and λ given in Ref. 36 (see Table 9),

$$\eta_0 = \eta_b \frac{(1+2S)(2+3S)}{(2+S)} \quad (63a)$$

$$\eta_b = \eta_0^{ISO} \frac{(1-S)^4}{(1+S/2)} \quad (63b)$$

where η_0^{ISO} is given by Eqn. (18) with $B=0$, so that η_0 decreases as S increases toward unity. With the α_i and λ given in Ref. 37 (see Table 9), $\lambda < 1$ and simple shear flow is predicted to be unstable. Since the calculation for the α_i is delicate, the significance of this result is unclear for the observed behavior, which results in stable steady-state shear stress at all κ studied. With the α_i given in Ref. 37,

$$\eta_b = \eta^{\text{ISO}} \frac{(1-S)^4}{105} \{4(4S+7) + 35(5S-2)^{-1}\} \quad (64)$$

which is smaller (about 20%) than η_b given by Eqn. 63b for given S . (Similarly, the elongational viscosity obtained with the α_i in Ref. 36 is about twice that for the α_i in Ref. 37 for comparable S).

Flow birefringence data indicate a substantial degree of orientation for shear flows with $\eta_p R_0^{(S)} \kappa > 1$. For example, at such κ , the strong turbidity characteristic of the quiescent nematic fluid is lost, and the fluid in flow is much like that for a well oriented isotropic solution, with similar characteristics for the transmission of polarized light. For smaller κ (e.g., $\eta_p R_0^{(S)} \kappa < 0.1$), the transmitted intensity is smaller than expected, and tends to fluctuate. In particular, with $\eta_p R_0^{(S)} \kappa > 1$, the sum $I_+ + I_{11}$ of the intensities I_+ and I_{11} transmitted between crossed and parallel polars, respectively, is smaller than that for the quiescent fluid, and the overall field appears optically homogeneous (albeit birefringent and oriented). For $\eta_p R_0^{(S)} \kappa < 0.1$, the sum $I_+ + I_{11}$ is markedly depressed and the overall field is mottled in appearance. This is not consistent with the flow predicted in connection with Eqn. 60 (and the α_i in Ref. 36), and may suggest some kind of flow instability, perhaps similar to the effect predicted in connection with α_i given in Ref. 37.

Values of η_p plotted in Figure 3b are much smaller than η_0 extrapolated for the isotropic fluid, in some cases being in the range expected for an isotropic fluid with $cL/M_L = \alpha^*$. Based on the preceding discussion, it is not clear whether η_p should be identified with η_b or η_0 in Eqn. 60, or with neither of these.

In addition to the complicated flow birefringence behavior at small κ , it is found that $\eta_\sigma = (\partial J_\sigma / \partial t)^{-1}$ determined in creep at stress σ increases with decreasing shear rate $\partial \gamma_{ss} / \partial t$,

and is larger than η_p , see Figure 31, whereas η_κ determined in stress-growth with shear rate $\kappa = \partial \gamma_{ss} / \partial t$ is about equal to η_p . This unusual behavior may be related to the flow birefringence behavior reported above. In other respects, the rheological behavior is similar to that given by Eqn. 57. Thus, as shown in Figure 30, the $R_\sigma(t)$ determined after steady-state flow with $\eta_p R_\kappa \kappa \approx 1$ is similar to $R_0(t)$ for the nematic solutions. Values of the (apparent) λ_i and R_i calculated with Eqn. 14 and $R_\sigma(t)$ so determined lead to (apparent) τ_i and η_i that reproduce η_κ / η_p reasonable well for $\eta_p R_\kappa \kappa > 1$ using Eqn. 21.

Table 9: Leslie Coefficient for Rodlike Polymers

Parameter ^a	Ref. 36	Ref. 37 ^b
a_1/k	$-S^2$	$-rS^2$
a_2/k	$-S(1+2S)/(2+S)$	$-(S/2)[3(r-1)+2(1+2S)]/[3(r-1)+2+S] = -S(4S-1)/(5S-2)$
a_3/k	$-S(1-S)/(2+S)$	$-(S/2)[3(r-1)+2(1-S)]/[3(r-1)+2+S] = S(1-S)/(5S-2)$
a_4/k	$(1-S)/3$	$(7-5S-2rS^2)/35 = (1-S)[1-(2/35)(1-S)(7+4S)]/3$
a_5/k	S	$S(5+2rS)/7 = S[1-(2/21)(1-S)(3-4S)]$
a_6/k	0	$-2S(1-rS)/7 = -2S(1-S)(3+4S)/21$
λS^c	$1-(1-S)/3$	$r-(1-S)/3 = -1-5(1-S)/3$
r	---	$1-4(1-S)/3$

a) $k = \eta_0^{\text{ISO}}(1-S)^2$; η_0^{ISO} given by Eqn. (18) with $B=0$.

Since $a_2 + a_3 = a_6 - a_5$, only five of the a_i are independent.

b) Based on asymptotic behavior for a_i given in ref. 37 and approximate relations for λ and r .

c) $\lambda = (a_2 + a_3)/(a_2 - a_3)$.

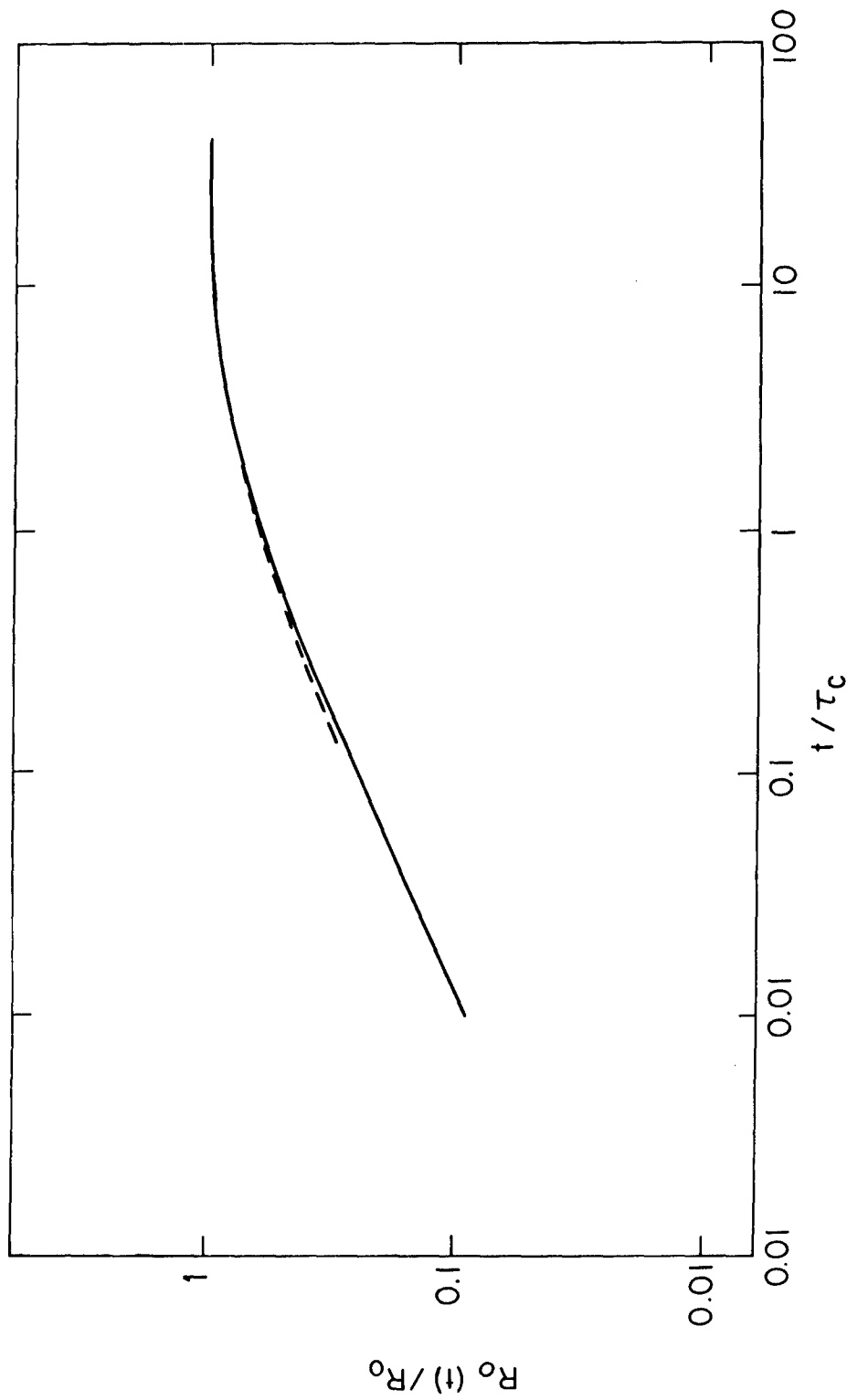


Figure 30:

$R_0(t)/R_0$ versus t/τ_c (with $\tau_c = \eta_0 R_0$) for an isotropic solution of PBT-53 (0.0294 weight fraction polymer), c_{∞} , and $R_0(t)/R_0$ versus $t/\eta_p R_0$ for a nematic solution of the same polymer (0.0323 weight fraction polymer), $\frac{t}{\eta_p R_0}$. For the latter, $R_0(t)$, R_0 , and η_p were determined after steady-state flow with $\eta_p R_0 \approx 1$.

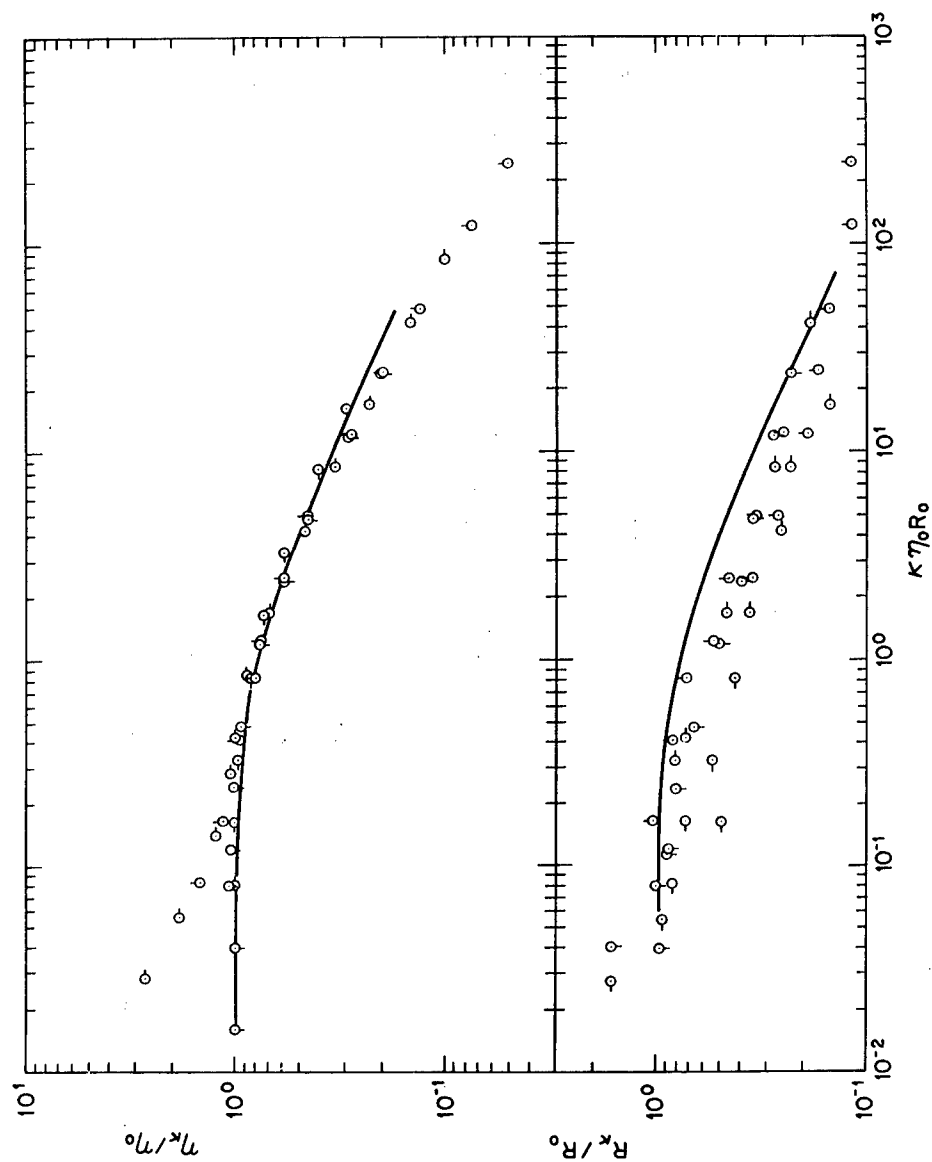


Figure 31: Rheological data³ for isotropic (—O, O) and nematic (O—, O) solutions of PBT-53 (0.0323 weight fraction polymer. With the latter, η_0 is replaced by $\eta_{\eta'}$, see text. The curves are calculated with Eqns. 3.3 and 3.4 using experimentally determined values of τ_i and η_i .

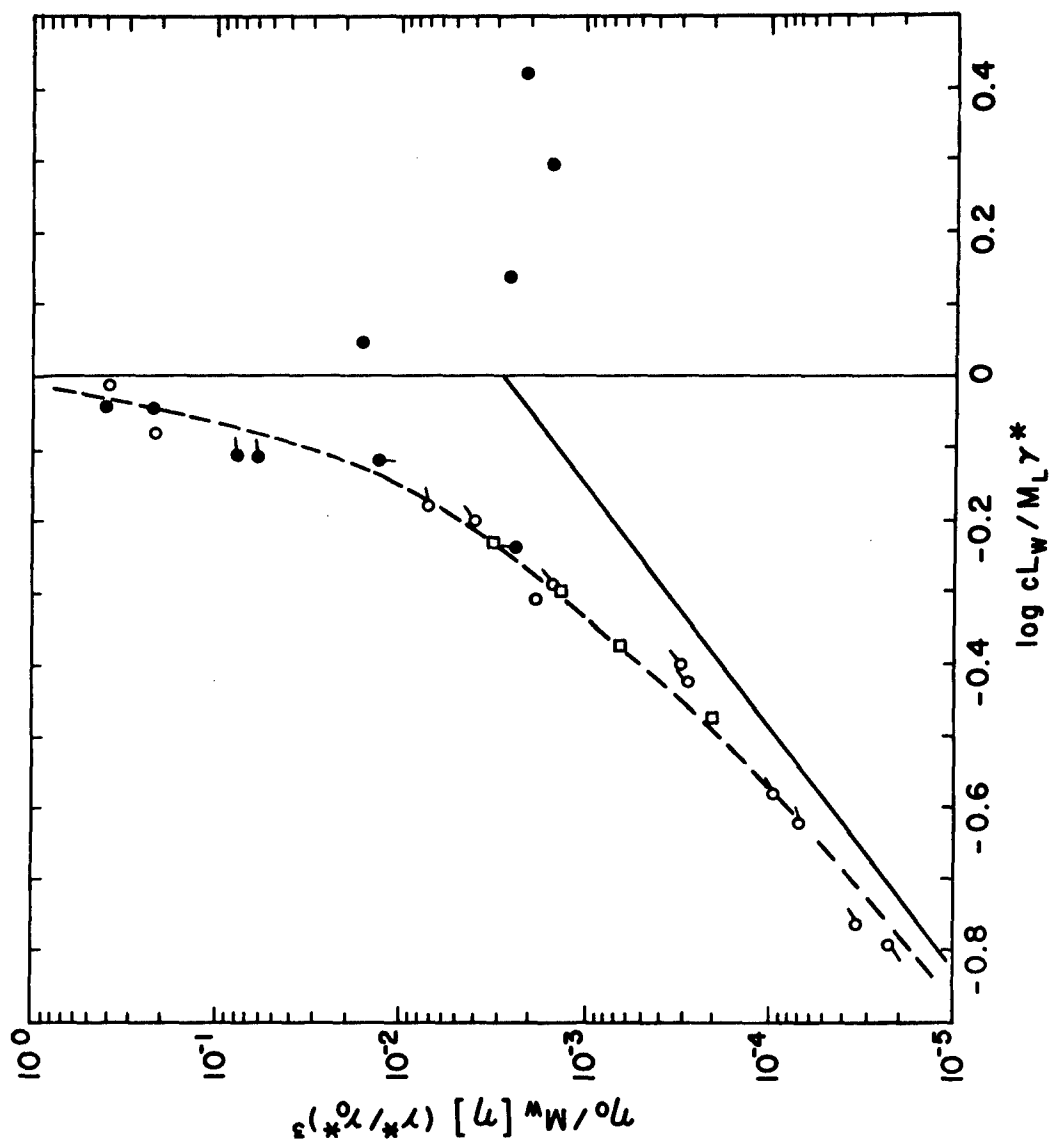


Figure 32: $\eta_0/M_w [\eta] (\gamma^*/\gamma_0^*)^3$ versus $BcL_w/M_L \alpha^*$ for isotropic and nematic solutions of PBT-53 and PBT-82. With the nematic solutions, η_0 is replaced by η_p (α^* is a constant).

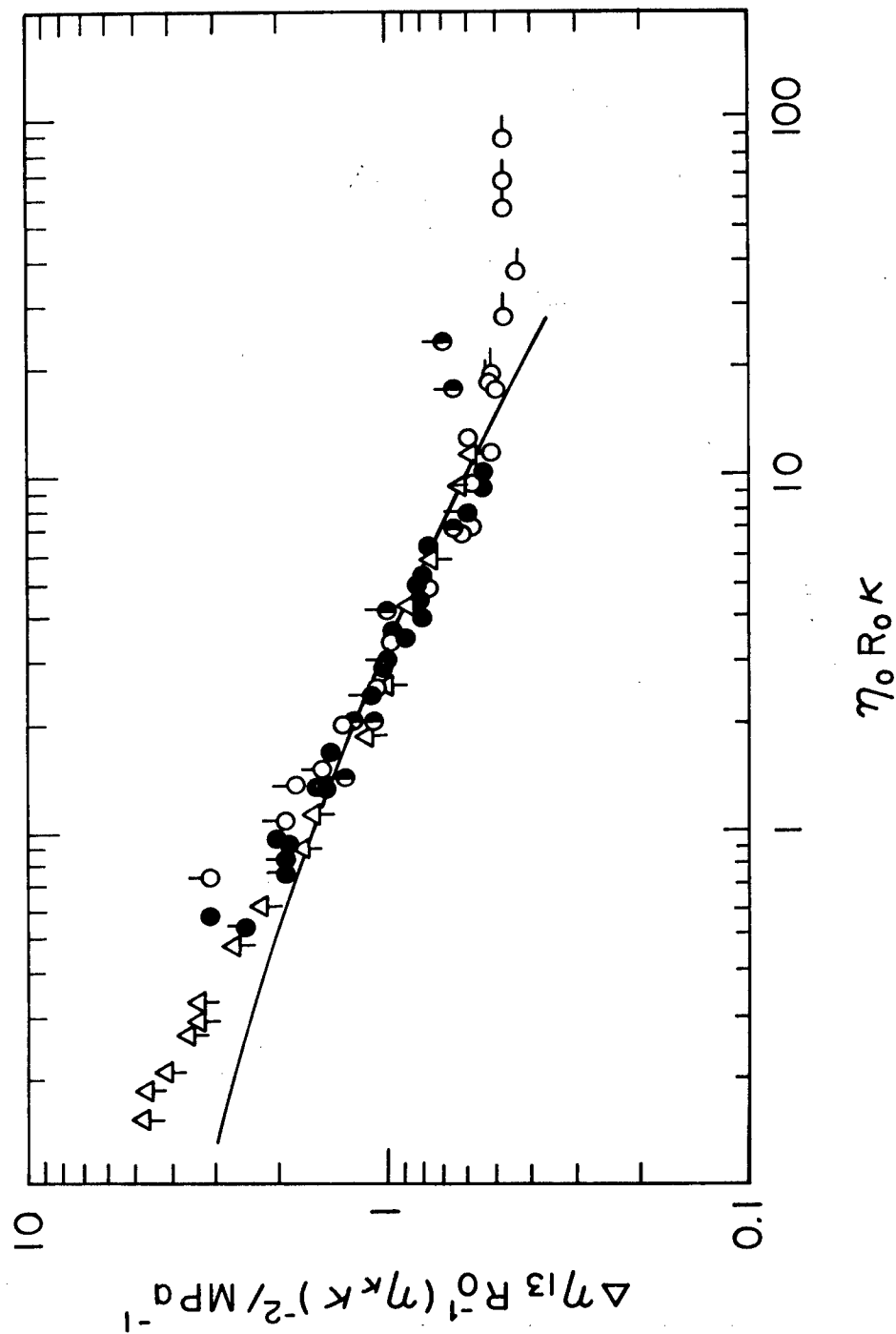


Figure 33:

The steady-state flow birefringence versus the reduced shear rate $\eta_0 R_0 K$ for an isotropic solution of PBT-53 (0.0255 weight fraction) at several temperatures. The curve is calculated with Eqns. 3.5 and 3.10 using experimentally determined values of τ_i and η_i .

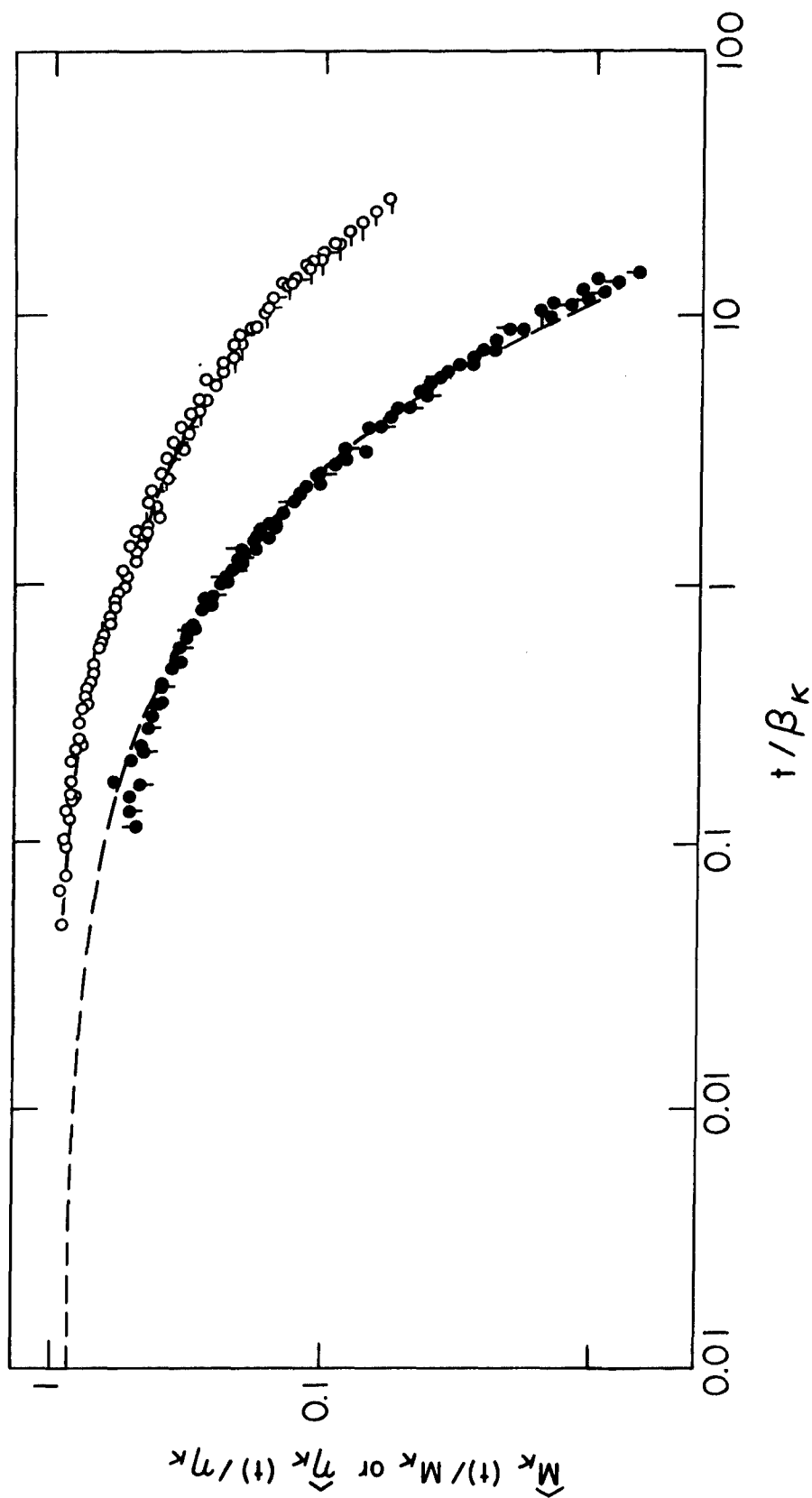


Figure 34:
The reduced flow birefringence relaxation function $\hat{M}_\kappa(t)/M_\kappa$ and stress relaxation function $\hat{\eta}_\kappa(t)/\eta_\kappa$ for anisotropic solution of PBT-53 (0.0294 weight fraction) for several shear rates, $\beta_\kappa \approx \tau_\kappa R_\kappa$.

4. STEADY-STATE AND TRANSIENT RHEOLOGICAL AND RHEO-OPTICAL PROPERTIES OF MIXTURES OF RODLIKE AND FLEXIBLE CHAIN POLYMERS IN ISOTROPIC SOLUTIONS

SUMMARY

Steady-state and transient rheological and rheo-optical properties have been studied for mixtures of PBT and nylon-66 in methane sulfonic acid solutions. The solutions were all isotropic. The zero-shear viscosity was found to exhibit an unusual dependence on composition, possibly related to constraints on translational diffusion of PBT parallel to the molecular axes. Reduced viscosity and flow birefringence behavior for the mixture can be represented using a single integral constitutive equation with a distribution of relaxation times that is similar to that for the nylon free solution, after normalization of the relaxation times by the terminal relaxation time.

INTRODUCTION

Rodlike molecules form nematic liquid crystalline solutions in which the molecular axes tend to be parallel. Such solutions may be oriented in flow, and formed into fibers and films which have well developed uniaxial orientation that confers ultrahigh stiffness and rigidity in the preferred direction (typically, the mechanical properties in the transverse direction are poor). In solution, blends of rodlike chains and flexible chain polymers will form a single isotropic phase under certain conditions (typically involving low concentration of the two components), or will form two phases, an isotropic phase rich in the flexible component and an ordered (usually nematic) phase rich in the rodlike component--a theoretical model of Flory and co-workers⁴⁴ predicts such behavior. Solution processing of the isotropic phase offers the possibility to prepare a molecular composite in which the rodlike chains are dispersed among the flexible chains. Since such an arrangement would not represent an equilibrium state, the dispersion would have to be trapped by manipulation involving the kinetics of the various operations. For example, the rodlike chains could be given a certain preferred orientation using shear or elongational deformations. Subsequently, it would be necessary to maintain this orientation as the solvent is removed, perhaps through a process involving coacervation.

The mechanical properties of a molecular composite should present features unavailable

with other materials. For example, these materials may exhibit superior (though not ultrahigh) rigidity and strength, either uniaxially or biaxially, depending on the orientation introduced in processing. It may also be possible to prepare heat-formable composites by judicious selection of the flexible chain polymer. In some cases, the rodlike polymer may exhibit useful optical properties that can be exploited if the flexible chain polymer is amorphous and transparent.

The successful imposition of molecular orientation through processing in materials comprising mixtures of rodlike and flexible chain polymers will require control and exploitation of the nonlinear rheological properties of the fluids. For the deformation rates of interest one can anticipate that the constitutive equation for the fluids of interest will be no simpler than the form (expressed within a hydrostatic pressure)

$$\sigma_{ij}(t) = - \int_0^\infty ds \frac{\partial G_0(s)}{\partial s} Q_{ij}(t,s) \quad (65)$$

found for certain rodlike polymers and for flexible^{3, 26} chains. Here $G_0(t)$ is the relaxation modulus of linear viscoelasticity and $\tilde{Q}(t,s)$ a tensor dependent on the strain history between times s and t --examples of \tilde{Q} for shear and elongational deformations are given in the Appendix B. (If the fluid is anisotropic at rest, this relation may be more complex, with $\partial G_0(t)/\partial t$ replaced by a tensor.) To the extent that Equ. (65) applies, the function $G_0(t)$ becomes central to understanding and predicting the processing behavior of the fluid of interest inasmuch as \tilde{Q} appears to take a nearly universal form for coil and rodlike chains.^{3, 26} Unfortunately, we are not able to predict $G_0(t)$ for heterodisperse mixtures, and systematic studies on $G_0(t)$ for mixtures of coil and rodlike chains are lacking. In this chapter, we report studies on solutions containing coil and rodlike chains to elucidate $G_0(t)$ as a function of composition and to evaluate the applicability of Equ. (65) to these materials for nonlinear deformations. The latter, of course, would be of central interest in attempts to design appropriate processing strategies for the fabrication of oriented samples. For rodlike fluids discussed in the preceding and coil like chains⁴¹, the steady-state birefringence $\Delta n_\kappa^{(13)}$ in shear deformation at shear rate κ can be represented by the expression

$$\Delta n_\kappa^{(13)} = 2CN_\kappa^{(1)}(t)(\eta_\kappa \kappa)^2 \quad (66)$$

where

$$N_{\kappa}^{(1)} = [\sigma_{11} - \sigma_{22}]_{\kappa} / 2(\eta_{\kappa} \kappa)^2$$

with $\eta_{\kappa} = \sigma_{12}/\kappa$ the steady-state viscosity at shear rate κ , and C is a material constant. Study of $\Delta n_{\kappa}^{(13)}$ provides information on the molecular orientation, and so is of direct interest in assessing the effects of flow on orientation. In principle, and practice for solutions of either rodlike or coil chains, Equ. (65) may be used to compute the functions $N_{\kappa}^{(1)}$ and η_{κ} appearing in the Equ. (66). The application of these relation for a solution of mixtures of rodlike and coil chains, is discussed in the following.

EXPERIMENTAL

Nylon-66 and PBT samples were provided through Dr. W. Adams, Wright-Patterson Air Force Base, Ohio. The PBT has $[\eta] = 3600$ ml/g, or a viscosity average contour length $L_{\eta} = 200$ nm. Mixtures were prepared with the compositions given in Table 10. In all cases, the compositions appeared isotropic and homogeneous when viewed with a polarizing microscope at temperatures between 0 and 60 degrees centigrade.

Rheological and rheo-optical experiments were carried out as described in preceding chapters of this report.

RESULTS

Values of the zero shear viscosity η_0 and the linear steady-state recoverable compliance R_0 are given in Table 10 (the data are reduced to 297K). Values of the time constant τ_c are also given in Table 10. Values of $\eta_0/\eta_s M[\eta]$ are shown as a function of cL_{η} in Figure 35. Data for PBT solutions are shown for comparison; in Figure 35. c refers to only the PBT concentration. The viscosity for nylon solutions containing no PBT is given in Figure 36; it may be seen that η_0 for the nylon solutions is very small.

The flow curve, η_{κ} versus κ ; and the dynamic viscosity, η^* versus ω , are shown in Figure 37 for one composition. Reduced curves for η_{κ}/η_0 , R_{κ}/R_0 , and $\Delta n_{\kappa}^{(13)} R_0$ versus $\tau_c \kappa$ are given in Figures 37 to 40; and reduced curves for the stress relaxation $\hat{\eta}_{\kappa}(t)/\eta_{\kappa}$; and the flow birefringence relaxation, $\hat{M}_{\kappa}(t)/M_{\kappa}$ versus t/β_{κ} are given in Figures 41 and 42.

DISCUSSION

As shown in Figure A, the data on $\eta_0/\eta_s M[\eta] c L_\eta$ for the mixture form a smooth curve. For the mixture with the smallest PBT concentration c studied, η_0 for the mixture is about equal to η_0 for a PBT solution with the same c , but with no nylon. For the mixture with the largest c studied, η_0 for the mixture is about ten-fold larger than the comparable nylon-free PBT solution. For the c -range studied, $\eta_0/\eta_s M[\eta]$ for the nylon free solutions is given by Eqn. 18, with the factor $(1-BX)^{-2}$ about equal to unity, i.e., $\eta_0/\eta_s M[\eta]$ is proportional to $(cL_\eta)^3$. The gradual departure from this behavior for the mixture with increasing c may indicate that a "free-volume" factor, similar in origin to the factor $(1-BX)^{-2}$, may become important for the mixtures. This would indicate restriction on the translational motion of the rodlike PBT chains parallel to their axes due to the presence of the nylon. Alternatively, the viscosity of the mixture could be enhanced by some more direct entanglement-like constraint on PBT by the nylon. We prefer the former explanation at this time, especially as the data in Figure 35 show that the nylon-66 is well below its own entanglement concentration (e.g., η_0/η_s is about proportional to the nylon concentration in the absence of PBT).

The data in Figure 37 show that the equivalence of η_κ and $\eta^*(\omega)$ for $\eta = \omega$, which is characteristic behavior of both rodlike and coil chains, is also obtained with the mixtures. Moreover, as shown in Figure 38, the flow curve η_κ/η_0 versus $\tau_c \kappa$ is independent of the composition, and is also the same for the mixtures and the nylon-free PBT solutions, despite the appreciable dependence of τ_c on these variables. Thus, as interpreted with Eqn. (21), the distribution of reduced relaxation times τ_i/τ_c is not affected by composition for these samples. This implies that the relaxation times for the nylon are far smaller than those for PBT. Similar behavior is observed in the reduced behavior for $\Delta n^{(13)} R_0$ versus $\tau_c \kappa$. Consequently, for these mixtures, the rheological behavior in steady-state flow is very similar to that discussed in the first chapter of this report.

Similarly the stress and flow birefringence relaxation shown in Figures 41 and 42 form reduced curves using a reduced time t/β_κ , with β_κ chosen empirically. As with the rodlike chain alone (e.g., see chapter 1), β_κ/τ_c appears to depend only on $\tau_c \kappa$; see Figure 43. Also, as with those solutions, $\beta_\kappa \approx \tau_\kappa$, so that β_κ decreases markedly with increasing η .

Table 10: Compositions of PBT-Nylon Solutions Studied

PBT NY	Wt% Polym.	Wt% PBT	Wt% Nylon	T °K	η_0 poise	$\eta_0 A^{-1a}$ poise	R_0 cm ² /dyne	τ sec
80/20	2.43	1.944	0.486	302	190×10^4	238×10^4	(0.0104) ^b	24800
100/0	1.80	1.80	0	301	2.3	2.76	0.0038	105
70/30	2.50	1.75	0.75	288	165	108	(0.0117)	12600
50/50	2.55	1.275	1.275	302	8.4	10.5	(0.0106)	1110
40/60	2.78	1.112	1.668	288	28.5	18.6	(0.0185)	3440
30/70	2.77	0.831	1.939	302	2.2	2.76	0.0130	359
100/0	0.82	0.82	0	302	0.47	0.59	0.0098	58
20/80	2.72	0.544	2.176	301	0.17	0.20	0.0082	17

(a) $A = \exp E(T^{-1} - T_r^{-1})$ with $E=4065K$ and $T_r=297$ °K

(b) R_0 in parenthesis are calculated as τ_c/η_0 with τ_c determined from fit of η_κ/η_0 vs. κ with curves of η_κ/η_0 vs. τ_κ .

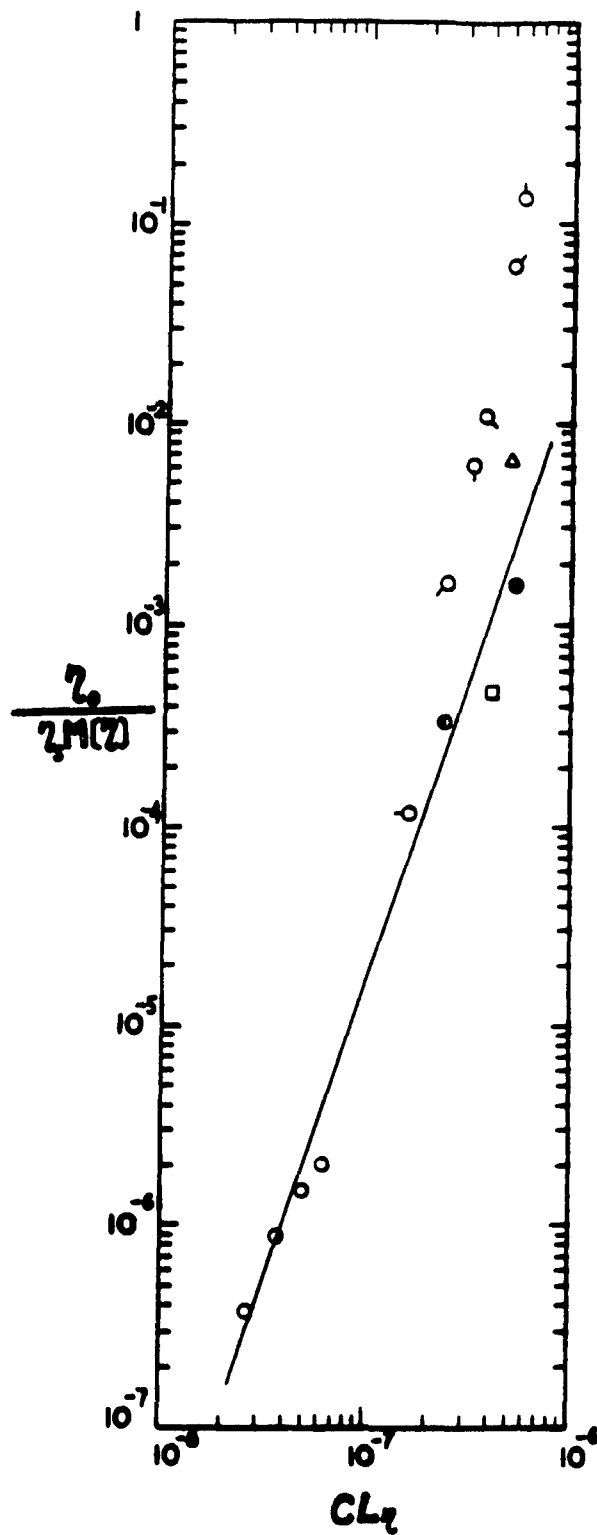


Figure 35:

The zero shear viscosity η as η_0/η , $M[\eta]$ vs. CL_T for PBT-nylon mixtures (circles with pipe) and PBT in nylon-free solutions --c refers to PBT concentration only, in methane sulfonic acid. For the mixture, the compositions are (see Table 10), 20/80, ; 30/70, ; 40/60, ; 50/50, ; 70/30, ; and 80/20, .

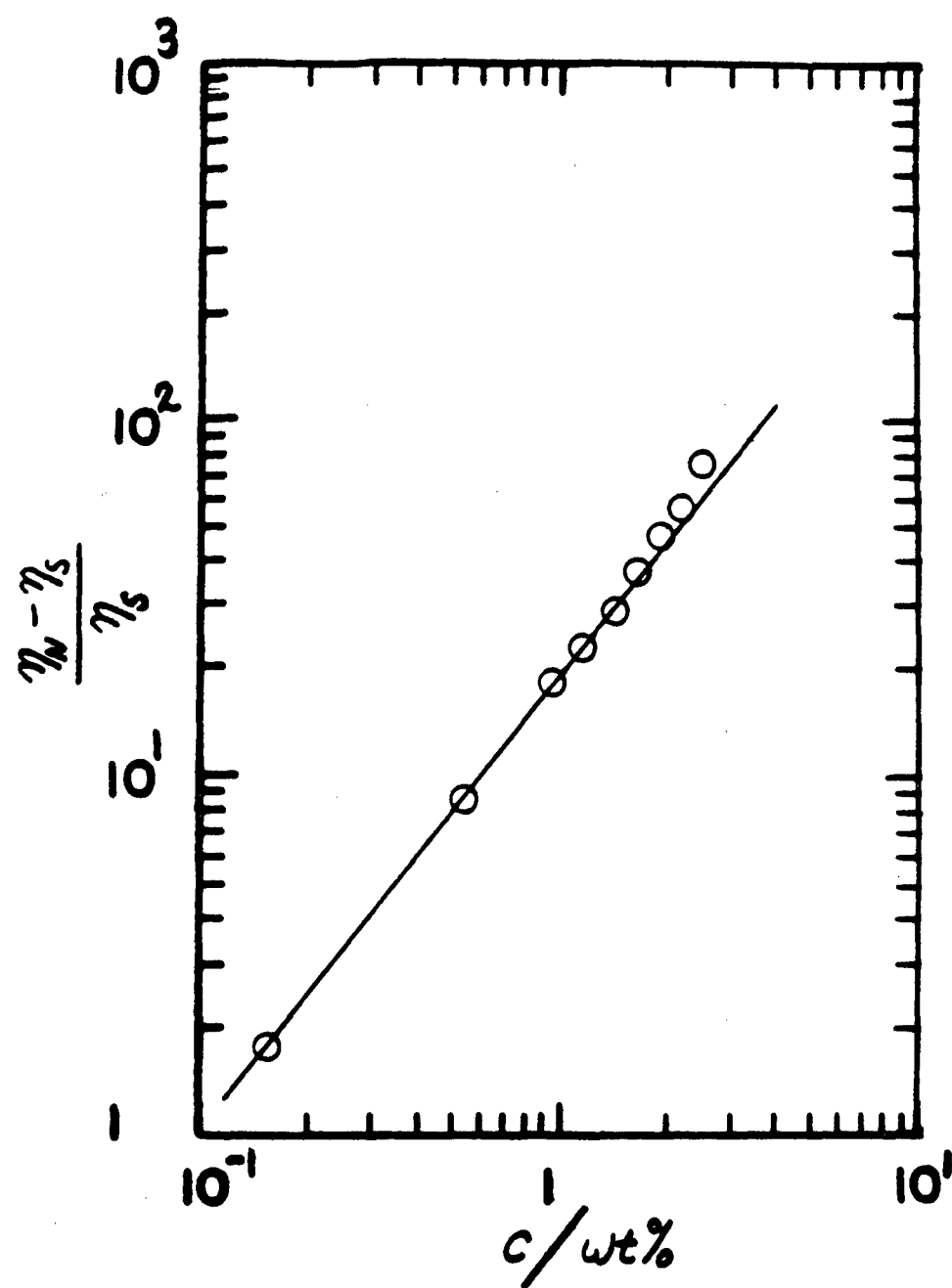


Figure 36:
The viscosity of the nylon-66 polymer used as a function of the nylon concentration (in PBT free solutions).

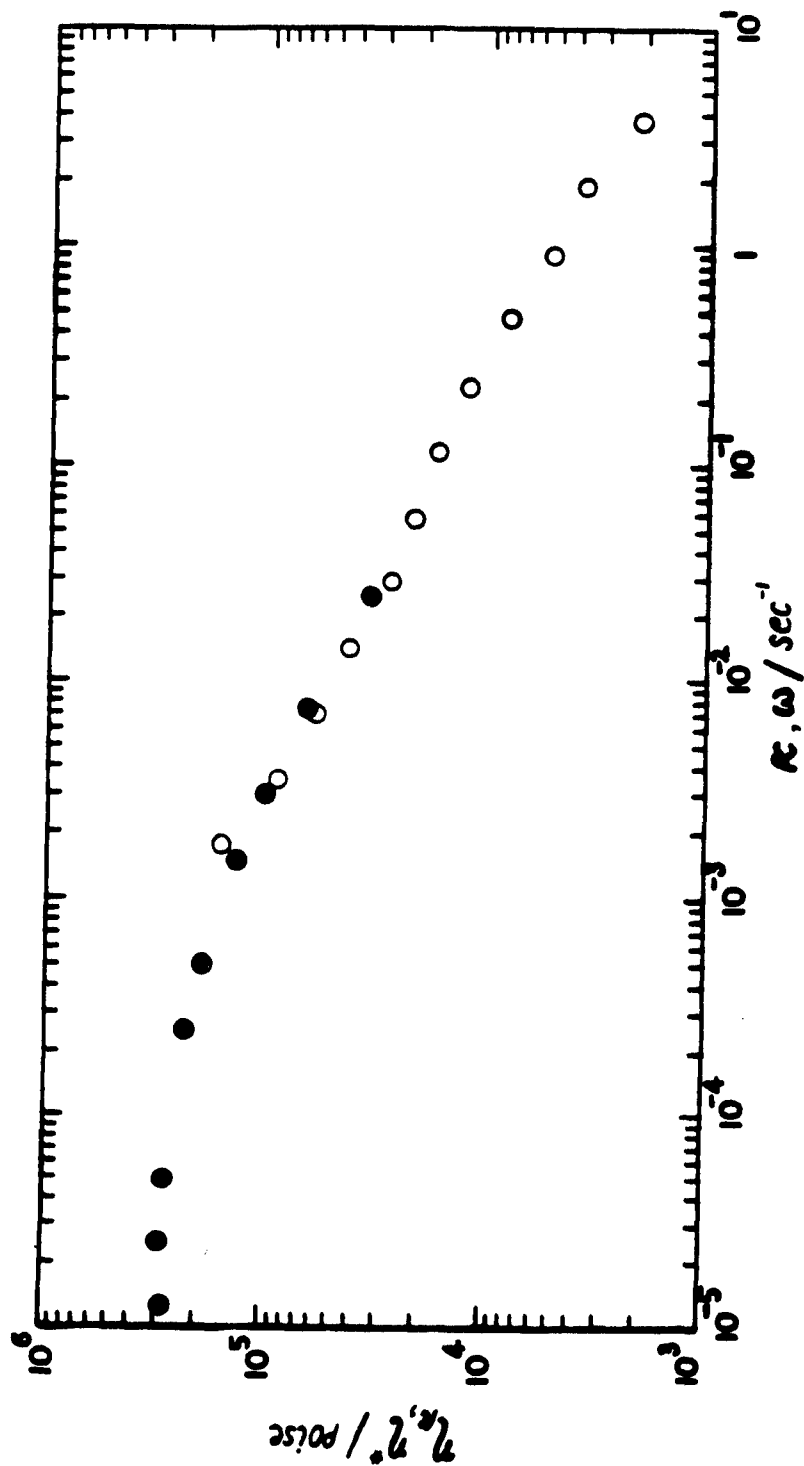


Figure 37:
The viscosity η_0 versus ω and the dynamic viscosity $\eta^*(\omega)$ versus ω for the 50/50 PBT/nylon mixture.

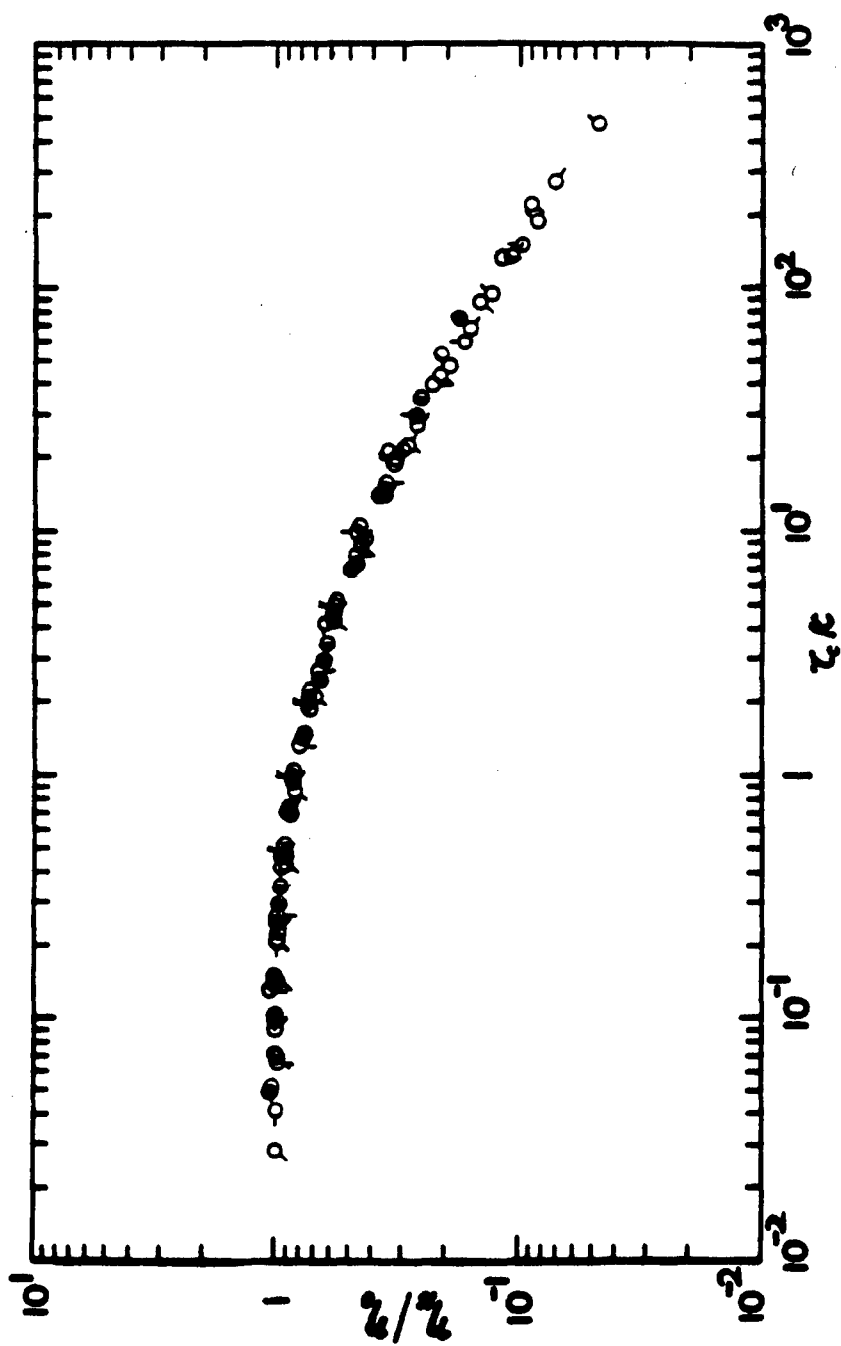


Figure 38: Steady-state flow curve for PBT-nylon mixture and PBT solutions; symbols are as in Fig. 35

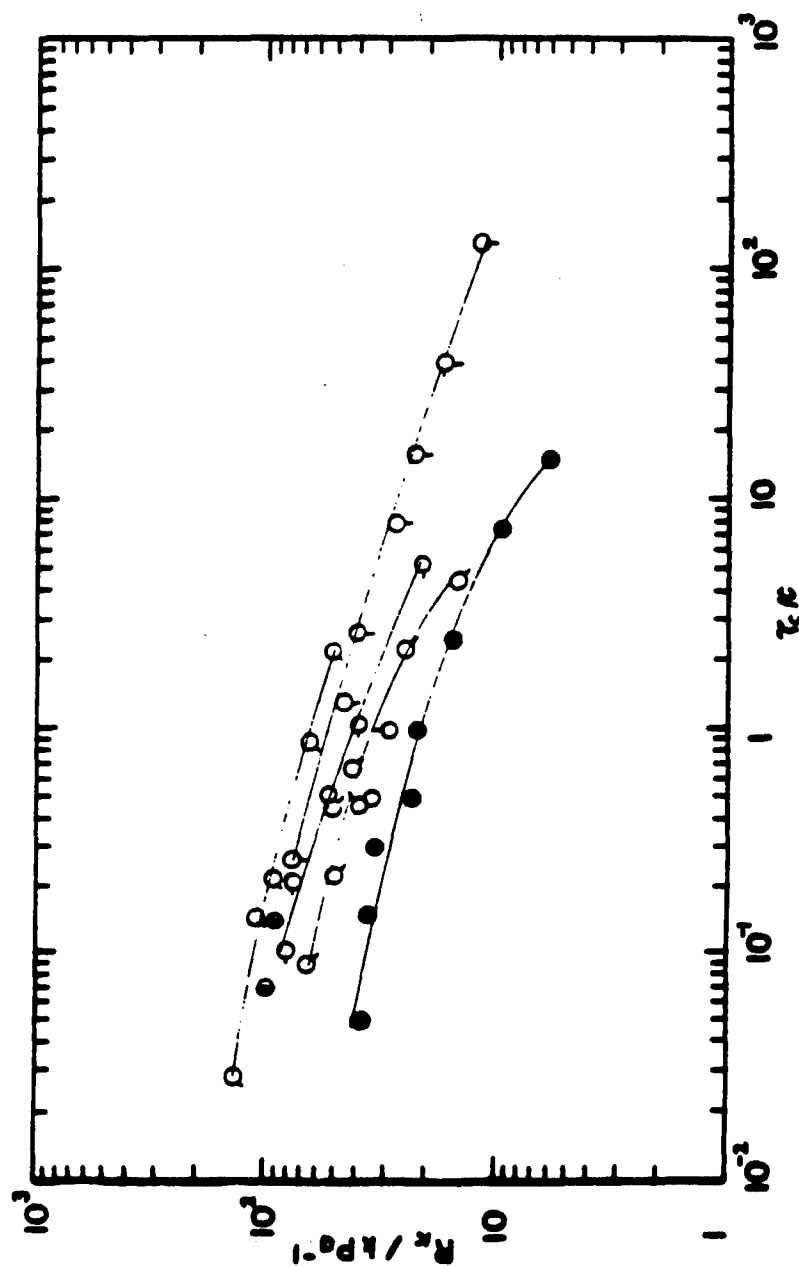


Figure 39:
Steady-state recoverable compliance curve for PBT-nylon mixture and PBT solutions; symbols are as in Fig. 35.

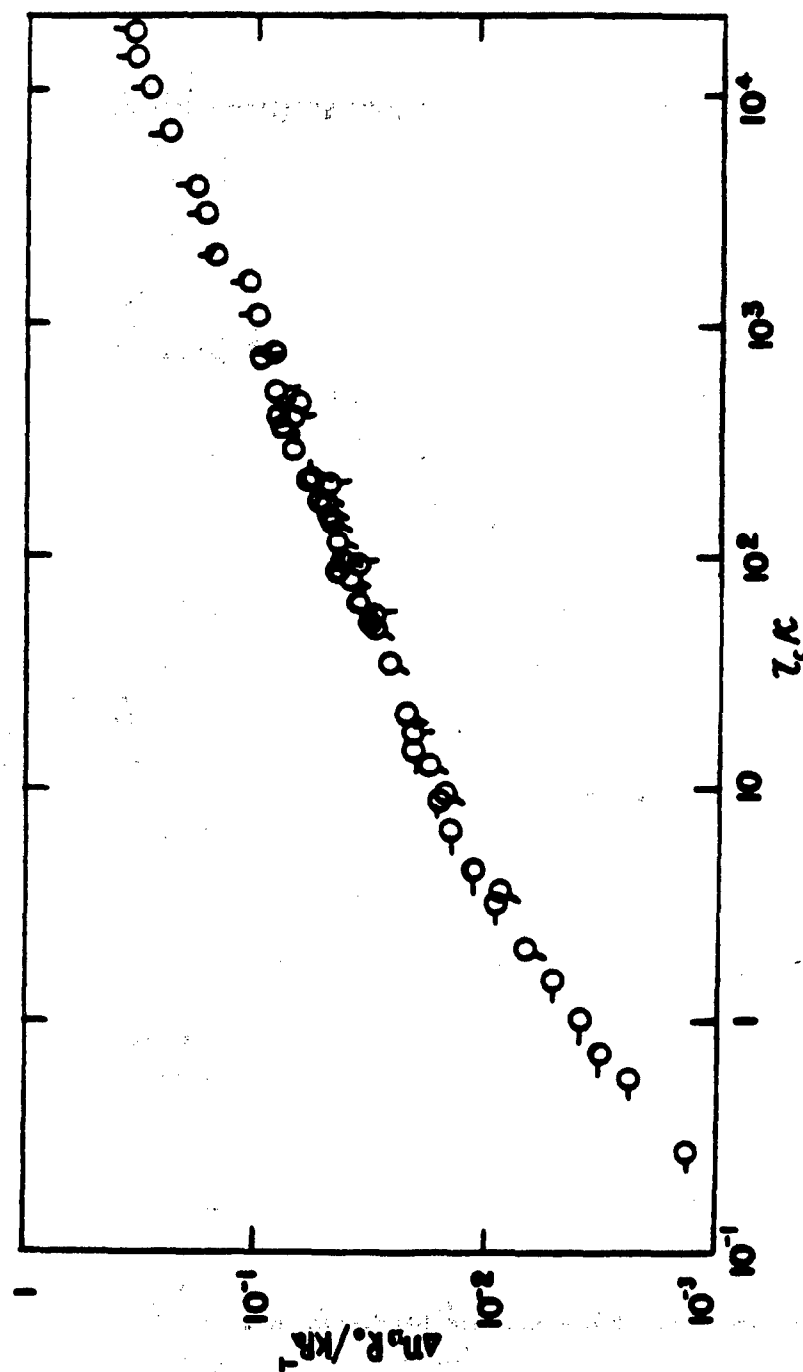


Figure 40:
Steady-state flow birefringence for mixtures (PBT and nylon in solution; symbols are as in Fig. 35.

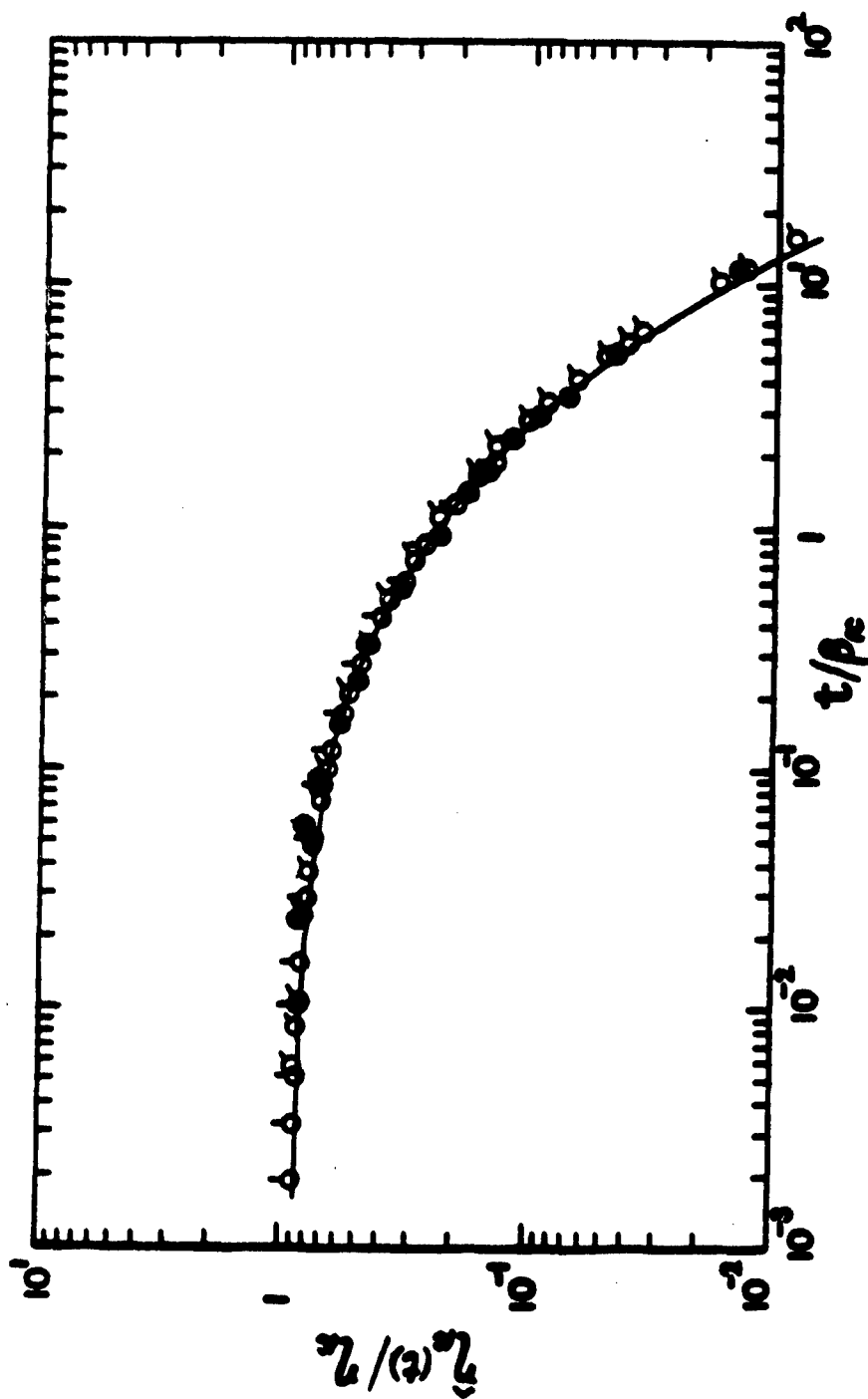


Figure 41:
Stress relaxation for mixture of PBT/nylon and PBT solutions; symbols are as in Fig. 35.

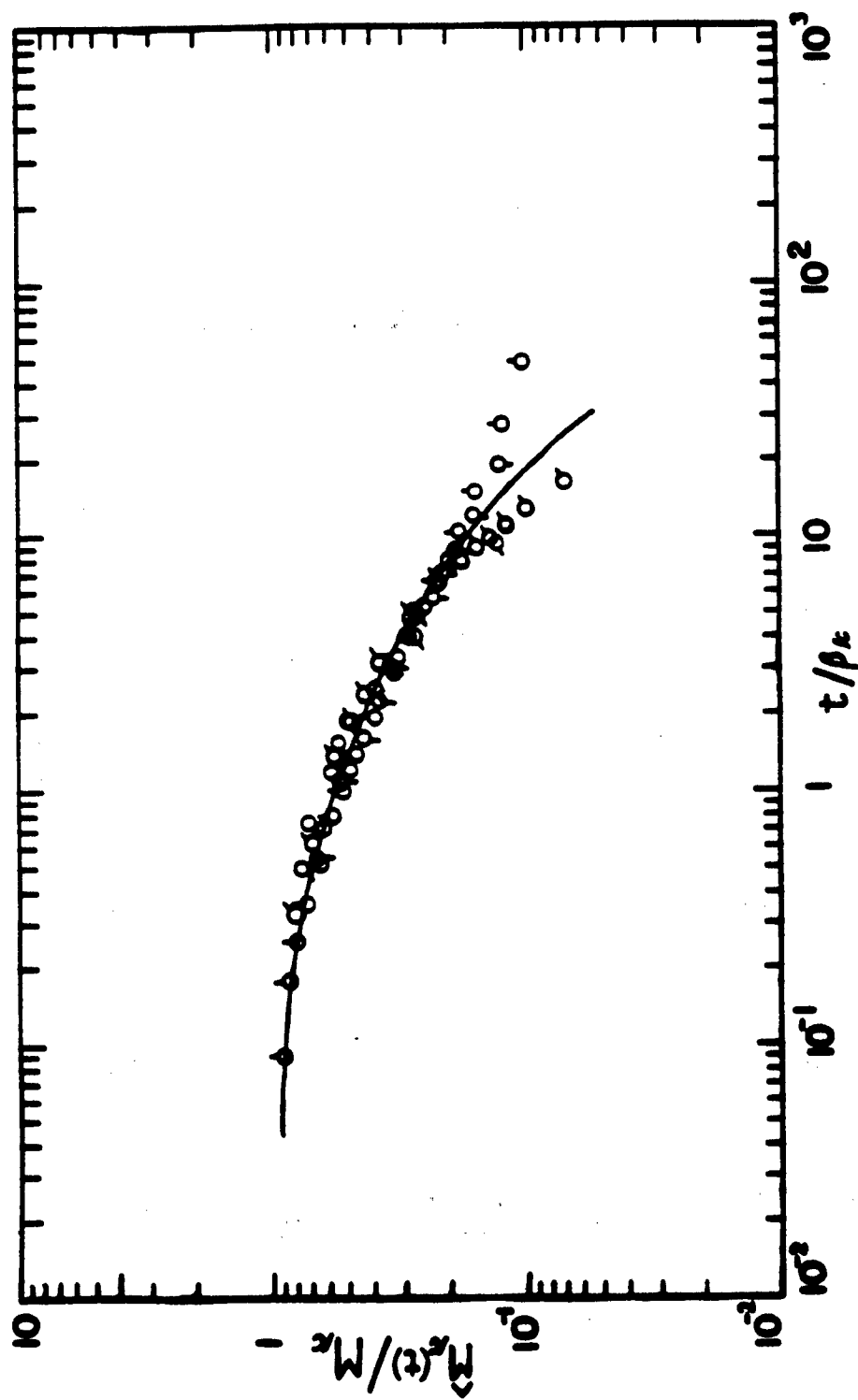


Figure 42:
Flow birefringence relaxation for PBT/nylon mixtures in solution; symbol as in Fig. 35.

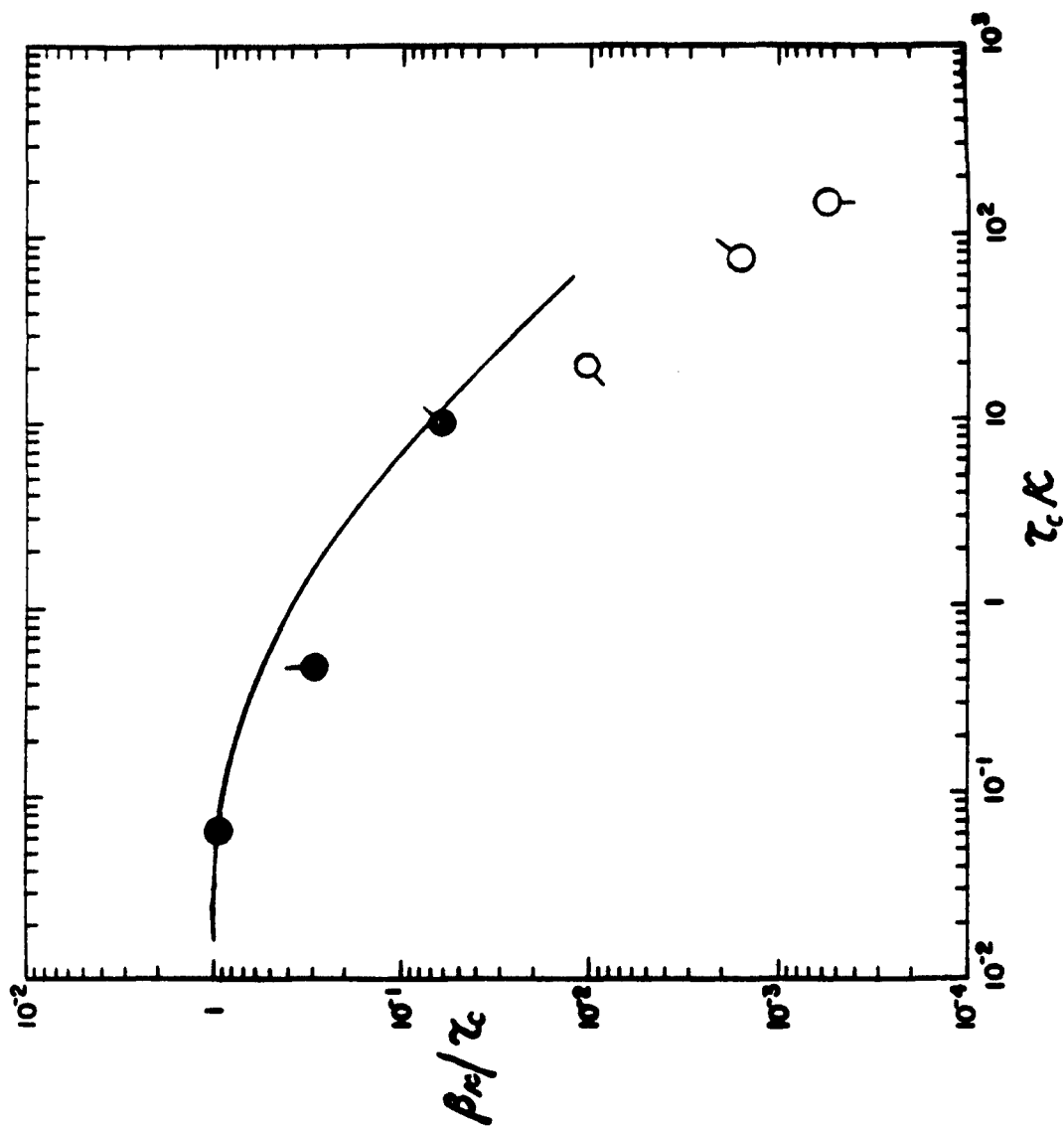


Figure 43:

The shift factor β_c versus $\tau_c \kappa$

References

1. S.-G. Chu, S. Venkatraman, G. C. Berry, and Y. Einaga, *Macromolecules* **1981** *14*, 939.
2. G. C. Berry, B. L. Hager, and C.-P. Wong, *Macromolecules* **1977**, *10*, 361.
3. K. Nakamura, C.-P. Wong, and G. C. Berry, *J. Polymer Sci., Polymer Physics Ed.*, **22**, 1119 (1984).
4. H. Markovitz and G. C. Berry, *Ind. Eng. Chem. Prod. Res. Div.* **1978**, *17*(2), 95.
5. H. Markovitz, in "*Am. Inst. Phys. 50th Anniversary Physics Vade Mecum*", Ed., H. L. Anderson, Am. Inst. Phys., New York, 1981, Chapter 19.
6. J. D. Ferry, *Viscoelastic Properties of Polymers*, Wiley, New York, NY, 3rd Ed., 1980.
7. R. Sips, *J. Polym. Sci.* **1951**, *7* 191.
8. H. Janeschitz-Kriegl, *Adv. Polym. Sci.* **1969**, *6*, 170.
9. B. D. Coleman, E. H. Dill, and R. A. Toupin, *Arch. Ration. Mech. Anal.* **1970**, *39*, 358.
10. C. C. Lee, S.-G. Chu, and G. C. Berry, *J. Polym. Sci., Polym. Phys. Ed.* **1983**, *21*, 1573.
11. C.-P. Wong and G. C. Berry, *Polymer* **1979**, *20*, 229.
12. G. C. Berry and C.-P. Wong, *J. Polym. Sci., Polym. Phys. Ed.* **1975**, *13*, 1761.
13. G. C. Berry, P. Metzger, D. B. Cotts, and S.-G. Chu, *British Polym. J.* **1980** *16*, 947.
14. E. V. Menezes and W. W. Graessley, *Rheol. Acta* **1980** *19*, 38.
15. K. Osaki, N. Bessho, T. Kojimoto, and M. Kurata, *J. Rheology* **1979** *23*, 457.
16. A. V. Tobolsky, *Properties and Structure of Polymers*, Wiley, New York, 1960, p. 188.
17. W. W. Graessley, *Adv. Polym. Sci.* **1974**, *20*, 229.
18. B. Bernstein, E. A. Kearsley, and L. J. Zapas, *Trans. Soc. Rheol.* **1963** *7*, 391.
19. L. Onsager, *Am. N.Y. Acad. Sci.* **1949** *51*, 627.
20. P. J. Flory, *J. Proc. R. Soc. London, Ser. A* **1956**, *234*, 73.
21. P. J. Flory and R. S. Frost, *Macromolecules* **1978**, *11*, 1126.
22. J. K. Moscicki and G. Williams, *Polymer* **1982**, *23*, 588.
23. H. Yamakawa, *Modern Theory of Polymer Solutions*, Harper and Row, New York **1971** p. 180.

24. G. C. Berry and D. B. Cotts, *Macromolecules* **1981** *14*, 930.
25. M. Doi, *J. Phys. (Paris)* **1975**, *36*, 607.
26. M. Doi and S. F. Edwards, *J. Chem. Soc., Faraday Trans. 2* **1978**, *74*, 560.
27. J. A. Odell, E. D. T. Atkins, A. Keller, *J. Polymer Sci., Polymer Lett. Ed.* **21**, 289 (1983).
28. G. Marrucci and N. Grizzuti, *J. Non-Newtonian Fluid Mech.*, **14**, 103 (1984).
29. V. N. Tsvetkov, et al. *Structure of Macromolecules in Solution* (English Translation); National Lending Library for Science and Technology: Boston Spa, England, 1971; Vol. 3, Chapter 7.
30. N. Y. Kuzuu and M. Doi, *Polymer J.* **1980** *12*, 883.
31. H. M. Laun, *Rheol. Acta* **1978** *17*, 1.
32. K. F. Wissbrun, *J. Rheology* **25**, 619 (1981).
33. M. Doi, *J. Polymer Sci., Polymer Phys. Ed.* **19**, 229 (1981).
34. G. C. Berry, P. Metzger Cotts and S.-G. Chu, *Brit. Polymer J.* **13**, 47 (1981).
35. T. Asada, H. Muramatsu, R. Watanabe and S. Onogi, *Macromolecules* **13**, 867 (1980).
36. G. Marrucci, *Mol. Cryst. Liq. Cryst. (Lett.)* **72**, 153 (1982).
37. N. Kuzuu and M. Doi, *J. Phys. Soc. Japan* **52**, 3486 (1983); **53**, 1031 (1984).
38. G. Kiss and R. S. Porter, *J. Polymer Sci., Polymer Symp.* **65**, 193 (1978).
39. F.M. Leslie, *Archs. Ration. Mech. Anal.*, 1968, **28**, 265.
40. J.L. Erickson, *Arch. Ration. Mech. Anal.*, 1960, **4**, 231.
41. K. Osaki, N. Bessho, T. Kojimoto and M. Kurata, *J. Rheol.*, 1980, **24**, 125.
42. M. H. Birnboim, G. C. Berry, J. O. Park, and D. J. Plazek, to be submitted.
43. N. J. Alderman and M. R. Mackley, *Faraday Disc. Chem. Soc.*, 1985, **79**.
44. M. Matheson and P. J. Flory, *Macromolecules*, 1981, **14**, 9 54.

Appendix A

The functions $q_{\kappa,i}$, $r_{\kappa,i}$ and $p_{\kappa,i}$ in Eqns. 21 - 23 are given by³

$$q_{\kappa,i} = (1 + af_i - f_i^2) \exp - g_i \quad (A1)$$

$$r_{\kappa,i} = \exp - R_{\kappa} \eta_{\kappa} / \tau_i \quad (A2)$$

$$p_{\kappa,i} = 1 - \frac{1 - f_i}{2} \frac{(f_i + g_i)^2 + f_i^2}{1 + af_i - f_i^2} \quad (A3)$$

where $f_i^{-1} = 1 + \tau_i \kappa / \gamma''$, $g_i = \gamma' / \tau_i \kappa$ and $a = \gamma' / \gamma''$. For $a = 0$,^{3,31}

$$(1 - q_{\kappa,i}) = (1 + \tau_i \kappa / \gamma'')^{-2} \quad (A4)$$

$$(1 - q_{\kappa,i} p_{\kappa,i}) = (1 + \tau_i \kappa / \gamma'')^{-3} \quad (A5)$$

The expression for $\eta_{\kappa}(t)$ for $\kappa t > \gamma'$ is given by

$$\eta_{\kappa}(t) = \sum \eta_i [1 - q_{\kappa,i} + q_{\kappa,i}(z)] \quad (A6)$$

$$q_{\kappa,i}(z) = (z f_i - f_i^2) \exp [-(z-a)/(1-f_i) - g_i]$$

where $z = \kappa t / \gamma''$

Appendix B

In general, the tensor \underline{Q} takes on the form

$$Q_{ij} = Q_{ij}^0 F_{ij}$$

where Q_{mn}^0 is the limiting behavior obtained for "recently small deformations" (e.g., very slow deformations, or arbitrarily fast deformations at short times), and F_{pq} accounts for nonlinear effects. For example for shear flows with shear strain history $\gamma(t)$, the tensor components are given by

$$\underline{Q}^0(t,s) = \begin{pmatrix} 1 + \gamma^2(t,s) & \gamma(t,s) & 0 \\ \gamma(t,s) & 1 & 0 \\ 0 & 0 & 0 \end{pmatrix}$$

$$\underline{F}(t,s) = \begin{pmatrix} F_1[\gamma(t,s)] & 0 & 0 \\ 0 & F_1[\gamma(t,s)] & 0 \\ 0 & 0 & F_2[\gamma(t,s)] \end{pmatrix}$$

with

$$\gamma(t,s) = \int_{u=s}^t d\gamma(u)$$

For elongational flows with strain history $\lambda(t)$,

$$\underline{Q}^0(t,s) = \begin{pmatrix} \lambda^{-1}(t,s) & 0 & 0 \\ 0 & \lambda^{-1}(t,s) & 0 \\ 0 & 0 & \lambda^2(t,s) \end{pmatrix}$$

$$\underline{F}(t,s) = \begin{pmatrix} F_1[\lambda(t,s)] & 0 & 0 \\ 0 & F_1[\lambda(t,s)] & 0 \\ 0 & 0 & F_2[\lambda(t,s)] \end{pmatrix}$$

with

$$\lambda(t,s) = \exp \int_{u=s}^t d\lambda(u)$$

Empirical and theoretical forms are available for the functions F_i appearing in $F(t,s)$, permitting calculation, for example, of the steady state shear viscosity η_K , and elongational viscosity $\bar{\eta}_E$ as functions of the shear rate, along with a number of other functions including the first normal stress difference $\nu^{(1)}(t) = \sigma_{11}(t) - \sigma_{22}(t)$ in shear deformation. The latter is strongly dependent on the molecular orientations in the fluid.